2013

A study of the mechanical behaviour of cemented soils via Structured Cam Clay

Jiangheng Liu
University of Wollongong

A study of the mechanical behaviour of cemented soils via Structured Cam Clay

A thesis submitted in the fulfilment of the
requirements for the award of the degree

MASTER OF ENGINEERING - RESEARCH
(CIVIL)

from

UNIVERSITY OF WOLLONGONG

by

Jiangheng Liu
BEng (Civil), MEng (Civil)

FACULTY OF ENGINEERING

School of Civil, Mining and Environmental Engineering

2013

Abstract

This thesis describes an investigation of the mechanical properties of soils. A systematic study of the Structure Cam Clay model (SCC) for describing the behaviour of cemented soils is presented. Mode parameters for the different soils are identified and their effects on model performance are investigated. Cementation effects on soil parameters are then investigated. After studying eight groups of experimental data, an empirical equation is proposed to define the relationship between cement content and swelling index. The failure envelope for cemented soil is assessed, based on the analysis of five groups of experimental data. Soils with cohesion including cemented clay and cemented sand are simulated and analysed. Loess could also be analysed as cemented soil with SCC due to its glutinous ingredient, and a special equation for predicting the virgin yield surface for loess is proposed with surface simulation. SCC performance is proved to be better than that of the Modified Cam Clay model (MCC) after a simulation comparison.

A study on yield surface was carried out. Defects of SCC yield surface in terms of its shape and the ratio of height to width are discussed. It was found that the extension of SCC to cemented soil failed to take into consideration the breakdown of cementation during a drained simulation. Thus, the decementation equation for drained soil behaviour is proposed to fix this problem. Through the test data and model analysis, it can be determined that the stress paths for cemented soil are usually distorted and SCC is incapable of reflecting sub yielding and decementation before peak stress. Further research in this area is needed.

Liu M. D., Liu J., Horpibulsuk S. and Huang W. (2013), "Simulating the stress and strain behaviour of loess via SCC model", *18th Southeast Asian Geotechnical Conference* (Approved).

Acknowledgements

Grateful acknowledgement is given to my supervisor Dr. Martin Liu of the University of Wollongong. The solid academic support, guidance and friendly working atmosphere improved this thesis in many ways. All the proposed equations and the outcomes were developed through discussion with and supervision from Dr. Martin Liu. Appreciation is also expressed to my Co-supervisor A/Prof. Wei Dong Guo, who provided me with plenty of valuable advice and tips on thesis development. Thanks also to the 'Web of Science' and 'Scopus' databases which provided me with most of the science papers for my study.

Table of Contents

Table of figure

Notations

A_w	Cement content.
C	True cohesion of soil.
e	Void ratio.
E^*	Tangential elastic Young's modulus.
G	Tangent shear modulus.
G_s	Specific gravity.
ICL	Intrinsic compression line, Burland (1990).
CSL	Critical state line.
SCC	Structured Cam Clay.
MCC	Modified Cam Clay.
I_L	Liquidity index.
K_0	Coefficient of earth pressure at rest.
LL	Liquid limit.
M^*	Critical state strength parameter, the value q/p' at critical state.
P_I	Plasticity index.
P_L	Plastic limit.
p'	Mean effective stress.
p'_c	Pre-shear effective confining pressure.
p'_0	Precompression pressure.
$p'_{y,i}$	Initial yield effective stress.
q	Deviatoric stress.

γ_b	Bulk density.
γ_d	Dry density.
ε_1	Axial strain.
ε_d	Deviatoric strain.
ε_v	Volumetric strain.
η	Stress ratio, q/p'.
κ^*	Swelling index.
κ	Swelling index dependent on cement content.
λ^*	Compression index in natural log scale (λ).
σ'_1, σ'_3	Principle effective stresses.
φ	Friction angle.
ω	Flow rule parameter.
Δe	Additional voids ratio.
ν^*	Poisson's ratio.
b	Destructuring index.
c	Voids ratio sustained permanently by structure.
γ	Parameter quantifying the effect of shearing on destrucuring.
$M(C)$	Effective Stress ratio, q/p' at critical state.
$\varphi(C)$	Effective frictional angle.

Chapter 1 Introduction

Soil is the product of nature and time, consisting of solid, liquid and gas. The different times, conditions and environments that form a soil lead to different soil particles and structures. Therefore, soil behaviour is irregular and developing a precise soil model is difficult. Soft clay is widespread in many big cities and it becomes an enormous engineering challenge due to its poor mechanical behaviour. Strengthening weak soil foundations is necessary for preparing a construction site. Cement reinforcement is one of the widely used methods for soil treatment. Adding a cement agent to soil changes soil structure, and this changes the mechanical characteristics of soil. To understand soil behaviour, many soil constitutive models were proposed. Some of these are complicated and include parameters which are difficult to identify. Moreover, the complexity of cemented soil behaviour challenges the model adoptability.

Through decades of development, the Cam Clay model has become one of the easiest and the most popular models and has potential to be improved. The Modified Cam Clay model (MCC) was first proposed by Roscoe and Burland (1968). Then Wood (1990) published a specific description and systematic study of this model. Effects of soil structure on soil behaviour are widely reported and need to be considered in modeling (e.g. Burland, 1990; Schmertmann, 1991). A recent model belonging to the Cam Clay model family is the Structured Cam Clay model (SCC) which was proposed by Liu and Cater (2002), and includes the effect of soil structure and cohesion based on MCC. SCC has already simulated many soil behaviours successfully. However, there are still some cases with special behaviour to be simulated.

This thesis is concerned with the behaviour and capacity of cemented soil using SCC. Specifically, test data was studied to discover the problems associated with SCC when special situations such as high cement content clay and cemented sand are simulated.

Also, the relationships between some parameters and cement content were investigated using extensive experimental data as a basis. Accordingly, adjustments to SCC and empirical equations are proposed. A further modification to the yield surface aspect of the model was made based on analysis of the model frameworks and test data. The thesis is outlined as follows:

Chapter 2 – A review of soil constitutive model development and some important contributions. These include the foundation of soil structure and the introduction of structure into the constitutive model and stress strain parameters.

Chapter 3 – An introduction to SCC extended to cemented soil. This part provides a mathematical and detailed description of the theory of the model.

Chapter 4 – Parametric studies especially for cemented soils. The meaning of parameters and the methods used to identify them are introduced.

Chapter 5 – Investigation of the influences of some parameters on soil behaviour. An empirical equation of cementation extending the failure envelope is assessed and an equation of cement content relating to swelling index is proposed.

Chapter 6 – A study on the behaviour of loess. SCC extended to cemented soil is applied to capture the distinct structure behaviour of this collapsible soil. The yield surface distorted by its special cementation is also studied.

Chapter 7 – Cemented soil simulation including Ariake clay, Singapore marine clay and gravel sand. The comparison between SCC and MCC as well as between cement independent swelling index simulation and cement dependent swelling index are made. Also, an equation for the breakdown of cementation in drained behaviour is developed.

Chapter 8 – Developing yield surface to suit cemented soil. The yield surface for cemented soil will be studied and a new yield surface is proposed and assessed.

Chapter 9 – Conclusions and recommendations for further study.

Chapter 2 Literature review

2.1 Soil structure and structured soil

Structure in soil was first examined in clay by Mitchell (1976) and was defined as the way individual soil particles clump or bind together, aggregate and incorporate pore water and air in soil. Its generation is mainly based on four effects: the alternation of wetting and drying; the alternation of freezing and thawing; root pressure and cultivation. As for soil structure in natural clay, Schmertmann (1991) stated that the aging of soil mechanically impacts soil and this should be considered in a constitutive model. Several researchers have performed tests on intact clays from various parts of the world (Lerouiel and Vaughan, 1990; Burland, 1990; Nagaraj et al., 2008; Liu and Cater, 1999; Asaoka et al., 2000; Baudet and Stallebrass, 2004; Low et al., 2008; Yao et al 2009) and this has yielded many useful conclusions including: A. soil structure does not affect elastic behaviour (κ^*) of soil; B. softening is likely to take place in structured soil; C. structure changes soil compression behaviour and it contributes to voids ratio sustainability based on corresponding reconstituted soil (Fig 2.1) and in particular D. the soil mathematical simulation model is proposed to simulate structured soil. Based on the development of structure in the constitutive model, many new models have been proposed by Gens and Nova (1993), Whittle (1993), Rouainia and Wood (2000), Taiebat et al. (2010), and Suebsuk et al. (2011).

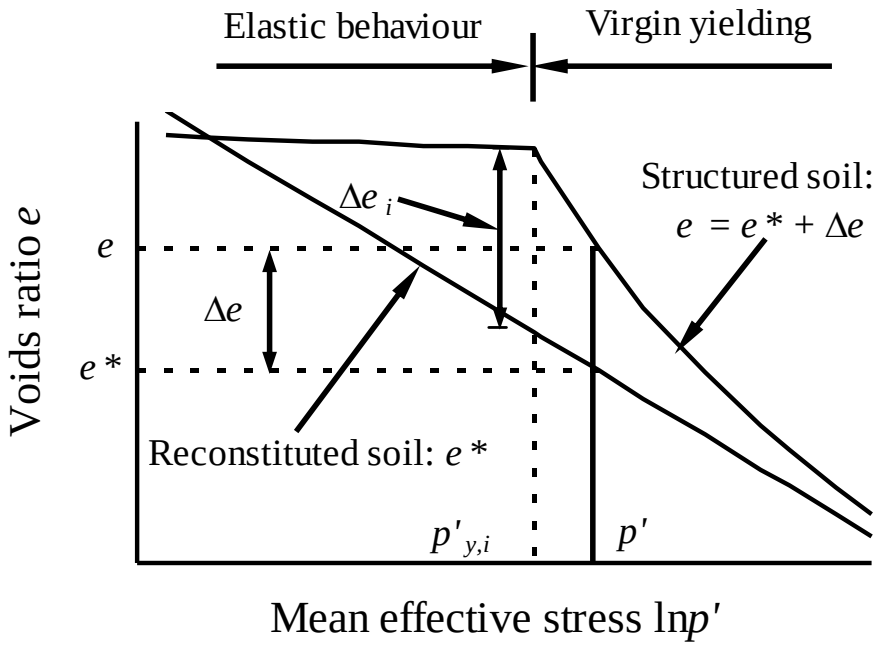

Fig 2.1 Compression behavior of structural soil

Mixing cement into unstable soil is a widespread application for unsound foundations. Portland cement, one of the most widely used stabilizing agents, consists of tricalcium silicate (C_3S), dicalcium silicate (C_2S), tricalcium aluminate (C_3A) and tetracalcium alumino-ferrite (C_4A) (Lea, 1956). When these chemical contents come in contact with the pore water in soil, hydration reactions occur and chemical ingredients in soil produce hydrated calcium silacates ($C_2S\ H_X$, $C_3S_2\ H_X$), hydrated calcium aluminates ($C_3A\ H_X$, $C_4A\ H_X$) and hydrated lime $\mathrm{Ca}(OH)_2$. The first two are the glutinous ingredients which provide cohesion force to soil. The process of curing of cement can be written as:

$C_3S + H_2O \longrightarrow C_3S_2H_X$ (hydrated gel) + $Ca(OH)_2$ (primary cementitious products)

$Ca(OH)_2 \longrightarrow Ca^{2+} + 2(OH)^-$ (hydrolysis of lime)

$Ca^{2+} + 2(OH)^- + SiO_2$ (soil silica) $\longrightarrow$ C-S-H (secondary cementitious product)

$Ca^{2+} + 2(OH)^- + Al_2O_3$ (soil alumina) $\longrightarrow$ C-A-H (secondary cementitious product)

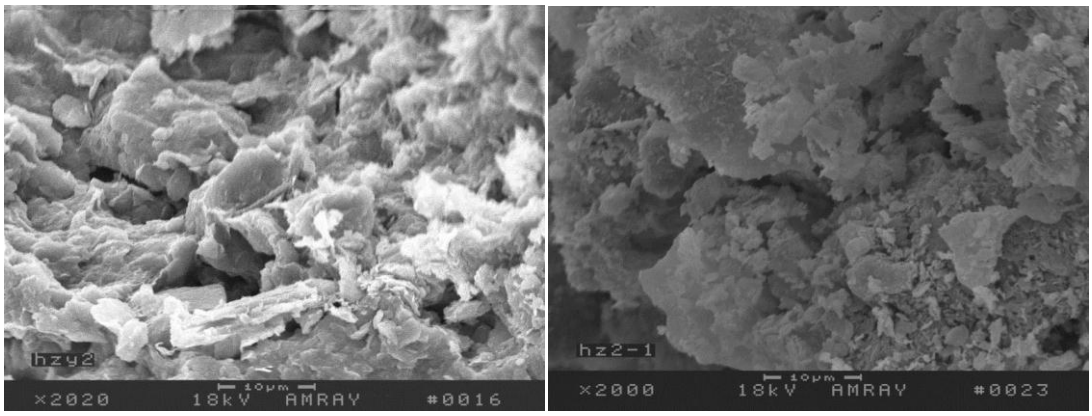

Original 1 day

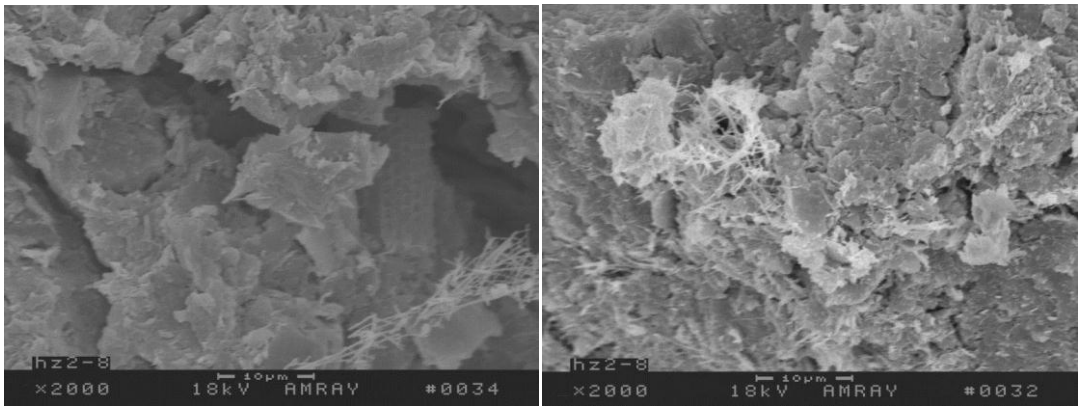

8 days 8 days

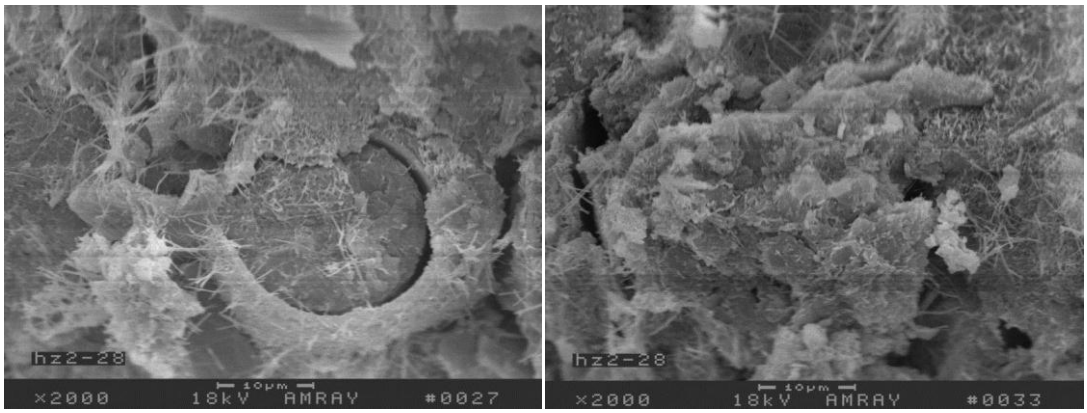

28 days 28 days

Fig 2.2 Microstructure features of cemented soil (Chen et al., 2011)

Chen et al. (2011) discovered granularmetric composition and microstructured features in soil that had been treated with cement via a deep mixing method (Fig 2.2). They

found that the high clay particle content would increase the complexity of the hardening behaviour of the cement treated soil. The process started with a slight increase in strength, followed by a dramatic increase at the end of curing. Electronmicrographs demonstrated few crystals in samples from the 8^{th} curing day but samples from the 28^{th} curing day contained many crystalline structures (Fig 2.2). Therefore, the curing process is one of microstructure generation and this is how cementation works in soil.

Cemented soil, where the original structure has been disturbed and replaced with a new artificial cement structure, behaves similarly to natural structured soil. The main difference between cemented structure and natural structure is that cementation increases its ability to bear tensile stress, which introduces the parameter of Cohesion to SCC. The conditions whereby soils can take utmost advantage of cementation have become a hot topic in cemented soil research. Horpibulsuk (2010) and Huawen (2009) simulated cemented soil with SCC and MCC respectively.

As a special natural soil that contains cementation, loess could be regarded as cement treated soil when simulating its behaviour. However, loess has different structure features compare to cemented clay. Cohesion contributes more to loess strength than structure does (Hu et al., 2004). The cementation in loess can be dissolved in water and this removes cohesion. Therefore, the saturated structural compression line represents the structural contribution to its strength as cohesion is completely removed. Shao and Deng (2008) concluded from experimental data that cementation in loess changes its strength along with soil structure break down (yielding and crushing). Cohesion reaches its peak when shear strain is as low as about 1%, followed by a cementation decrease as shear strain grows until soil structure is completely removed. As confining stress increases, loess in the same water ratio shows larger shear strength. Meanwhile, stress-

strain behaviour tends to shift from a softening pattern to a hardening one due to increasing destructure with the rise of preconsolidation stress (Shao et al., 2006).

Since structured soil is far more complicated than reconstituted soil, developing an appropriate structured soil model is significant and urgent. Many soil models have been proposed based on reconstituted soil and the Cam Clay family is one of the most popular for its wide adaptability. After adjusting the yield surface to elliptical, MCC is well recognized in solving boundary problems on reconstituted soil in geotechnical engineering practice (e.g., Gens and Potts, 1988; Yu, 1998; Potts and Zdravkovic, 1999 and Liu and Cater, 2002) and the proposed SCC is based on MCC. Following this, Liu et al. (2006) extended the model to suit both natural structured soil and cemented soil.

2.2 Stress and strain parameters

For stress and strain states of soil elements in the cylindrical specimen and soil cube element as in Fig 2.3, two stress parameters, mean effective stress and deviatoric stress, need to be defined in conventional triaxial tests to calculate the stress ratio. In the axial symmetric situations:

$$p' = \frac{1}{3}(\sigma_1' + 2\sigma_2') \quad 2.1$$

$$q = (\sigma_1' - \sigma_2') \quad 2.2$$

The stress ratio is written as

$$\eta = \frac{q}{p'} \quad 2.3$$

Correspondingly, the incremental volumetric and deviatoric strains are written as

$$d\varepsilon_v = d\varepsilon_1 + 2d\varepsilon_2 \quad 2.4$$

and

$$d\varepsilon_d = \frac{2}{3}(d\varepsilon_1 - d\varepsilon_2) \qquad 2.5$$

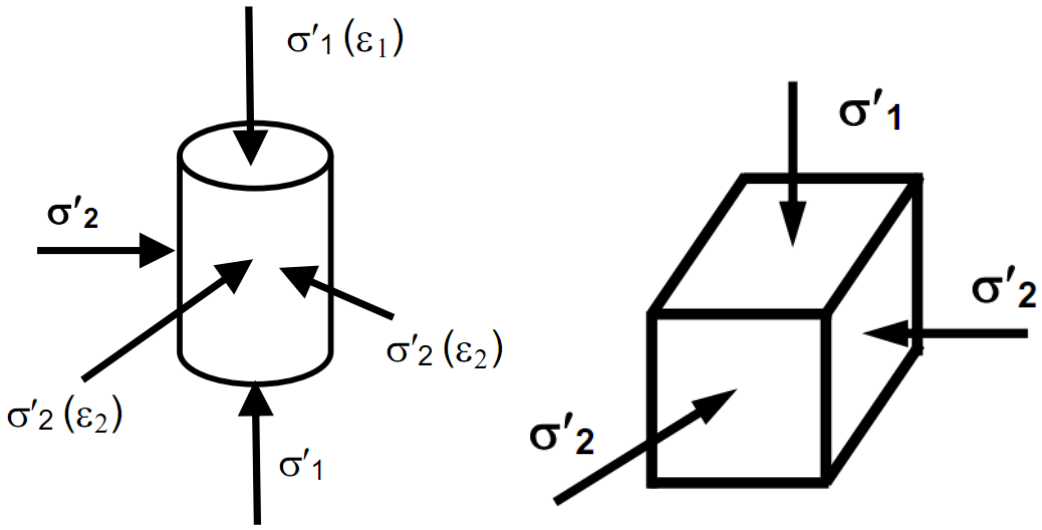

Fig 2.3 Stress and strain state for soils in conventional triaxial tests

Chapter 3 Structured Cam Clay for cemented soil

The Structured Cam Clay model (SCC) is proposed for simulating uncemented soil behaviour, especially for triaxial tests on clay. Based on some material assumptions and former Cam Clay frameworks, the original SCC is introduced step by step (section 3.1 to section 3.7) from the compression model to describe elastic and plastic behaviour. Then, SCC for cemented soil is introduced in section 3.8. All the work performed in this thesis is based on this version of the model.

3.1 Influence of soil structure on isotropic virgin compression line

The soil is assumed to be elastic and virgin yielding material. Referring to the compression behaviour of structured soil, it is obvious that the compression line exhibits a sharp drop after stable slightly reduced elastic behaviour. The inflection point of the compression line corresponds to the virgin yield mean effective stress, which brings soil from elastic deformation to plastic deformation. The introduction of soil structure allows the consideration of the extra voids ratio sustained by structure. The extra voids ratio is referred to as Δe (Fig 2.1) (Liu and Carter , 2003; and Liu et al., 2003), where:

$$e = e^{*} + \Delta e \qquad 3.1$$

where the extra voids ratio during isotropic virgin compression of natural clays as proposed by Liu and Cater (1999, 2000a) as:

$$\Delta e = a\left(\frac{p'_{y,i}}{p'}\right)^{b} + c \qquad 3.2$$

Where b is the structure index representing the stiffness of soil structure and $p'_{y,i}$ is the virgin yielding mean effective stress. Parameters a and c are described as follows:

$$c = lim_{p' \to \infty} \Delta e \qquad 3.3$$

and

$$a = \Delta e_i - c \qquad 3.4$$

Δe_i is the additional voids ratio at the point $p'=p'_{y,i}$.

3.2 Yield surface for structured clay

SCC is developed from MCC. In the model, it is assumed that on the p'-q space, there is a virgin yield surface corresponding to a soil in a virgin yielding stress state, which is related to the largest stress that soil has experienced. Elastic deformation only takes place in soil when the soil stress state is in the virgin yield surface. Once the stress state reaches or surpasses the virgin yield surface (the historically greatest stress state is surpassed by the current stress state), plastic deformation occurs. In this case, the virgin yield surface will be extended then replaced by the current yield surface. Hence, both elastic and plastic deformation happens when the stress state crosses the virgin yield boundary. During the lengthy development of the Cam Clay model, the equation used to simulate soil yield surface has undergone a few adjustments in the quest for a more precise simulation. In the recent study of Cam Clay model, MCC and SCC, the yield surface is assumed to be elliptical and it is given by (see Fig 3.1)

$$f = q^2 - M^* p'\left(p'_s - p'\right) = 0 \qquad 3.5$$

The idealisation and assumptions associated with soil for SCC yield surface can be summarized as:

a. Soil is an isotropic material, which implies the yield surface has no distortion because of cementation or special grain component etc. In addition, the yield surface will also extend isotropically with no distortion. So ignoring the rotation of the yield

surface simplifies both the shape of yield surface and extension of the yield surface. The extension of the yield surface is based on the values of yielding mean effective stress on the right tip of the elliptic and critical state line.

b. The yield surface separates elastic behaviour and plastic behaviour. Only elastic deformation occurs inside of the yield surface, otherwise both plastic deformation and elastic deformation occurs.

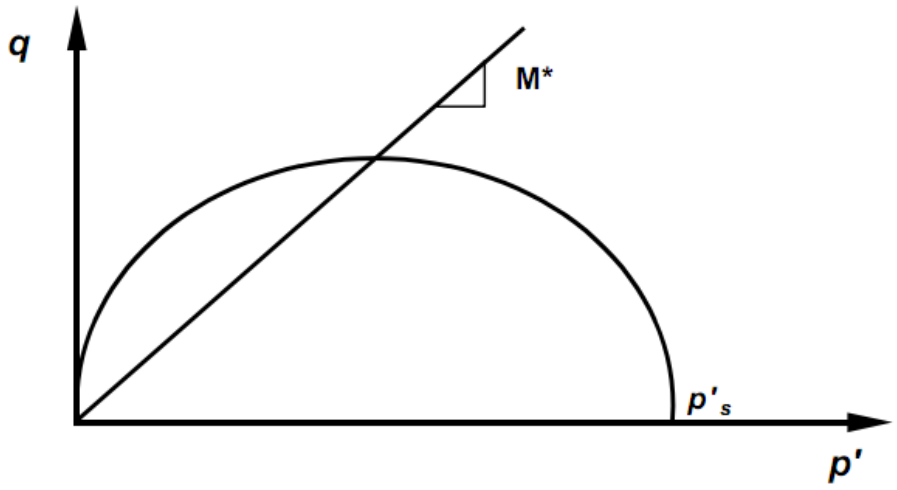

Fig 3.1 The yield surface for structured soils

3.3 Elastic behavior

Elastic deformation (inside the virgin yield surface) can be described by Hooke's law (Equation 3.6). This corresponds to the slightly diagonal straight line in Fig 2.1.

$$\sigma = E\varepsilon \qquad 3.6$$

$$d\varepsilon_v^e = \frac{3(1-2\nu^*)}{E^*} dp' \qquad 3.7$$

$$d\varepsilon_d^e = \frac{2(1+\nu^*)}{3} \frac{dq}{E^*} \qquad 3.8$$

where ν^* is Poisson's ratio and E^* is Young's modulus. E^*, ν^*, p', and the elastic swelling index κ^* are related by:

$$E^* = \frac{3(1-2\nu^*)(1+e)}{\kappa^*} p' \quad 3.9$$

Equations 3.7 and 3.8 can be replaced by Equation 3.9 which describes the elastic strain increment without Young's modulus.

3.4 Flow rule

The plastic deviatoric strain increment over the plastic volumetric strain increment for MCC is defined through the flow rule. The ratio of plastic deviatoric strain increment to plastic volumetric strain increment is:

$$\frac{d\varepsilon_d^p}{d\varepsilon_v^p} = \frac{2\eta}{M^{*2}-\eta^2} \quad 3.10$$

For the structured soil, the flow rule is generally lower than that of corresponding reconstituted soil. Structured soil has less plastic deviatoric strain than the reconstituted soil at the same plastic volumetric strain increase. The flow rule for SCC is given as follows:

$$\frac{d\varepsilon_d^p}{d\varepsilon_v^p} = \frac{2(1-\omega\Delta e)\eta}{M^{*2}-\eta^2} \quad 3.11$$

Where ω is the flow rule parameter representing the influence of soil structure on flow rule. The modifier range from 0 to 1 is as follows:

$$0 < 1 - \omega\Delta e_i \leq 1 \text{ or } 0 < \omega \leq \frac{1}{\Delta e_i} \quad 3.12$$

It cannot have a negative value as the plastic deviatoric strain could not locate inside of the yield surface. Its value could not surpass one, as the plastic deviatoric strain

increment will be less than that of flow rule of MCC, which reflects the effect of soil structure.

3.5 Virgin yielding behaviour

When the stress state reaches the yield surface, virgin yielding occurs.

$$e = e^* + \Delta e_i (\frac{p'_{y,i}}{p'})^b \quad 3.13$$

where e^* is the voids ratio of corresponding reconstituted soil and Δe_i is the additional voids ratio at the virgin yielding stress state.

As the reconstituted soil compression behaviour is assumed as a straight line in e-lnp' space, the reconstituted compression behaviour can be referred to as:

$$e^* = e^*_{IC} - \lambda^* \ln p' \quad 3.14$$

Substituting Equation 3.14 into Equation 3.13 gives:

$$e = e^*_{IC} + \Delta e_i (\frac{p'_{y,i}}{p'})^b - \lambda^* \ln p' \text{ for } p'_s \geq p'_{y,i} \quad 3.15$$

If the current yield surface is larger than the initial yield surface, the whole loading process could not start from an elastic stress state. In this case, soil simply shows plastic behaviour and no elastic parameter κ^* is involved in the equation. As for the case when initial load is smaller than initial yield mean effective stress, soil deformation will start from elastic behaviour and transition to plastic behaviour. The elastic behaviour can be written as $\kappa^* \ln p'$ and this reflects elastic deformation taking place in the whole process of tests even during the plastic stress state. The plastic part that works on the voids ratio drop is given by $(\lambda^* - \kappa^*) \ln p'_s$. To describe purely plastic behaviour, the elastic swelling index is subtracted from this equation. Thus, the virgin compression tests can be described as follows:

$$e = e_{IC}^{*} + \Delta e_i (\frac{p'_{y,i}}{p'})^b - (\lambda^* - \kappa^*)\ln p'_s - \kappa^* \ln p' \quad 3.16$$

When p' in Equation 3.16 is equal to or larger than $p'_{y,i}$ (the initial value of p'_s), Equation 3.16 includes Equation 3.15, as they can be simplified into the same formula.

For the assumption that soil deformation is solely attributed to the change in voids, at the yielding stage, the decrease of the volume of soil is equal to the decrease of the voids ratio. The decrease in both differentia follows the same equation. Therefore, the volumetric deformation in virgin yielding can be written as:

$$d\varepsilon_v = (\lambda^* - \kappa^*) \frac{dp'_s}{(1+e)p'_s} + b\Delta e \frac{dp'_s}{(1+e)p'_s} + \kappa^* \frac{dp'}{(1+e)p'} \quad 3.17$$

This equation can be divided into the elastic part and the plastic part of the volumetric deformation as in Equation 3.16, so

$$d\varepsilon_v^e = \kappa^* \frac{dp'}{(1+e)p'} \quad 3.18$$

and

$$d\varepsilon_v^p = (\lambda^* - \kappa^*) \frac{dp'_s}{(1+e)p'_s} + b\Delta e \frac{dp'_s}{(1+e)p'_s} \quad 3.19$$

The two parts in Equation 3.19 are attributed to soil intrinsic properties and soil structure. The first part, described as $(\lambda^* - \kappa^*) \frac{dp'_s}{(1+e)p'_s}$, reflects the soil intrinsic volumetric compressibility and is as applied in MCC. The associated parameters are from reconstituted soil compression behaviour. The second part reflects the soil structure sustainability of the voids ratio via the destructuring index. As seen in Equation 3.19, the plastic part of the volumetric deformation varies with yield surface but is independent of the current shear stress. Hence, the current deviatoric stress (with modification on Equation 3.19) is given as follows:

$$d\varepsilon_v^p = \left\{(\lambda^* - \kappa^*) + b[(\Delta e - c) + \frac{\eta \Delta e}{M^* - \eta}]\right\} \frac{dp_s'}{(1+e)p_s'} \quad 3.20$$

Parameter *c* refers to the voids ratio that is sustained by soil permanently. Adding modified plastic and elastic volumetric strain increments together gives the total volumetric strain increment of:

$$d\varepsilon_v = \kappa^* \frac{dp'}{(1+e)p'} + (\lambda^* - \kappa^*) \frac{dp_s'}{(1+e)p_s'} + b\Delta e \left(\frac{M^*}{M^* - \eta}\right) \frac{dp_s'}{(1+e)p_s'} \quad 3.21$$

The plastic volumetric strain increment is multiplied by the SCC flow rule (i.e. Equation 3.11) and is added to the elastic deviatoric strain increment of Equation 3.8 to yield the total deviatoric strain increment:

$$d\varepsilon_d = \frac{2(1+\nu^*)}{9(1+2\nu^*)} \left(\frac{\kappa^*}{1+e}\right) \frac{dp'}{p'} + \frac{2(1-\omega\Delta e)\eta}{M^{*2} - \eta^2} [(\lambda^* - \kappa^*) + b\Delta e \left(\frac{M^*}{M^* - \eta}\right)] \frac{dp_s'}{(1+e)p_s'} \quad 3.22$$

3.6 Softening

In the event that the stress state surpasses the critical state line within the virgin yield surface and assuming that only elastic deformation occurs inside the yield surface, it is possible that the stress could cross over the critical state line without soil destructuring. Soil structure remains intact and exhibits elastic behaviour until the stress state on the virgin yield surface is reached. After that, softening occurs and soil structure breaks down. During softening, the yield surface shrinks and the volumetric deformation associated with intrinsic soil properties is negative. This process is described as dry behaviour while the normal hardening consolidation is referred to as wet behaviour. In this stress state, $M^* < \eta$ and $dp_s' < 0$. Therefore, the structural volumetric strain is negative when Δe is negative and structural volumetric strain is positive when Δe is positive.

$$d\varepsilon_v^p = 2(1-\omega\Delta e)[(\lambda^* - \kappa^*) - b\Delta e(\frac{M^*}{M^*-\eta})]\frac{\eta}{M^{*2}-\eta^2}\frac{dp'_s}{(1+e)p'_s} \quad 3.23$$

3.7 Crushing of structure

After virgin yielding, the stress state reaches the critical state line ($\eta = M^*$) and tends to move along the critical state line upward or downward if the structure has not been completely removed. The stress strain relationship for structure crushing is described by:

$$\begin{cases} dq = M^* dp' \\ dp' \geq 0 \text{ for } p'_s < p'_e \text{ and } dp' \leq 0 \text{ for } p'_s > p' \\ d\varepsilon_v = \left(\dfrac{\kappa*}{1+e}\right)\dfrac{dp'}{p'} + d\varepsilon_v^p \\ d\varepsilon_d = \dfrac{2(1+\nu^*)}{9(1-2\nu^*)}\left(\dfrac{\kappa^*}{1+e}\right)\dfrac{dq}{p'} + \dfrac{2\left|d\varepsilon_v^p\right|}{\omega\eta\left|1-\sqrt{p'_o/p'_s}\right|} \end{cases} \quad 3.24$$

3.8 Soil with cohesion

If cementation is considered as reinforcement to mean effective stress then the behaviour of cemented soil should remain similar to cohesionless soil. Two basic modifications are made to the original SCC to extend the model in order to describe cemented soil: modification on the mean stress parameter and decementation after peak stress. For the SCC extended to cemented clay, cohesion will enlarge the yield surface isotropically. The modified mean stress parameter is written as Equation 3.25.

$$\bar{p'} = p' + {C}/{M^*} \quad 3.25$$

The stress ratio should be changed to

$$\bar{\eta} = \frac{q}{\bar{p'}} \quad 3.26$$

Consequently, the SCC extended to cemented clay is defined by stress parameters: $\overline{p}'$, q and $\overline{\eta}$.

The yield surface of cemented soil is extended to:

$$f = q^2 - M^* \overline{p}' (p_s' - \overline{p}') \tag{3.27}$$

where p_s' is the size of the yield surface extended by C/M^* as shown in Equation 3.25. The yield surface of cemented soil is illustrated in Fig 3.2.

Although evidence demonstrates that cementation can be broken down when yielding begins, the breakdown of cementation mainly takes place when the stress state is on the critical state line. In SCC, cementation breakdown is assumed to only occur during structure breakdown on the critical state line. The process of cementation breakdown is written as:

$$dC = -2\left(\frac{C}{C_{in}}\right)\frac{dp\prime}{\sqrt{\left(q/p\prime - M^*\right)}} \tag{3.28}$$

Therefore, the stress strain relationship for structure crushing with cemented soil is described by:

$$\begin{cases} dq = M^* dp' - dC \\ d\varepsilon_v = \left(\dfrac{\kappa^*}{1+e}\right)\dfrac{dp'}{\overline{p}'} + d\varepsilon_v^p \\ d\varepsilon_d = \dfrac{2\left(1+\nu^*\right)}{9\left(1-2\nu^*\right)}\left(\dfrac{\kappa^*}{1+e}\right)\dfrac{dq}{\overline{p}'} + \dfrac{2\overline{\eta}\left|d\varepsilon_v^p\right|}{\omega\left(1-2\nu^*\right)\left|1-\sqrt{p_o'/p_s'}\right|} \end{cases} \tag{3.29}$$

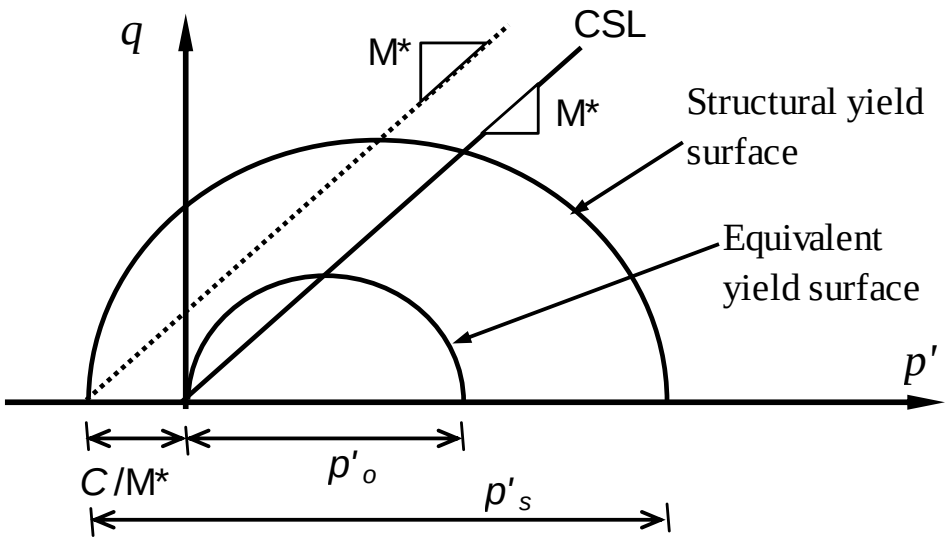

Fig 3.2 Structural and equivalent yield surfaces

Chapter 4 A study of the parameters for Structured Cam Clay

In this chapter, the significance of SCC parameters as well as methods of identifying these parameters will be introduced. The effects of these parameters on soil behaviour predicted by the model are extensively investigated. Undrained triaxial simulations are presented in this discussion to illustrate the effect graphically.

4.1 Physical meanings and identification of parameters for Structured Cam Clay

The core work for applying SCC to simulate soil behaviour should be the identification of parameters. In SCC, there are five parameters, denoted with the * symbol (i.e. $M^*, e_{IC}^*, \lambda^*, \kappa^*, \nu^*$), which are considered as intrinsic soil properties and which are independent from soil structure. The rest of parameters, those without the '*' (b, $p'_{y,i}$, C, Δe_i *and* ω), change with soil structure. The quantitative relationship between these parameters is illustrated specifically for compression behaviour and yield surface in Fig 4.1 and Fig 4.2. Paramaters are described as follows:

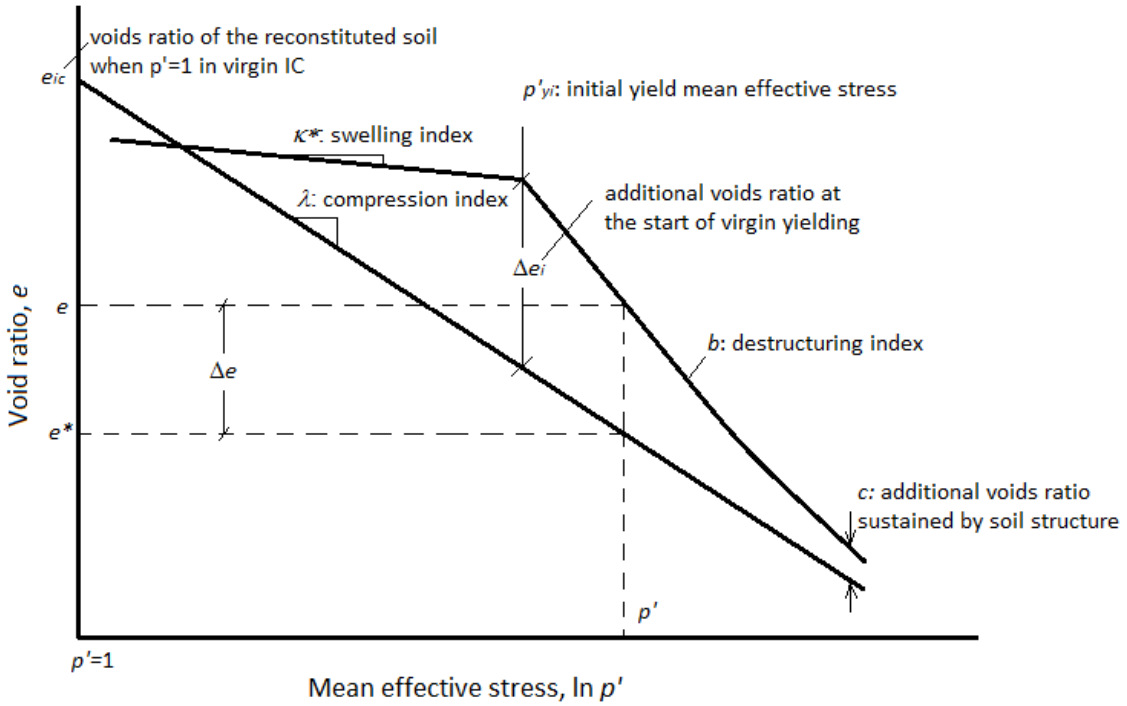

Fig 4.1 Definition of physical parameters in soil isotropical compression behavior

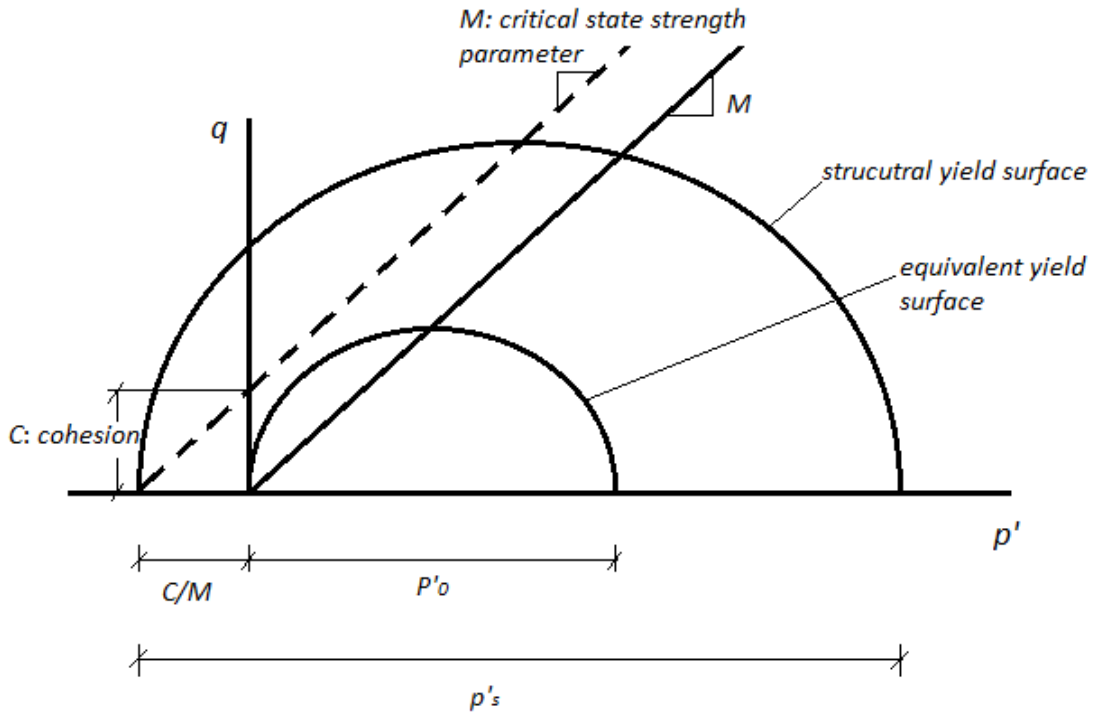

Fig 4.2 Definition of physical parameters in yield surface

a. M^* is the critical state strength parameter. It is the slope of the critical state line in p'-q space. It can be identified using test data for the stress path. The critical state refers to the deviatoric strain which increases with stable deviatoric stress. Cementation, a type of soil structure, cannot change the value of M^*. Therefore, the stress state at the end of the soil test should represent the critical state of soil for cementation and is recognized as completely broken down at this stage. The value of M^* increases with the friction angle so soil can sustain greater deviatoric stress. Therefore, the larger the friction angle, the stiffer the soil. At the critical state the soil starts cracking under shear and the intrinsic critical state friction angle and M^* are related as follows:

$$M^* = \frac{6sin\varphi_{cs}}{3-sin\varphi_{cs}} \quad 4.1$$

b. e_{IC}^* is referred to as the voids ratio of the reconstituted soil when the mean effective stress p' is equal to 1 kPa in virgin isotropic compression. Soil compression tests indicate the value of e_{IC}^*. Plotted on the logarithmic scale of mean effective stress, the value of lnp' for p'=1 is zero on the isotropic compression line.

c. λ^* , compression index, is the slope of the compression behaviour of reconstituted soil in e-lnp' space.

d. Destructuring index b indicates the rate of destructuring during virgin yielding and reflects the vulnerability of soil structure. The rate of structured soil compression decreases to that of reconstituted soil to generate the value of b. Structured soil is regarded as that with the ability to sustain a greater voids ratio than reconstituted soil. Therefore, decreases in the rate of voids ratio reflect destructuring and decementation processes.

e. $p'_{y,i}$ is the initial yield mean effective stress. It is the mean effective stress at the turning point in compression from elastic behaviour to plastic. The parameters of λ^*,

κ^* and b, can be determined from compression tests, but the constant stress ratio, $p'_{y,i}$ should be identified though isotropic compression tests. $p'_{y,i}$ is the size of the initial yield surface on the right tip of the yield surface where deviatoric stress is zero.

f. Swelling index κ^* refers to the slope of elastic behavior of soil. It is obtained via the rebound line at the unloading stage of compression tests, or the elastic compression line, as the slope of these two lines is theoretically equal. In addition, soil structure is independent of elastic deformation. Structured soil adopts the same swelling index as that of a corresponding reconstituted soil, because they use the same method to calculate elastic volumetric and deviatoric strain increment.

g. Δe_i is the additional voids ratio at initial yield mean effective stress. This reflects the voids ratio sustainability of soil structure and can be measured in a compression behaviour chart.

h. c is referred to as the voids ratio sustained permanently by soil structure. It can be identified as the gap between the lines between structural soil compression and reconstituted soil at the end of the test. Therefore, the net extra voids ratio from soil structure can be given as $\Delta e_i - c$.

i. C is referred to as cohesion, and describes the tensile stress that soil can bear. This can be defined from the peak strength line (failure envelope) of cemented soil in p'-q space. Specifically, the distance that the peak strength line rises above the critical state line is the value of cohesion. The effect of cementation on soil behaivour is shown in Fig 4.3.

Most of the soils are unable to sustain tensile force and hence, they do not have cohesion. However, cement treated soil and loess can sustain tension due to cementation and other glutinous chemical ingredients. The cohesion will extend the yield surface

without changing the shape of the yield surface. The left tip of the yield surface tends to move toward the negative side of the p' axis, which represents tensile mean effective stress.

In SCC, the complex process of decementation is considered to happen only after soil passes peak stress. Fig 4.3 illustrates the change of undrained soil behaviour with cementation. The most remarkable change is that the soil deviatoric strength increases with cohesion. Because of this, soil with higher cohesion tends to show more obvious softening during testing. This behaviour can be simply attributed to the cement structure in soil.

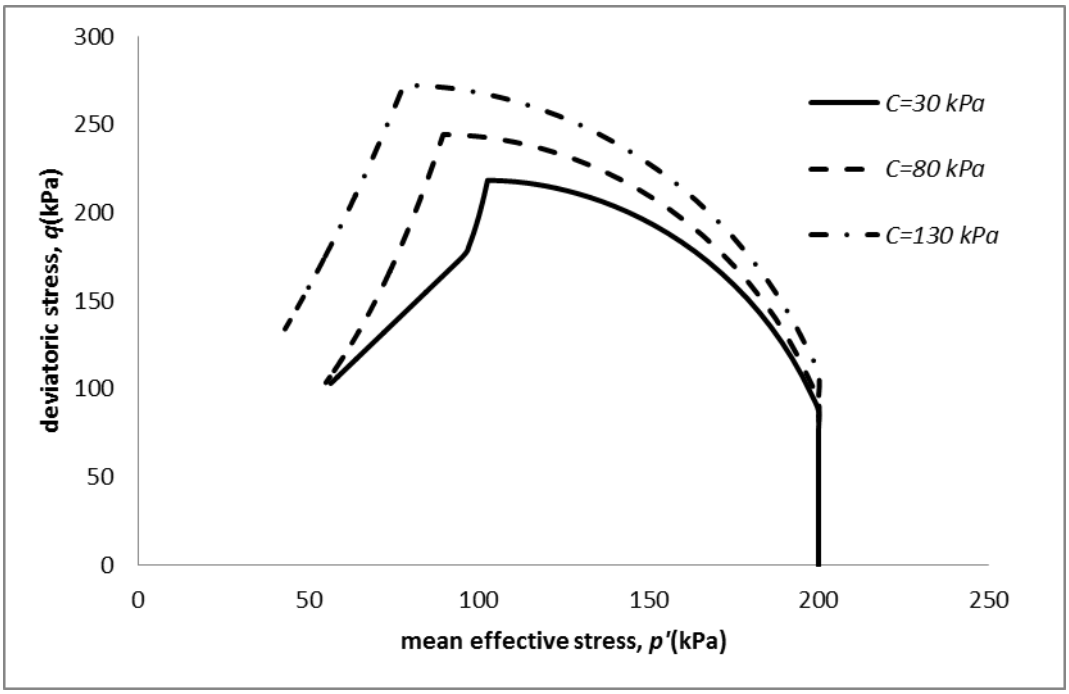

(a) Stress path

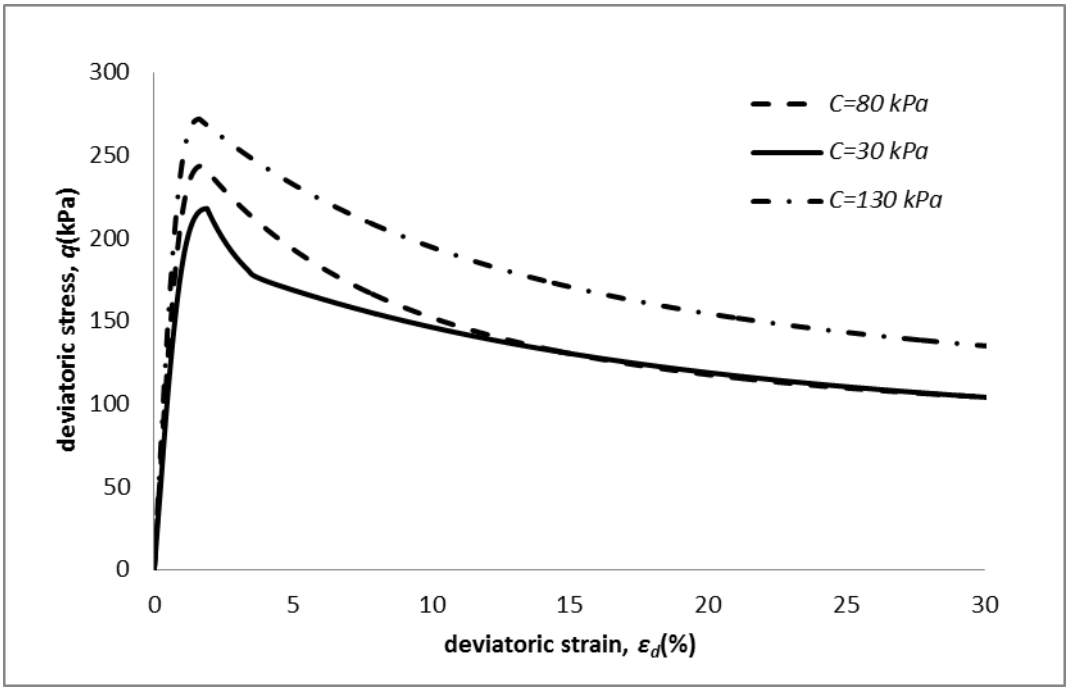

(b) Deviatoric stress and deviatoric strain

Fig 4.3 Influence of cohesion on undrained simulated soil behavior

4.2 Parametric study

This section explains the influence of some parameters (λ^*, κ^*, Δe_i, b, ω) on soil behaviour. Differences between soil behaviour, related to different values of these parameters, will mainly be demonstrated by the relationships between deviatoric strain and volumetric strain as well as between deviatoric strain and deviatoric stress. The soil data is mainly based on drained soil and the loading stress states generally start from virgin yielding mean effective stress (confining stress equals yielding stress). Values of soil parameters are listed below.

Table 4.1 Model parameters

λ^*	κ^*	Δe_i	M^*	${e_{IC}}^*$	ν^*	b	$p'_{y,i}$ (kPa)	C (kPa)	ω	γ
0.15	0.03	0.2	1.2	1.3	0.3	1	100	0	1	1

4.2.1 *b*

A series of soils with *b* values of 0, 0.5, 1 and 10 were selected to study the difference of soil behaviour in SCC. The simulations are shown in Fig 4.4 and Fig 4.5.

Parameter *b* reflects the stiffness of soil structure and therefore it affects the process of plastic deformation. The compression behaviour, (Fig 4.4), shows how structure index affects plastic behaviour. Generally, *b* values vary from 0 to 10. In the unlikely case of *b* equalling 0, soil structure remains intact as the stress increases. The compression behaviour of structured soil is parallel to that of reconstituted soil in *e*-ln*p'* space and therefore Δe_i does not change. As the parameter *b* becomes larger, the compression behaviour of structured soil decreases at a faster rate than that of the isotropic compression line of reconstituted soil. If *b* is very large (set at 10 in this simulation), the

soil is so vulnerable that the structure deteriorates suddenly and completely at the initial yielding mean effective stress.

As for the deviatoric stress strain relationship (Fig 4.5a), the deviatoric strain tends to increase to a stable point at the deviatoric stress of 200kPa, which is the intersection between the critical state line and the stress path. A small value of *b* brings stiffness to soil as the same deviatoric stress produces less deviatoric strain.

For drained soil behaviour (Fig 4.5b), parameter *b* does not change the final volumetric soil deformation at the critical state. This is because for this type of soil structure, strength does not change the voids ratio but does change the rate of volumetric deformation as the structure retains a proportion of the voids ratio. Deviatoric strain has a greater effect in soil when *b* equals 0 than in soils with a larger *b* value, since soil destructuring directly affects plastic volumetric deformation. The greater the value of *b*, the greater the volumetric strain. Therefore, the additional voids ratio is a measurement of increased soil structure, as the breakdown of soil structure is closely linked to a decrease in voids ratio.

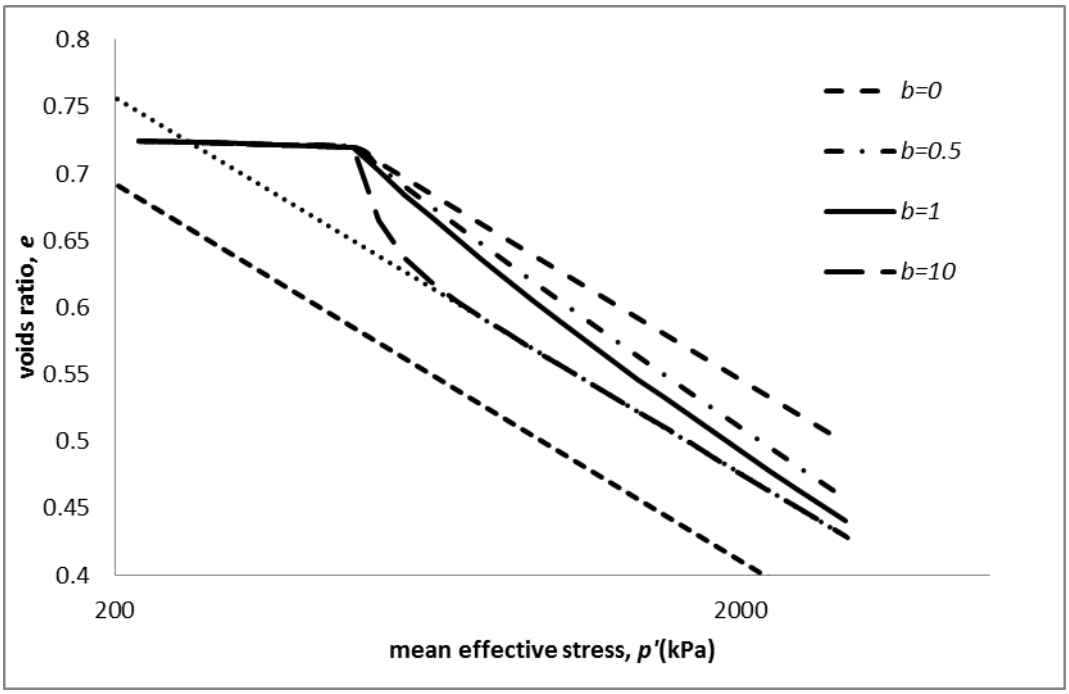

Fig 4.4 Influence of structure index on simulated isotropic compression soil behavior

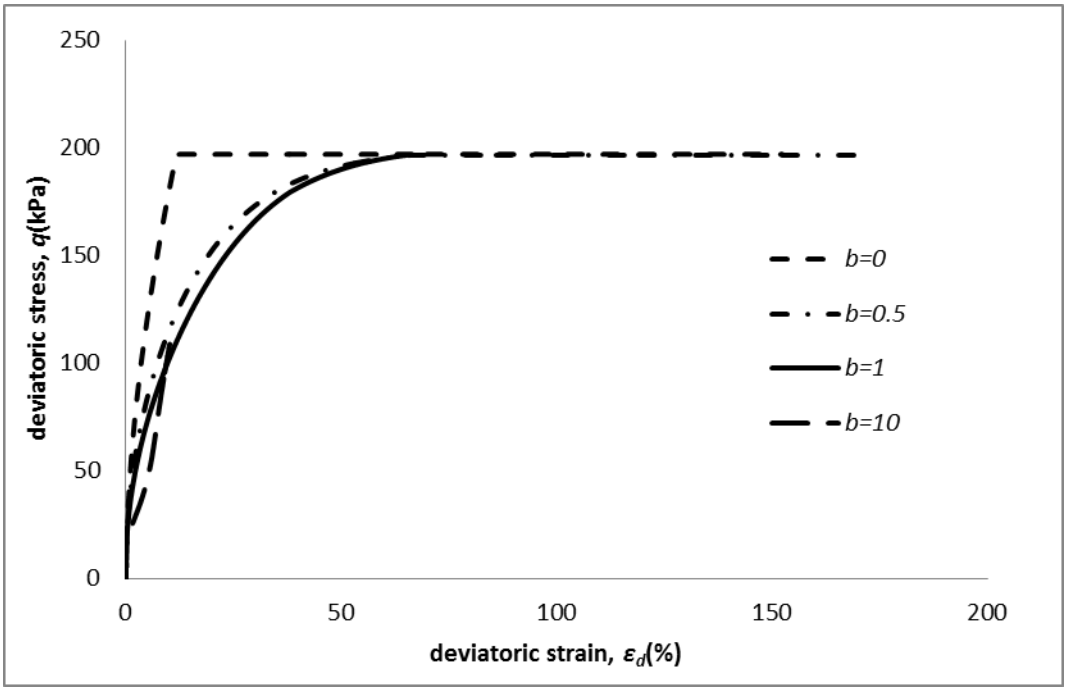

(a) Deviatoric strain and deviatoric stress

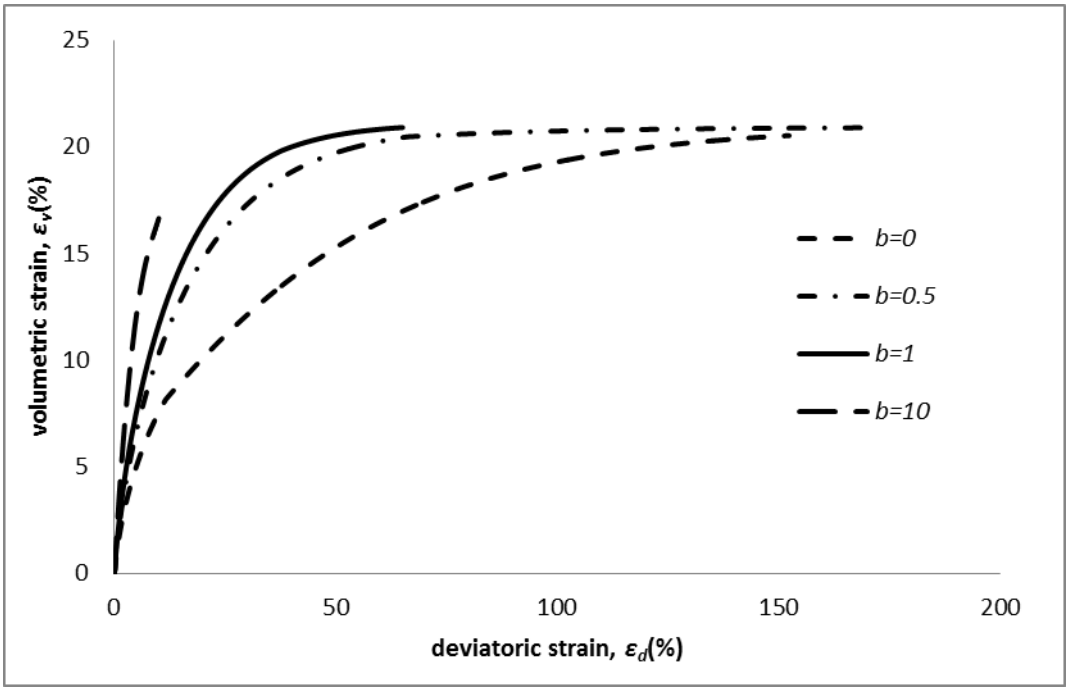

(b) Deviatoric strain and volumetric strain

Fig 4.5 Influence of structure index *b* on drained simulated soil behavior

4.2.2 Δe_i

The significance of Δe_i was investigated in both drained and undrained soil by using examples with four different values of Δe_i including 0.01, 0.1, 0.2 and 0.5. Distinctive variances are indicated in Fig 4.6 and Fig 4.7.

The initial voids ratio at the initial yield stress is the voids ratio held by soil structure. A larger value of Δe_i gives soil a greater volumetric deformation and a larger deviatoric deformation, which are linked by the flow rule (Fig 4.6b). Although there are differences in deviatoric strain, all of the soils reached their maximum strain at the same deviatoric stress. In addition, soil with a small Δe_i has a smaller deviatoric strain (than soil with a large value for Δe_i) as the deviatoric stress increases (Fig 4.6a). The stress path in undrained soil (Fig 4.7a), indicates a slight difference between the soil groups with varied Δe_i values. The small initial voids ratio of 0.01 tends to extend the yield surface more than the rest of the soil groups with higher Δe_i values. More importantly, this test is terminated sooner due to the earlier collapse of structure. Due to this short interval before soil structure breakdown for a low value of Δe_i soil, the degree of softening in deviatoroic stress strain behaviour is smaller than that of a higher Δe_i soil (Fig 4.7b). Unlike drained soil behaviour, there is no obvious gap in total deviatoric strain.

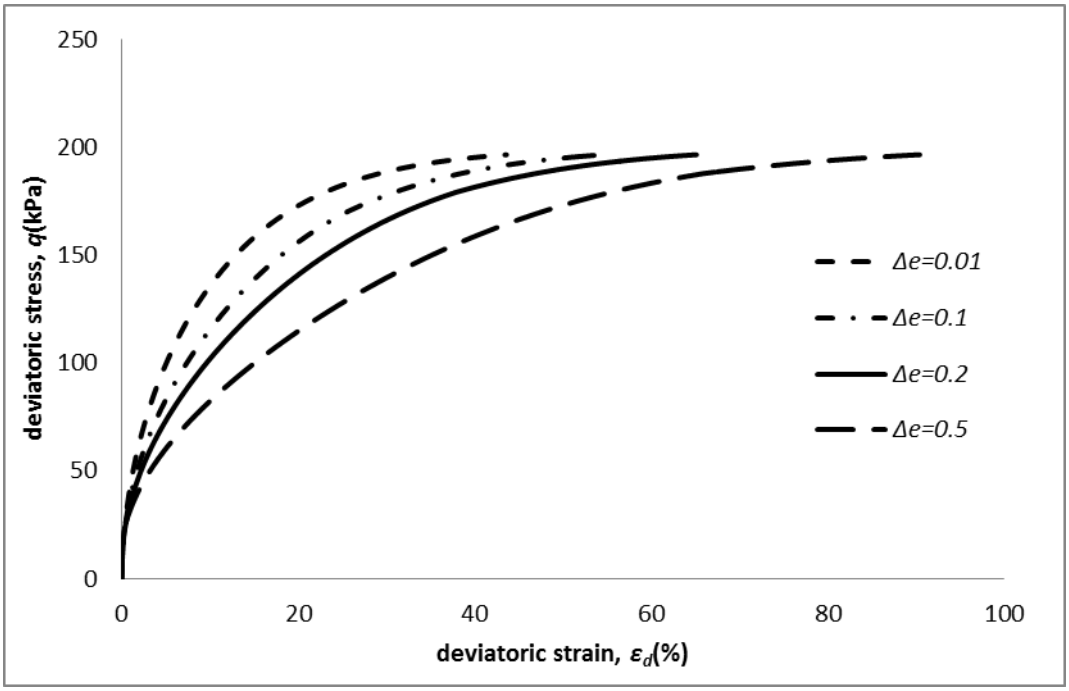

(a) Deviatoric strain and deviatoric stress

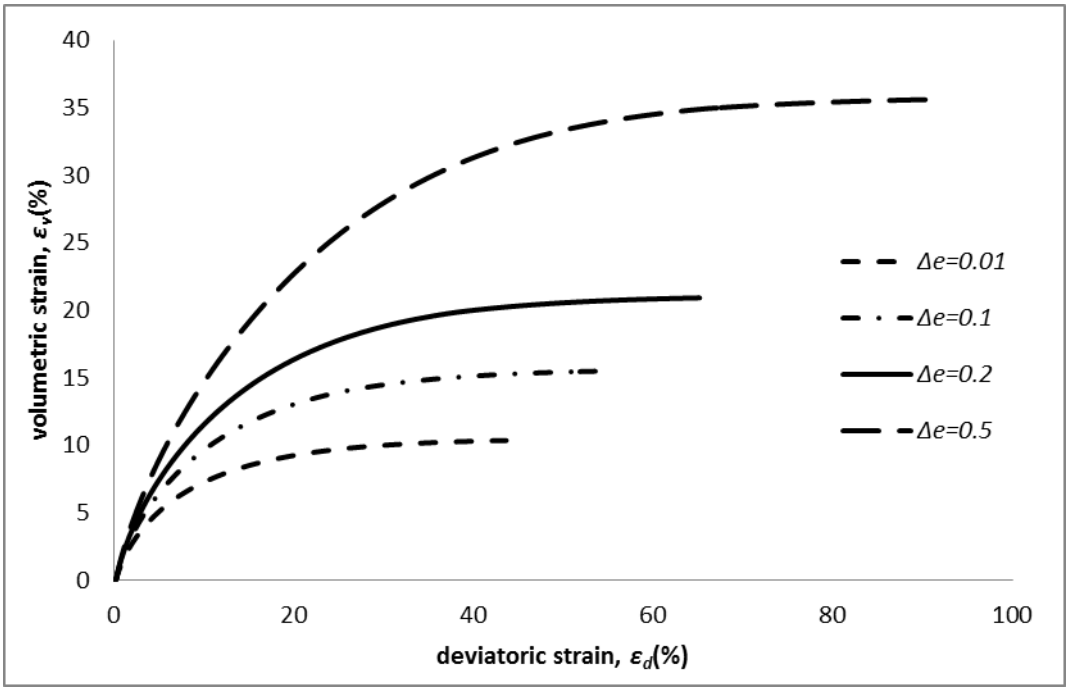

(b) Deivatoric strain and volumetric strain

Fig 4.6 The influence of Δ*e* on drained soil behavior

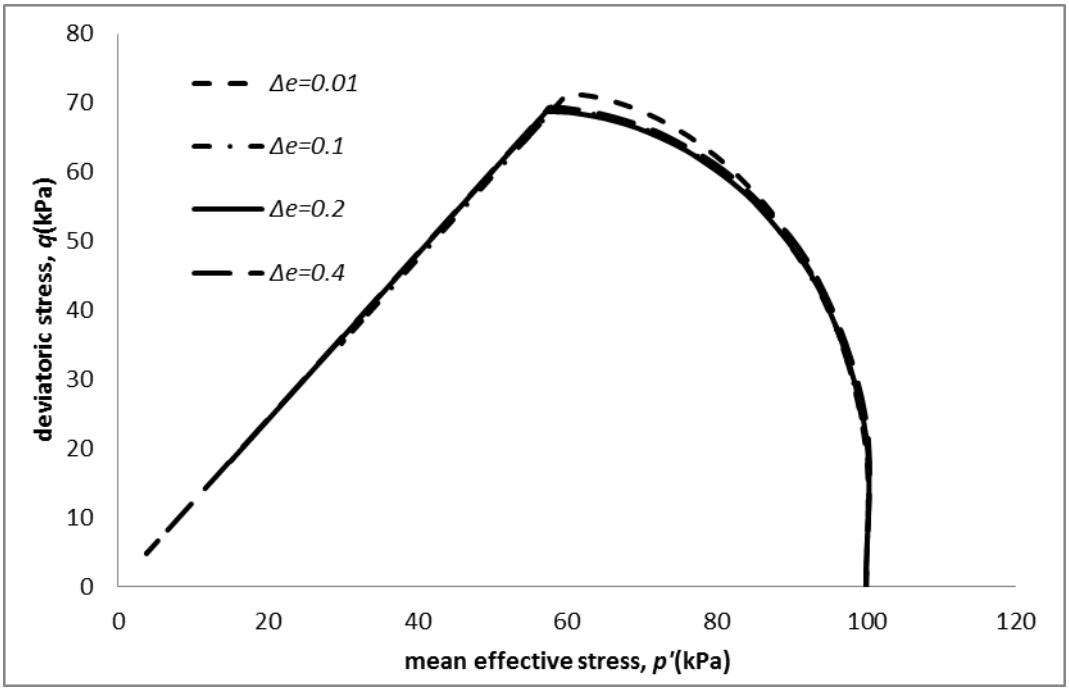

(a) **Stress path**

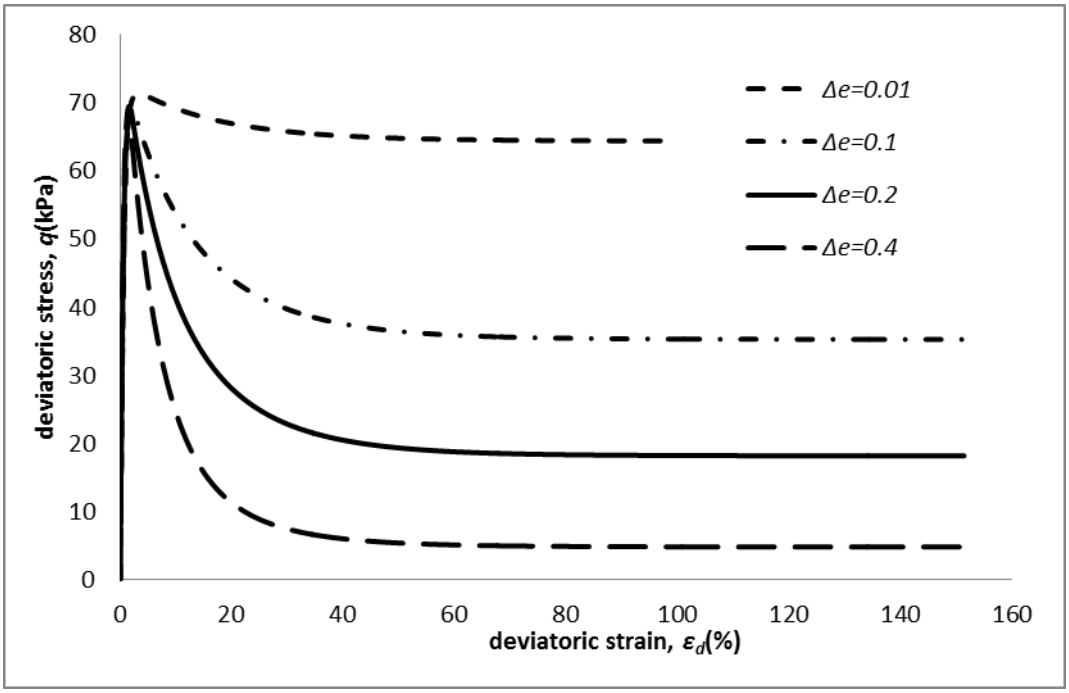

(b) **Deivatoric strain and deviatoric stress**

Fig 4.7 The influence of Δ*e* on undrained soil behavior

4.2.3 κ^*

To discover the effect that parameter κ^* has on soil behaviour, three cases of drained soil triaxial trials with different κ^* value were conducted with κ^* values of 0.01, 0.03 and 0.1. Since swelling index has a key role in elastic behaviour, in this trial calculation, the initial yield mean effect stress was set at 60kPa, while the stress was keep constant at 100kPa so soils would undergo elastic deformation. The results are shown in Fig 4.8.

Because λ^* is constant for a particular kind of soil, the value of κ^* determines plastic behaviour. In this simulation, the volumetric strain of all the groups tends to plateau at a maximum of 16% while large κ^* values lead to lower deviatoric strain at the end of the tests. For each group, an obvious pivotal point, which divides elastic behaviour from plastic behaviour, was observed (Fig 4.8a). The greater the soil swelling index the smaller the deviatoric stress at which this turning point was reached. All the groups tended to finish the test at the same deviatoric stress.

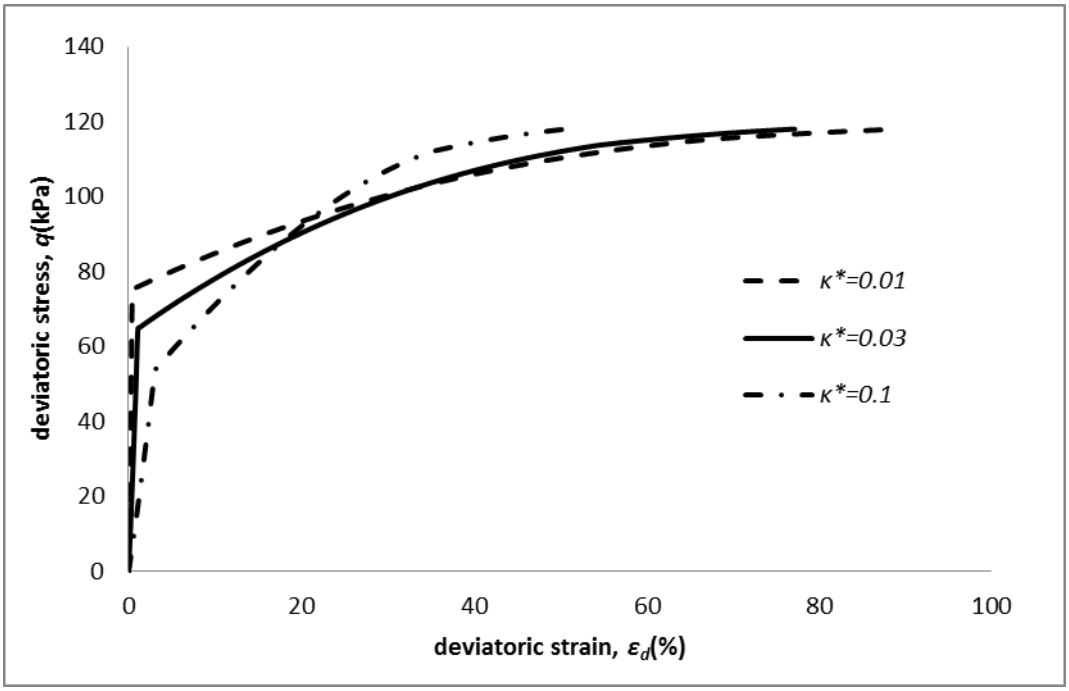

(a) Deviatoric strain and Deviatoric stress

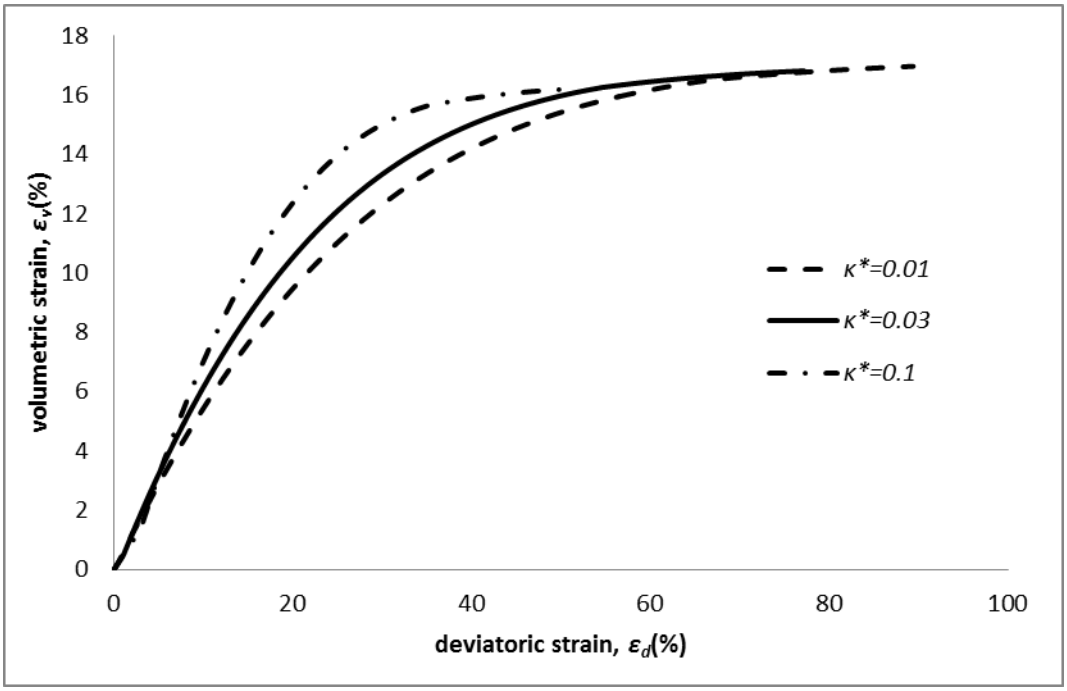

(b) Volumetric strain and deviatoric strain

Fig 4.8 The influence of κ^* on drained soil behavior

4.2.4 λ^*

As the plastic compression index, λ^* is independent from elastic behaviour, it influences plastic behaviour significantly. The calculations are made with three different values of λ^*; 0.05, 0.15 and 0.2, to compare the behaviour of simulated soil (Fig 4.9).

The higher the value of the compression index λ^*, the greater the amount of deviatoric strain and volumetric strain (Fig 4.9). Moreover, the groups with small value for λ^* show less deviatoric strain than the groups with a higher value of λ^* during the tests. When the critical state is reached, the shear stress for all tests reaches a final value of 200kPa.

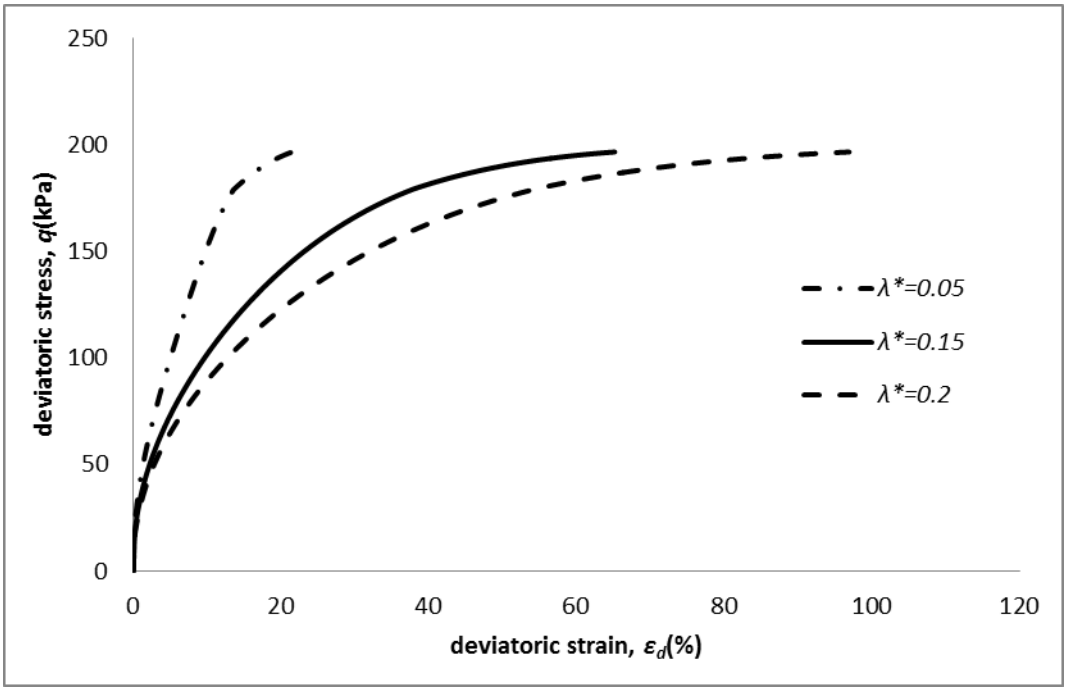

(a) Deviatoric strain and Deviatoric stress

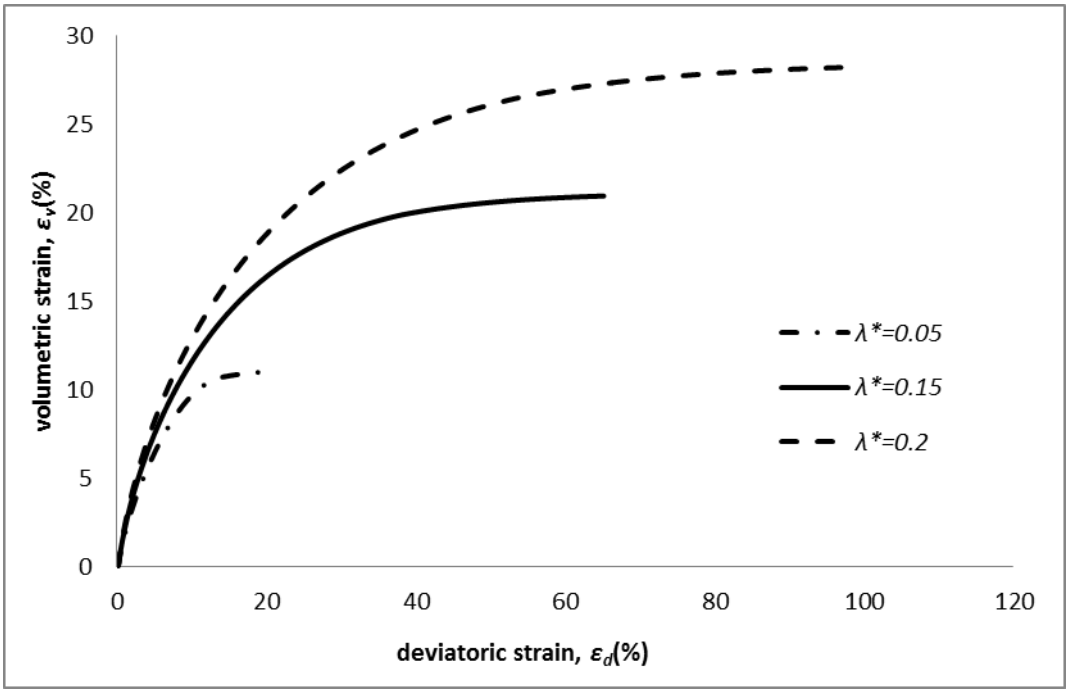

(b) Volumetric strain and deviatoric strain

Fig 4.9 The influence of λ^* on drained soil behavior

4.2.5 ω

ω is a new parameter introduced to reflect the effect of soil structure on the soil flow rule. The calculations are made with 4 different values of ω; 0, 1, 2 and 5 to compare the behaviour of simulated soils. From Equation 3.8, $(1 - \omega \Delta e)$ is the modifier of the flow rule for structured soil. This results from modifier values of 1, 0.8, 0.6 and 0 and corresponds to Δe is given as 0.2 in this trial calculation. The simulations are shown in Fig 4.10.

According to Fig 4.10, the shear strength and volumetric strain at the end of the tests do not vary with the flow rule parameter value. However, a larger flow rule parameter results in stiffer soil behaviour.

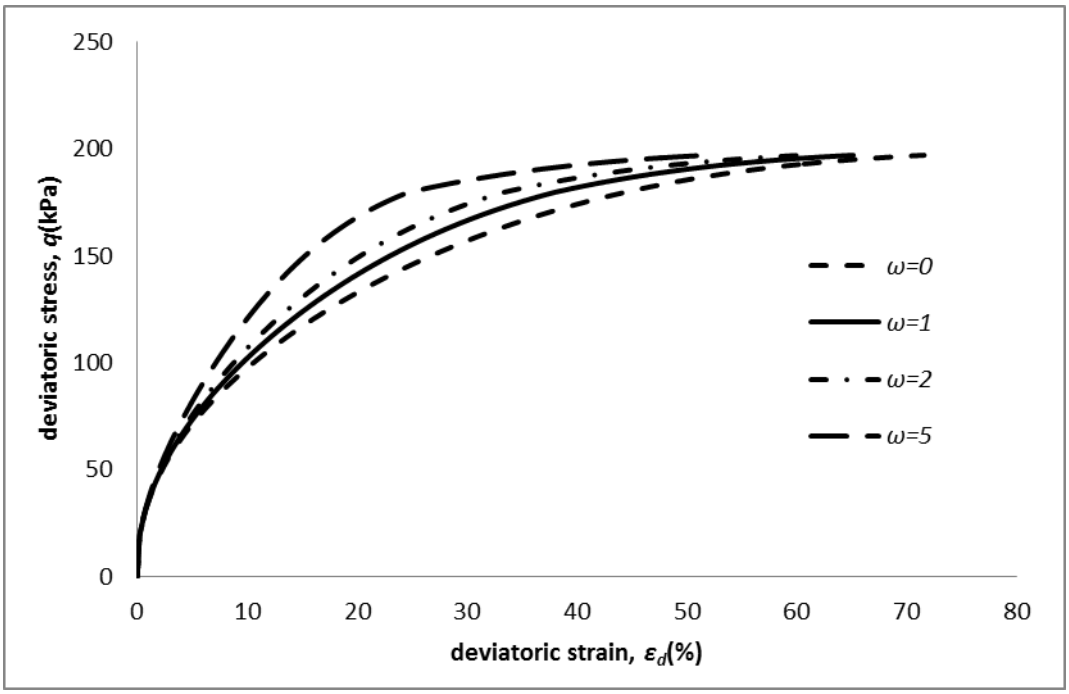

(a) Deviatoric strain and deviaotric stress

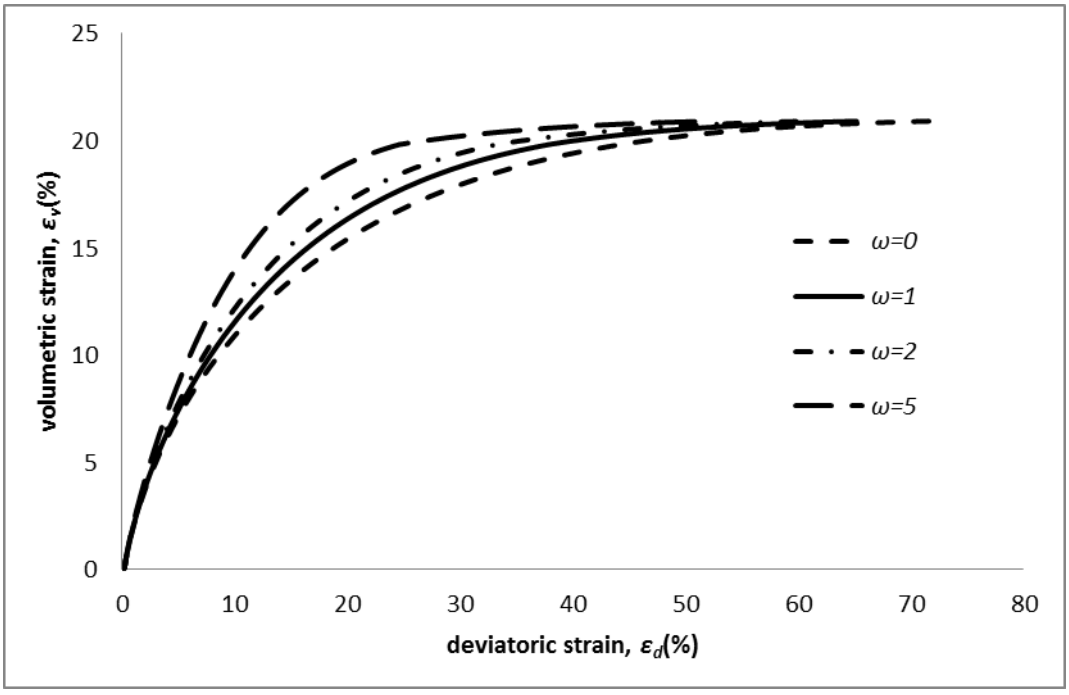

(b) Deviatoric strain and volumetric strain

Fig 4.10 The influence of ω on drained soil behavior

4.2.6 Conclusion of parametric study

The undrained soil simulations on the five parameters studied are summarized in Table 4.2. Deviatoric strength is independent of all of these five parameters, while deviatoric strain is affected by all of them. Volumetric strain is strongly dependent on Δe_i and λ^* while the remaining parameters do not affect volumetric strain.

The parameter of structured soil ω is introduced in the flow rule to represent the compressive nature of soil, and it has no influence on soil strength. Flow rule describes the plastic strain increment ratio and the introducing of ω and Δe_i in structured soil flow rule reflects soil structure can also influence the strain increment ratio. It is found in the model simulations for both drained and undrained tests that there is no influence on soil strength.

Table 4.2 Influence of parameters on soil behaviour

Parameters	Deviatoric strain	Volumetric strain	Deviatoric strength
b	-	/	/
Δe_i	+	+	/
κ	-	/	/
λ	+	+	/
ω	-	/	/
C	/	/	+

+ positive correlation; - negative correlation; / no correlation.

Chapter 5 Empirical equation proposed for model parameters

In this Chapter, the effects of cementation on model parameters are studied. An experimental equation is proposed to correlate cement content and swelling index. More than 5 groups of test data are analysed to assess the ability of cementation to increase deviatoric strength. The relationship between cement content and cohesion is also studied. All these studies will be adopted in the simulation chapter and reflect the benefits of introducing experimental equations.

5.1 Cementation versus deviatoric strength

As the effects of cementation in soil on SCC are discussed, the formula that describes the failure envelope should also be able to describe soil deviatoric strength. The deviatoric strength is written as:

$$q_{peak} = Mp' + C \qquad 5.1$$

According to Equation 5.1 when soil has no cementation, parameter *C* is equal to 0. The strength of soil is contributed only by friction. If soil is treated with cement or shows cohesion, the value of *C* will increase accordingly. The degree that CSL moves to the left and extent the yield surface is affected, reflects the amount of cementation and its effects on soil deviatoric strength. The line described by Equation 5.1 is no longer the failure envelope when the value of C is not equal to 0. Instead, it is the maximum possible deviatoric stress envelope. The more cementation in soil, the greter the value of *C* in the equation so the analysis of experimental data of cemented soil is designed to investigate the correlation between cement content and the value of *C* and to determine the intrinsic soil changes with cementation.

5.1.1 Weathered sandstone

Low cement content soil specimens with 3 different percentages of cement content; 1%, 3% and 5% were used in drained triaxial tests by Consoli et al. (1999). This soil base is from Port Algere in southern Brazil and it is classified as weathered sand stone and has the greatest dry density of 17.5kN/m^3 and saturated moisture content of 16.4%. The specific gravity G_s of specimens is 2.7 and effective diameter D_{10} is equal to 0.003mm. The uniformity coefficient, which represents the equation $C_u = D_{60}/D_{10}$, is as high as 48. The liquid limit of the soil is 21% and the plastic limit is 17%. The special points in p'-q space are represented in Fig 5.1.

The simulation of the failure envelope with Equation 5.1 in this case is reasonable. Strength increases with cement contents and M^* retains its value even with cementation changes. The equation that describe experiment data is:

$$q_{peak} = 1.599p' + C \qquad 5.2$$

The values of cohesion parameter *C* from this simulation are shown in Table 5.1 below.

Table 5.1 Measured cohesion from simulation of tests data

Cement content (%)	Cohesion parameter C (kPa)
1	125
3	333
5	528

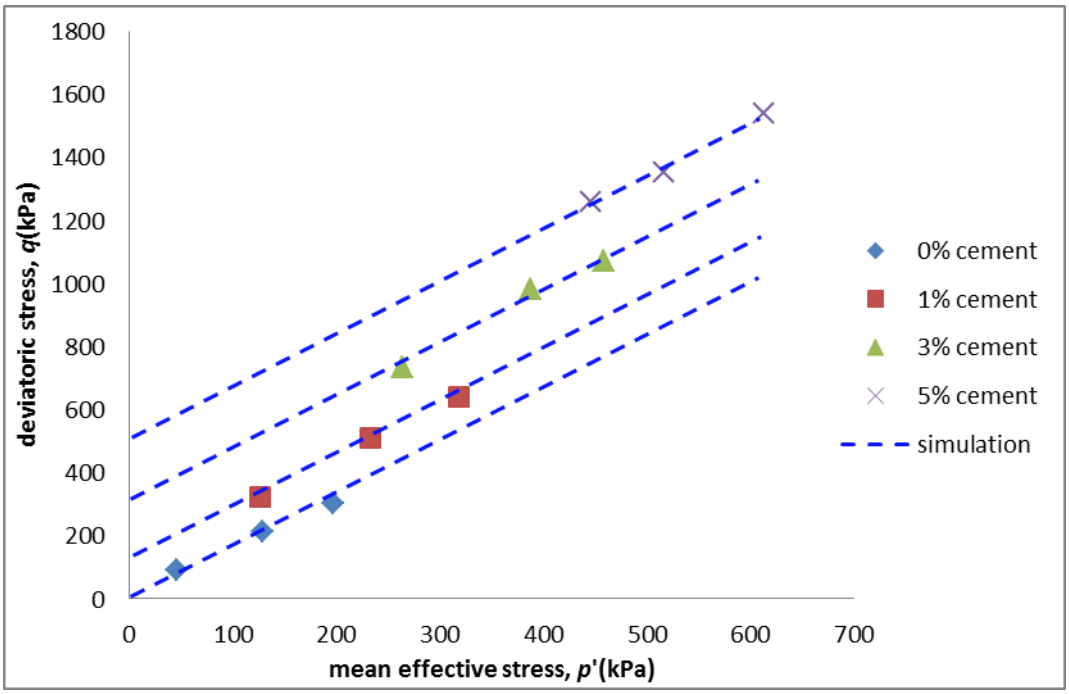

Fig 5.1 Variation in peak strength with cement content (Consoli et al., 1999)

5.1.2 Gravely sand

To discover triaxial behaviour of a cemented gravely sand, Asghari et al. (2003) conducted tests on cemented coarse-grained Tehran alluvium specimens. This soil is basically gravely sand with 45% gravel, 49% sand and 6% fine material and is treated with hydrated lime ($C_a(OH)_2$). The specimens were carefully controlled as follows:

Table 5.2 Average physical properties of the base soil

Property	Value
Specific gravity (G_s)	2.58
Effective diameter (D_{10})	0.2 mm
Uniformity coefficient (C_u)	27.8
Percent gravel (>4.76mm)	45%
Percent fine material (<0.074mm)	6%
Liquid limit of passing 425um	44%
Plastic index of passing 425um	16%
Unified classification of soil	SW-SM

The formula that incorporates the test data of the failure envelope is written as:

$$q_{peak} = 1.52p' + C \qquad 5.3$$

The values of the cohesion parameter *C* from this simulation are shown in Table 5.3 below. The simulation of the failure envelope is shown in Fig 5.2.

Table 5.3 Measured cohesion from simulation of test data

Cement content (%)	Cohesion parameter C (kPa)
1.5	237
3	300
4.5	519

Once again, cementation test data can be simulated by the simple failure envelope equation as M^* does not change with cementation. Compared with former tests, the data

in this case shows greater irregularity with much fluctuation. In addition, specimens with cement contents of 1.5% and 3% are located close to the same simulation line. The strength is almost unchanged in the scale of 1.5% to 3%. Therefore, excluding the experimental variability, it can be concluded that the strength of cemented soil is not correlated only with cement content. There are some other factors at work, in particular, scale such as that encountered with the lower cement content range or the scale of the stress state.

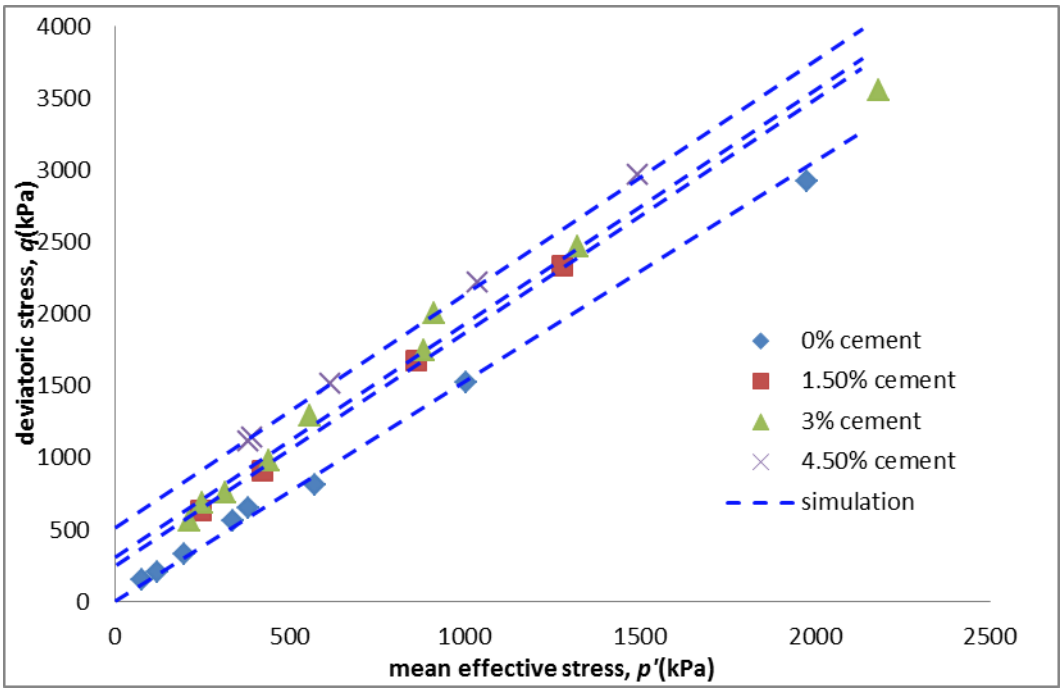

Fig 5.2 Variation in peak strength with cement content (Asghari et al., 2003)

5.1.3 Ariake clay from Horpibulsuk et al.

Cemented Ariake clay has been well researched in Japan. Horpibulsuk et al. stabilized Ariake clay and reported a compression index ($\lambda^* = C_c/2.303$) of 0.446 and a swelling index ($\kappa^* = C_s/2.303$) of 0.044 by mixing 6%, 9% and 12% of cement content separately (Table 5.4).

Table 5.4 Average physical properties of the base soil

Physical properties	Value
Specified density	2.70
Natural water content	135-150%
Liquid limit	120%
Plasticity index	63%
Liquidity	1.24-1.47
Clay fraction	55%
Silt fraction	44%
Sand fraction	1%

The formula derived from the test data of the failure envelope is written as:

$$q_{peak} = 2.03p' + C \qquad 5.4$$

The values of cohesion parameter *C* from this simulation are shown in Table 5.5 below. The simulation of the failure envelope is shown in Fig 5.3.

Table 5.5 Measured cohesion from simulation of tests data

Cement content (%)	Cohesion parameter C (kPa)
6	0
9	75
12	143

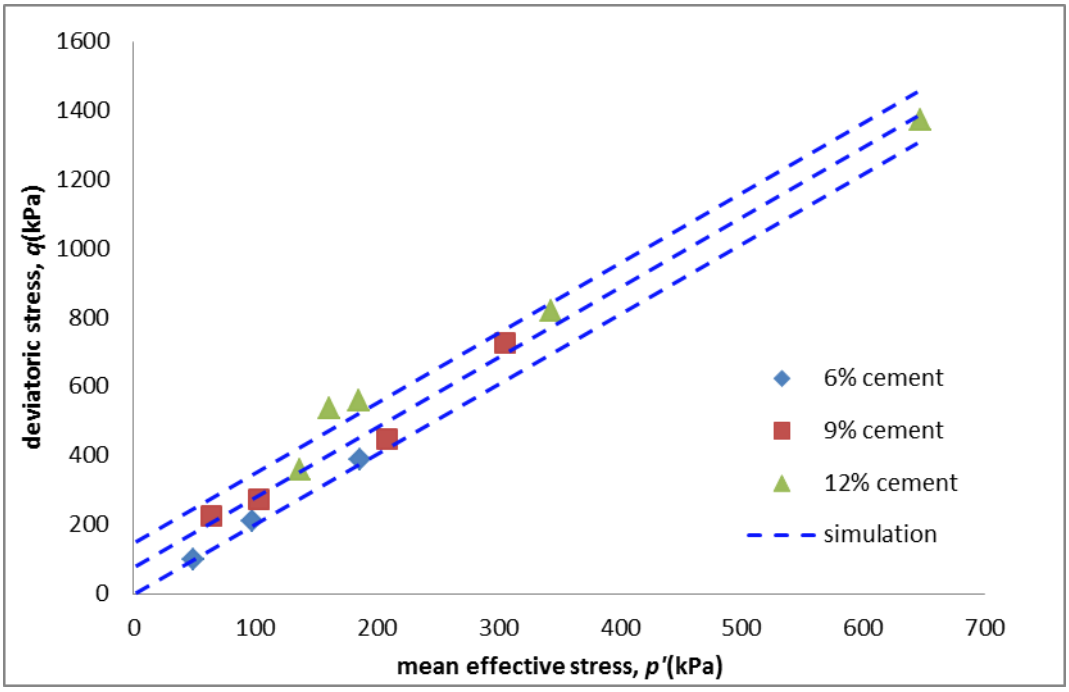

Fig 5.3 Variation in peak strength with cement content (Horpibulsuk et al., 2004)

5.1.4 Ariake clay from Kasama et al.

Light cemented samples are combined with Portland cement and Ariake clay in the tests. Some basic properties of soil are listed in Table 5.6. The clay is in a slurry of $2\omega_L$ when it is mixed with cement. These consolidation tests and undrained triaxial tests were carried out following the JGS (Japanese Geotechnical Society) standards 0411-1990 and 0523-1990.

The formula that best explains the test data of the failure envelope is written as:

$$q_{peak} = 1.51p' + C \qquad 5.5$$

The values of the cohesion parameter C from this simulation are shown in Table 5.6 below. The simulation of the failure envelope is shown in Fig 5.4.

Table 5.6 Measured cohesion from simulation of test data

Cement content (%)	Cohesion parameter *C* (kPa)
1	6
3	13
5	54
7	79
10	123

Referring to the first Ariake clay tests, 6% cemented Ariake clay shows no cohesion based on the simulation. At the same time, the remaining tests of 9% and 12% cemented specimens, appear to display high variability, and each set of data seems skip over to the neighbouring failure envelope. But, the tendency for the failure envelope to enlarge with higher cement contents is undebatable. The second group of Ariake clay test data, which concerns low cement content (0% to 10%) Ariake clay, exhibits different behaviour. The three lowest cement contents specimens produced data located within a very narrow failure envelope. It is hard distinguish between different cement content test groups. This implies that Ariake clay is not "sensitive" to the lower cement treatments from 0% to 3%. Once the cement content reaches 5%, however, cohesion changes noticeably.

According to the two series of tests on Ariake clay, clayey soil contains much smaller particle elements than sandy soil. The former does not fit the failure envelope equation. The sandy soil tends to follow it better. The increase of the failure envelope extension for cementation is not distinctive. The testing data seems to straddle more than one failure envelope.

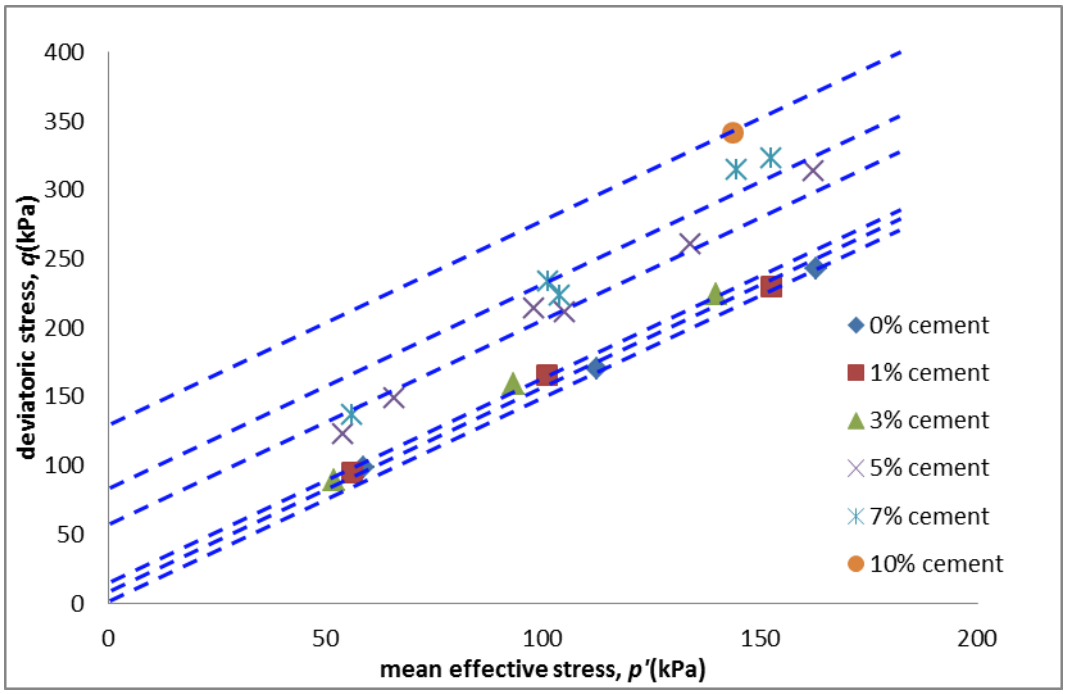

Fig 5.4 Variation in peak strength with cement content (Kasama et al., 2000)

5.1.5 Singapore marine clay

The soil base was sampled from 4-5m below the seabed offshore from Pulau Tekong. The soil belongs to the Singapore upper marine clay of Kallang formation.

Table 5.7 Average physical properties of the base soil

Properties	Values
Liquid limit, LL (%)	88
Plastic limit, PL (%)	38
Plasticity index, PI (%)	50
In-situ moisture content, m	72%
Liquidity index, I_L	0.68
Initial void ratio, e_o	1.93

Specific gravity, G_s	2.7
Grain size distribution:	
Sand (%)	8
Silt (%)	72
Clay (%)	20
Total unit weight, γ_b (kN/m^3)	15
Dry unit weight, γ_d (kN/m^3)	8.72
K_o	0.62

The formula that captures the test data of the failure envelope is written as:

$$q_{peak} = 2.977p' + C \qquad 5.6$$

The tests show high cementation clay behavior from 10% to 50%. It appears that the distinguishing character of the tests on different cement contents is that the results fall within the same failure envelope and show no cohesion. In addition, the value of M^* is as high as 2.977. This almost reaches the maximum value of 3. It is possible that cementation increases the soil friction angle and aspect ratio rather than cohesion. This also demonstrates that sensitivity to cementation of clayey soil is not as high as sandy soil. Considering the former two sets of Ariake clay test data, a rough conclusion can be made that the cohesion of clayey soil tends to remain stable when the cement content surpasses 10%. The simulation of the failure envelope is shown in Fig 5.5.

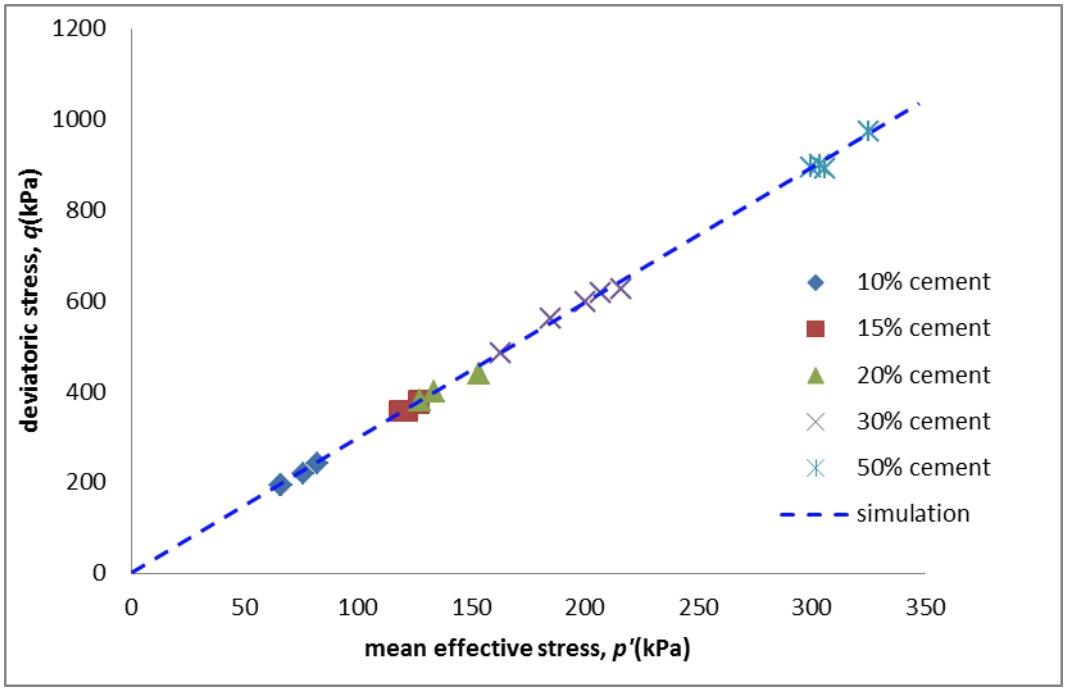

Fig 5.5 Variation in peak strength with cement content (Huawen, 2009)

5.1.6 Analysis

The results of the five groups of data are listed in Table 5.8. The relationship of cement content versus cohesion parameter *C* is shown in Fig 5.6.

Table 5.8 Values of parameters *C* and M^* obtained from test data

Soil	Aspect ratio, M^*	Cement content, A_w	Cohesion, *C* (kPa)
Weathered sandstone	1.599	1%	125
		3%	333
		5%	528
Gravely sand	1.52	1.5%	237
		3%	301

		4.5%	519
Ariake clay from Horpibulsuk et al	2.03	6%	0
		9%	75
		12%	143
Ariake clay from Kasama et al.	1.51	1%	6
		3%	13
		5%	54
		7%	79
		10%	123
Singapore marine clay	2.977		

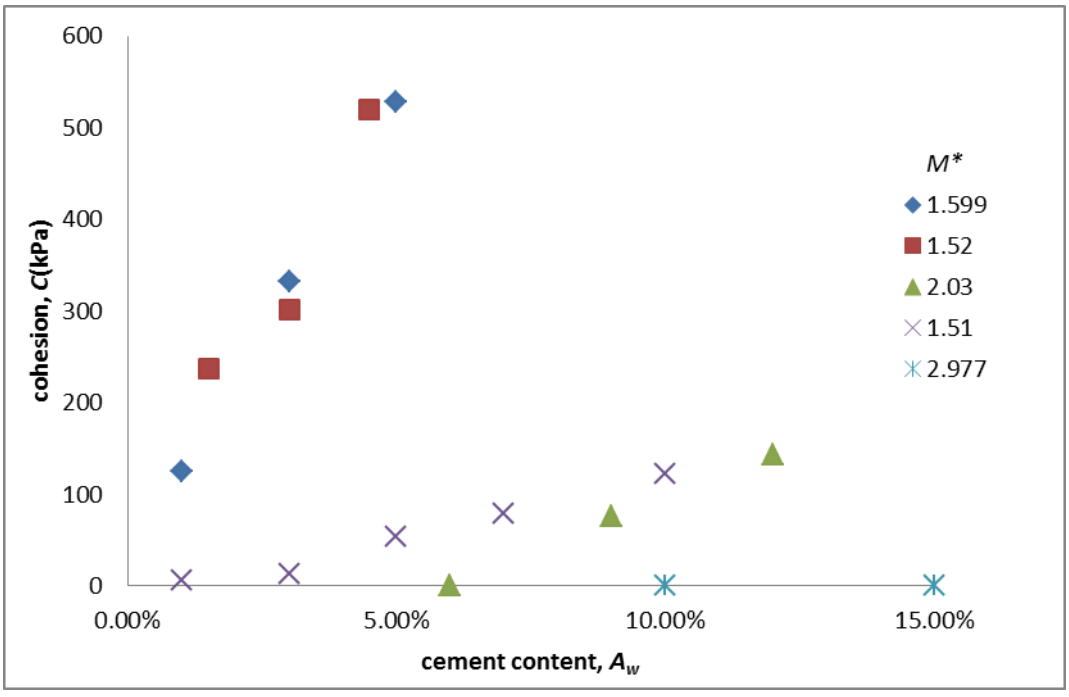

Fig 5.6 Cohesion and cement content relationship

According to the cement content and the cohesion relationship shown in Fig 5.6, sandy soil is more sensitive to cement treatment than clay. Thus sand can raise the deviatoric strength more than clay with same cement content. However, in this analysis, for simplification, the cementation is considered as a constant and irrelevant to different stress states before the peak deviatoric stress is reached. The process of decementaion is hard to define and this leads to the huge variation of the test data.

5.2 Swelling index κ versus cement content A_w

Although the swelling index is originally taken as structure independent parameter, the research in this work shows clearly cementation has influence on swelling index. The results are presented in Figs 5.14 to 5.17. A detailed study on the influence is made. Two important parameters for soil deformation are compression index λ and swelling index κ. The influence of cementation on λ has been already described in the model. The influence of cementation on κ is studied. Because cement content is a simple and direct parameter to represent the weight of cement in soil and the proposed equation describes their relationship. The value of swelling index is obtained from experimental data to assuming the initial elastic deformation is linearly in the e and $\ln p'$ space. There is some degree of uncertainty in deciding the ending point of the elastic deformation.

The value of swelling index is captured from elastic compression line as illustrated in Fig 4.1.

5.2.1 Bangkok clay

Bangkok clay was sampled at the campus of the Asian Institute of technology (ATI), Klong Luang, Pathumthani, Thailand. Specimens were combined with a cement slurry

with a water-cement ratio (W/C) of 0.6. Lorenzo and Bergado (2004) conducted both unconfined compression tests and oedometer tests on specimens. The base soil properties are listed in Table 5.9.

Table 5.9 Physical properties of the base soil

Properties	Values
Liquid limit, LL (%)	103
Plastic limit, PL (%)	43
Plasticity index, PI (%)	60
Water content, w (%)	76-84
Liquidity index, LI	0.62
Grain size distribution	
Clay (%)	69
Silt (%)	28
Sand (%)	3
Total unit weight, γ_t (kN/m^3)	14.3
Dry unit weight, γ_d (kN/m^3)	7.73
Initial void ratio, e	2.31
Color	Dark gray
Activity	0.87
Sensitivity	7.4

The measured swelling indices for each test are listed in Table 5.10 below.

Table 5.10 Measured κ from simulation of tests data

Cement contents	Swelling index, κ
0%	0.079
5%	0.051
10%	0.025
15%	0.029

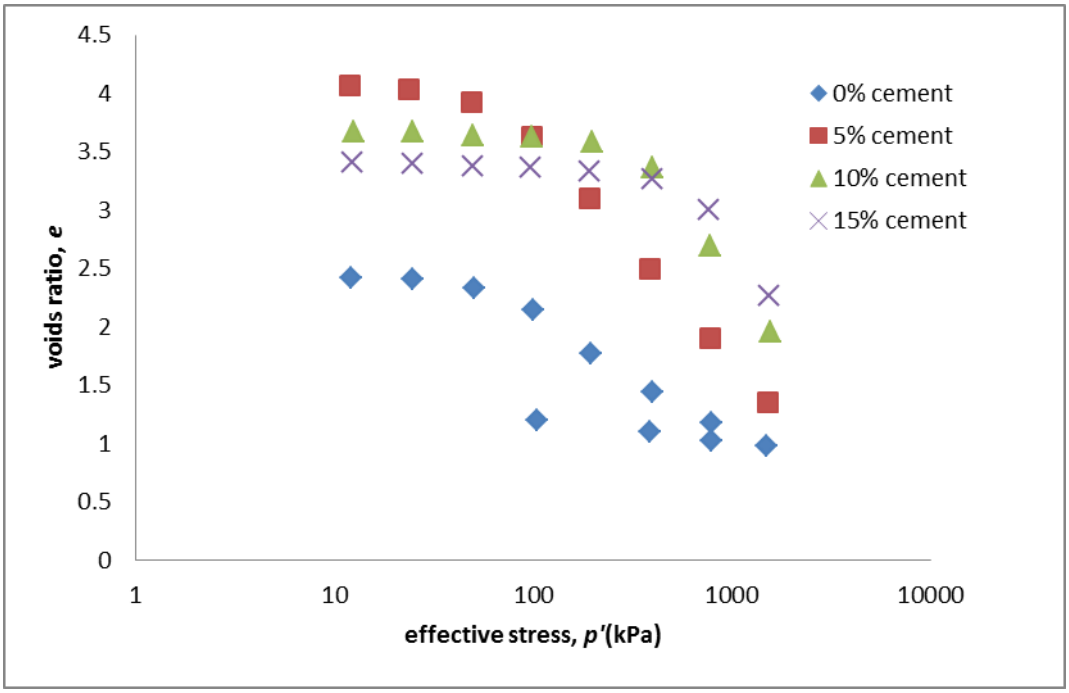

Fig 5.7 One-dimensional compression behavior of Bangkok clay (Lorenzo and Bergado, 2004)

5.2.2 Singapore marine clay

The compression data is a part of the tests on Singapore marine clay from Huawen (2009) mentioned previously in the failure envelope analysis. The measured swelling index for each test is listed in Table 5.11 below.

Table 5.11 Measured κ from simulation of tests data

Cement contents	Swelling index, κ
10%	0.012
15%	0.01
20%	0.013
30%	0.011
50%	0.01

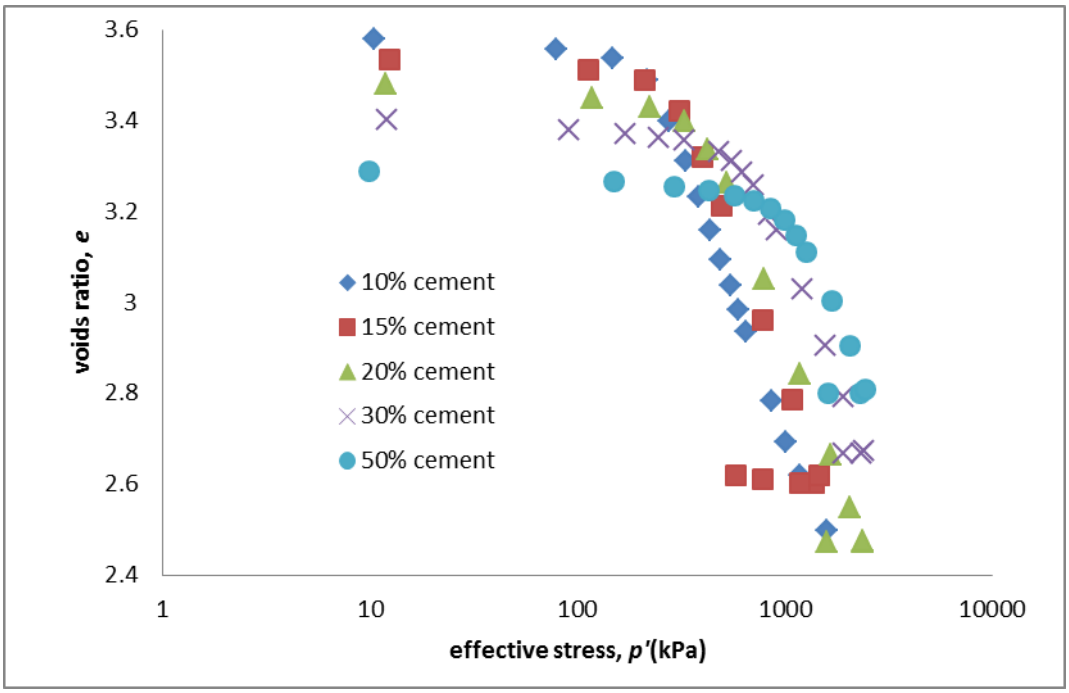

Fig 5.8 Isotropic compression behavior of Singapore marine clay with various cement content curing 7 days (Huawen, 2009)

5.2.3 Organic soil

Soil at the south end of the "Celery Bog" in West Lafayette has been sampled and mixed with cement. This soil sample is highly organic with loss on ignition (LOI) of 40% to 60% and around 2% of fibre content. Therefore, sample properties varied from one to another. Its plastic limit (PL) is 114%-253% and liquid limit (LL) is from 228% to 406%. The measured swelling index for each test is listed in Table 5.12 below.

Table 5.12 Measured κ from simulation of test data

Cement contents	Swelling index, κ
0%	0.09
8%	0.028
19%	0.017
51%	0.009
103%	0.024

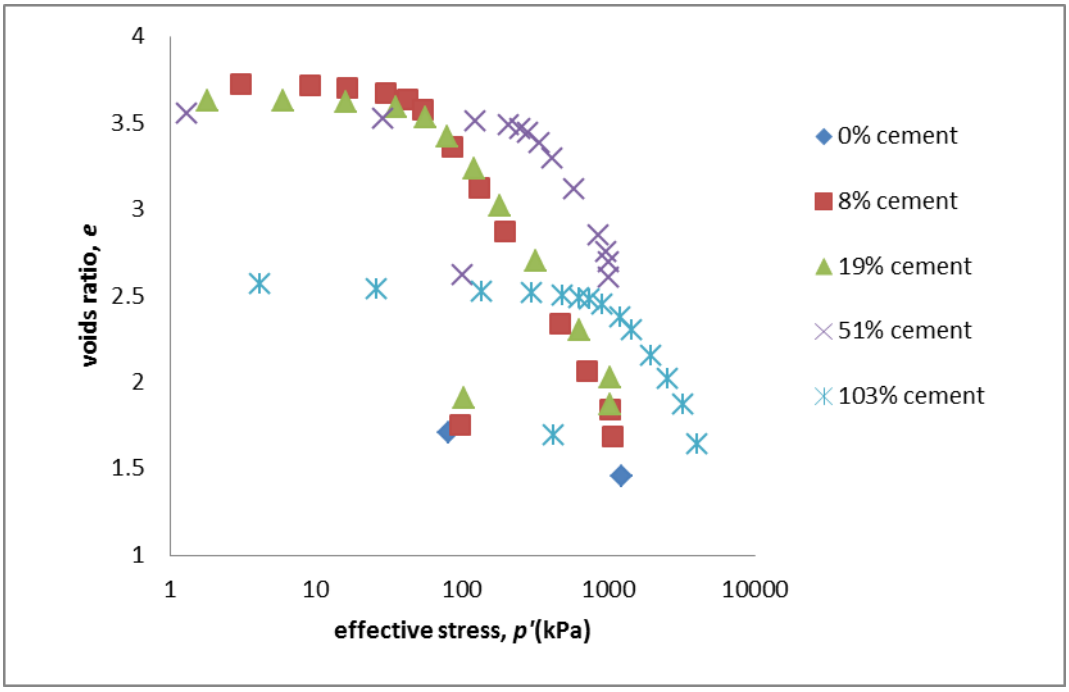

Fig 5.9 One-dimensional compression behavior of organic soil (Bobet et al., 2011)

5.2.4 Dredged sediment

Specimens used in these tests are the sediment from the harbour of Ouistreham (Normandy, France) mixed with dry cement (CEM II/B-M [LL-S] 32.5). A wide range of cement contents: 2%, 5%, 8% and 10% and two different curing times for a full series of cemented specimens were tested. The base soil properties are listed in Table 5.13.

Table 5.13 Average physical properties of the base soil

Properties	Value
Relative water content	120
Liquid limit	104
Plastic limit	38
Plastic index	66
Organic content	7
Grain-size distribution	
Clay (<2 um) content	25
Silt (2-63 um) content	50
Sand (63um-2mm) content	25

The measured swelling index for each tests is listed in Table 5.14 below.

Table 5.14 Measured κ from simulation of test data

Cement contents	Swelling index, κ
7days	
2%	0.152
5%	0.028
8%	0.023
10%	0.005
28days	
2%	0.205
5%	0.014
8%	0.007
10%	0.001

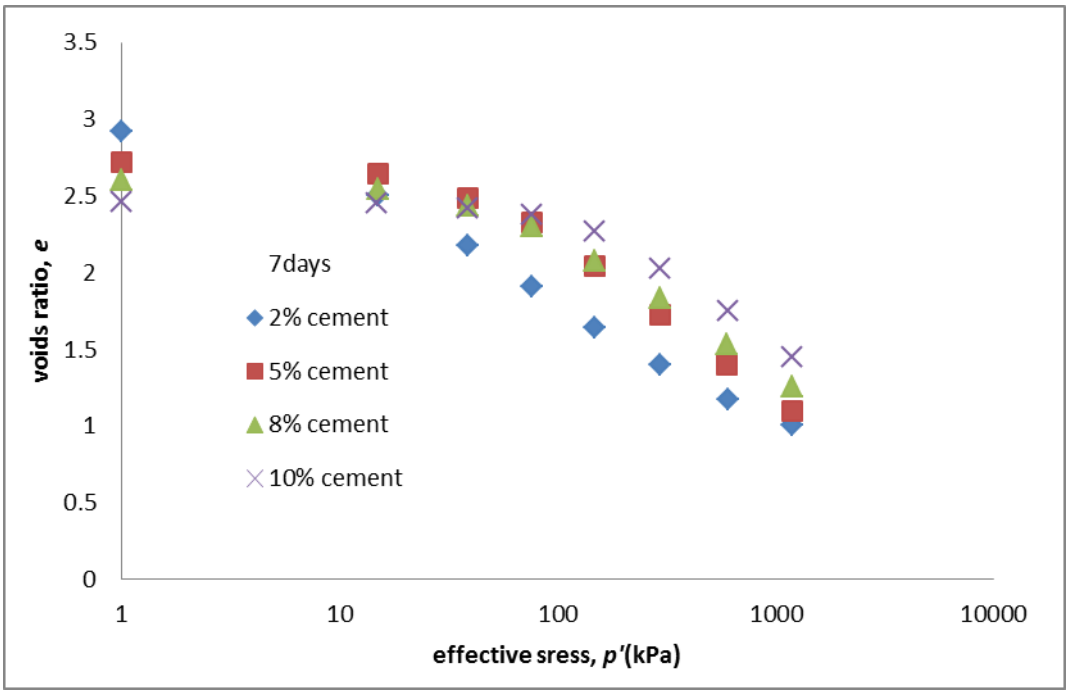

Fig 5.10 One-dimensional compression behavior of dredged sediment with cement content at curing time 7 days (Rekik and Boutouil, 2009)

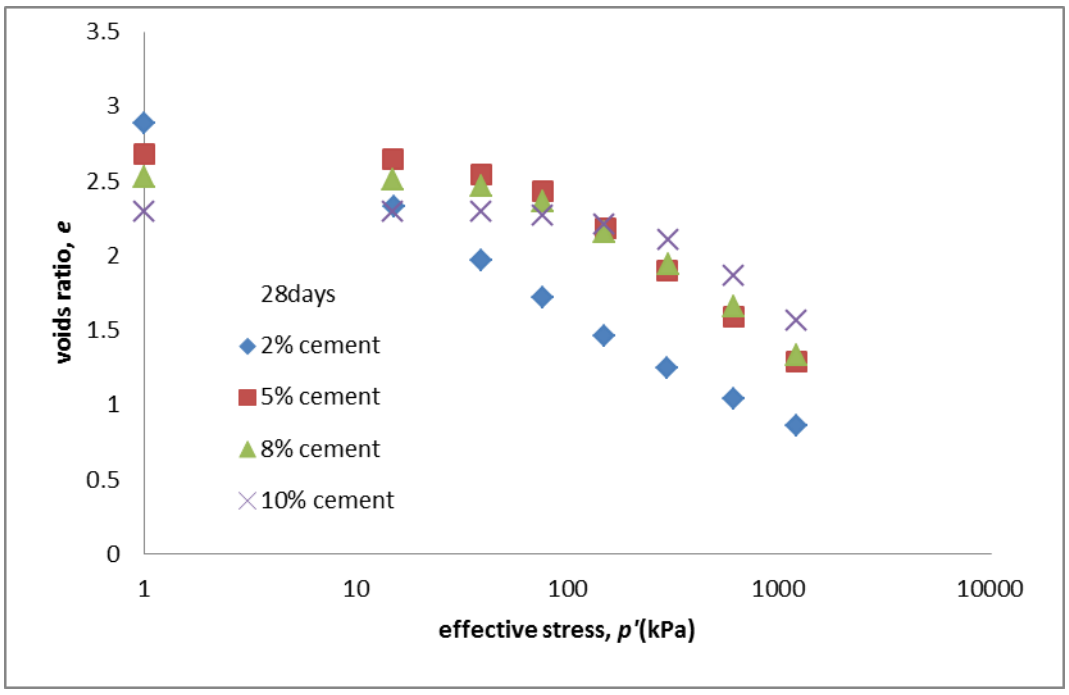

Fig 5.11 One-dimensional compression behavior of dredged sediment at curing time 28 days (Rekik and Boutouil, 2009)

5.2.5 Ariake clay from Horpibulsuk et al.

The compression data forms part of the tests on Ariake clay from Horpibulsuk et al, (2004) mentioned previously in the failure envelope analysis. The measured swelling index for each tests is listed in Table 5.15 below.

Table 5.15 Measured κ from simulation of tests data

Cement contents	Swelling index, κ
6%	0.076
9%	0.028
12%	0.011
18%	0.006

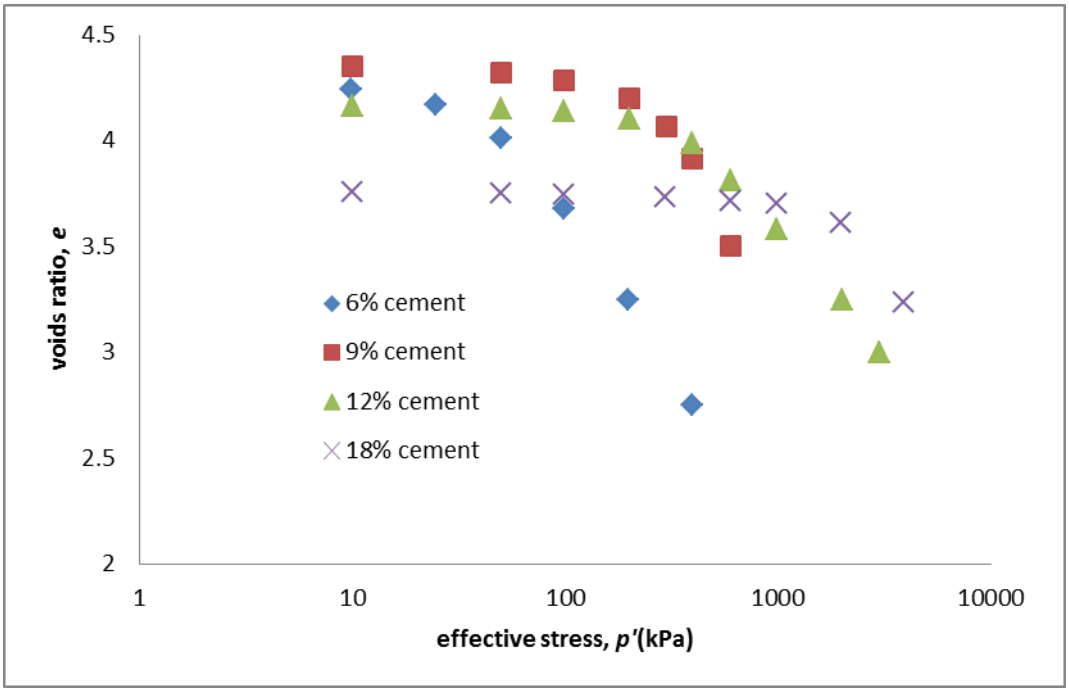

Fig 5.12 One-dimensional compression behavior of Ariake clay with cement content (Horpibulsuk et al., 2004)

5.2.6 Ariake clay from Kasama et al.

The compression data is part of the testing on Ariake clay from Kasama et al, (2000) mentioned previously in the failure envelope analysis. Kasama and Zen (2000) have analysed the influence of cementation on Ariake clay on the value of the swelling index. The treated Ariake clay base has a specific gravity of 2.609 and a mean grain size D_{50} (mm) of 0.0034. It has 96% of fine grain. The measured swelling index for each test is listed in Table 5.16 below.

Table 5.16 Measured κ from simulation of tests data

Cement contents	Swelling index, κ
0%	0.056
1%	0.036
3%	0.036
5%	0.036

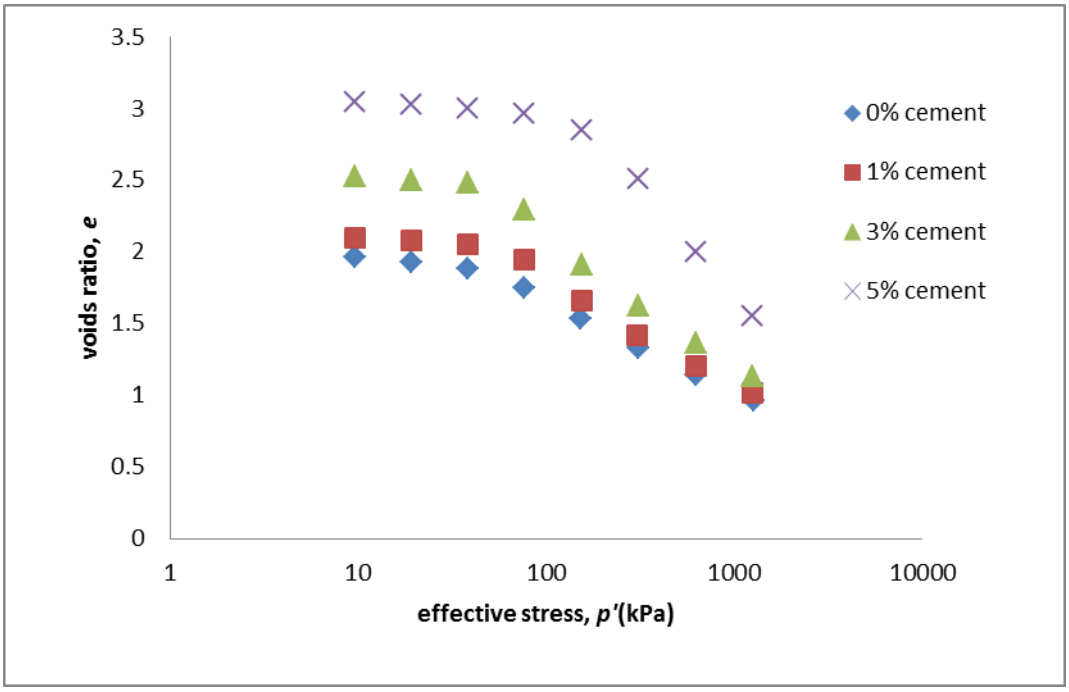

Fig 5.13 One-dimensional compression behavior of Ariake clay with cement content (Kasama et al., 2000)

Table 5.17 Measured κ from simulation of tests data

Cement contents	Swelling index, κ
5%	0.048
7%	0.039
10%	0.035

5.2.7 Simulation of swelling index κ versus cement content A_w

All the data are shown in Table 5.18. The plotted dots of those data in Fig 5.14 illustrate the relationship between cement content and swelling index. The highest cement content data from Bobet et al. behaves abnormal (κ=0.02372644). Its swelling index value

shows slight increase with cement content increased and could not be simulated by this equation.

Table 5.18 Measured κ from simulation of all the eight tests

	Cement contents	Swelling index, κ
Bangkok clay	0%	0.079
	5%	0.051
	10%	0.025
	15%	0.029
Singapore marine clay	10%	0.012
	15%	0.01
	20%	0.013
	30%	0.011
	50%	0.010
Organic soil	0%	0.09
	8%	0.028
	19%	0.017
	51%	0.009
	103%	0.024
Dredged sediment 7days	2%	0.152
	5%	0.028
	8%	0.023

	10%	0.005
Dredged sediment 28days	2%	0.205
	5%	0.014
	8%	0.007
	10%	0.001
Ariake clay from Horpibulsuk et al.	6%	0.14
	9%	0.084
	12%	0.048
	18%	0.028
Ariake clay 1. from Kasama et al.	0%	0.056
	1%	0.036
	3%	0.036
	5%	0.036
Ariake clay 2. from Kasama et al.	5%	0.048
	7%	0.039
	10%	0.035

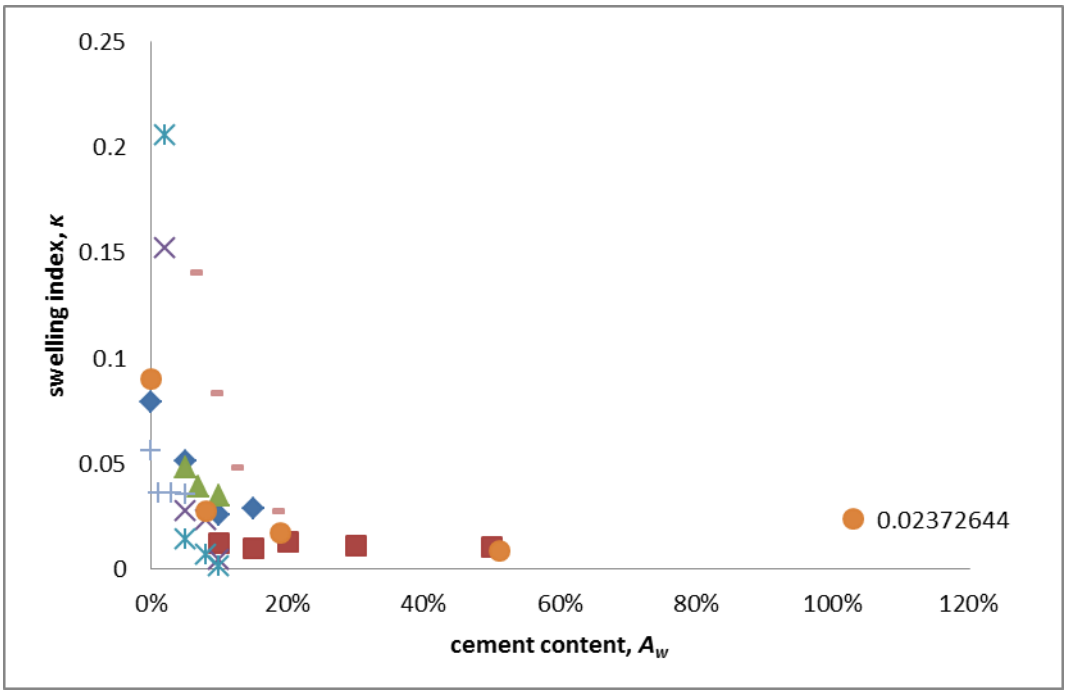

Fig 5.14 Cement content and swelling index relationship for different soils

As is seen from Fig 5.14, the value of the swelling index deceases with that of cement content. The rate of the decrement decreases with the value of cement content. When the cement content is larger than 10%, the effects of cement content on swelling index is not very significant. Based on this, the equation is formed.

$$\kappa = \frac{\kappa_0}{e^{A\sqrt{A_w}}} \qquad 5.7$$

Where:

κ_0 is the initial swelling index when soil is untreated and

A_w is cement content.

A is a parameter that reflects the rate of increase of cementation as it reduces the swelling index. The greater parameter A, the faster the swelling index will decrease in an inverse relationship with cement contents. The parameters used to simulate the change in swelling index with varied cement content are listed in Table 5.19 and the

simulations are plotted in Fig 5.15, Fig 5.16 and Fig 5.17. Although the test data is varied from one soil to another, the experimental equation captures all of the behaviour appropriately.

Table 5.19 Value of parameters for simulation

	A	κ_0
Bangkok clay	2.6	0.079
Singapore marine clay	1	0.018
organic soil	4	0.09
Dredged sediment 7days	16	1.1
Dredged sediment 28days	19	1.2
Ariake clay from Horpibulsuk et al	10	1.5
Ariake clay 1. from Kasama et al.	2.6	0.056
Ariake clay 2. from Kasama et al.	3.5	0.1

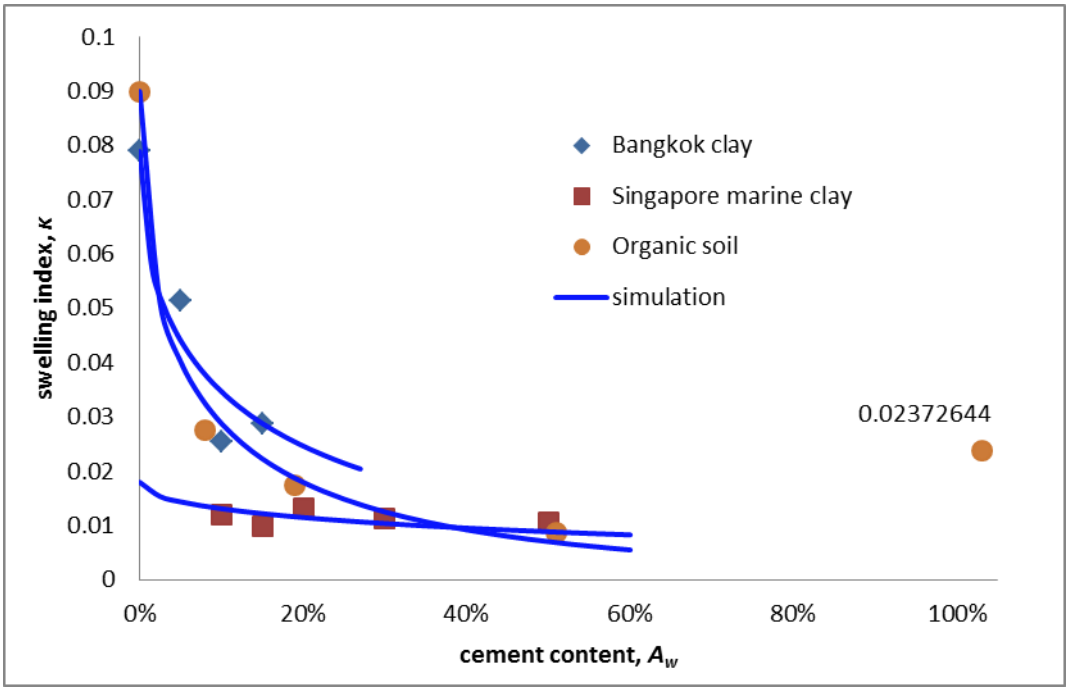

Fig 5.15 Cement content and swelling index simulation

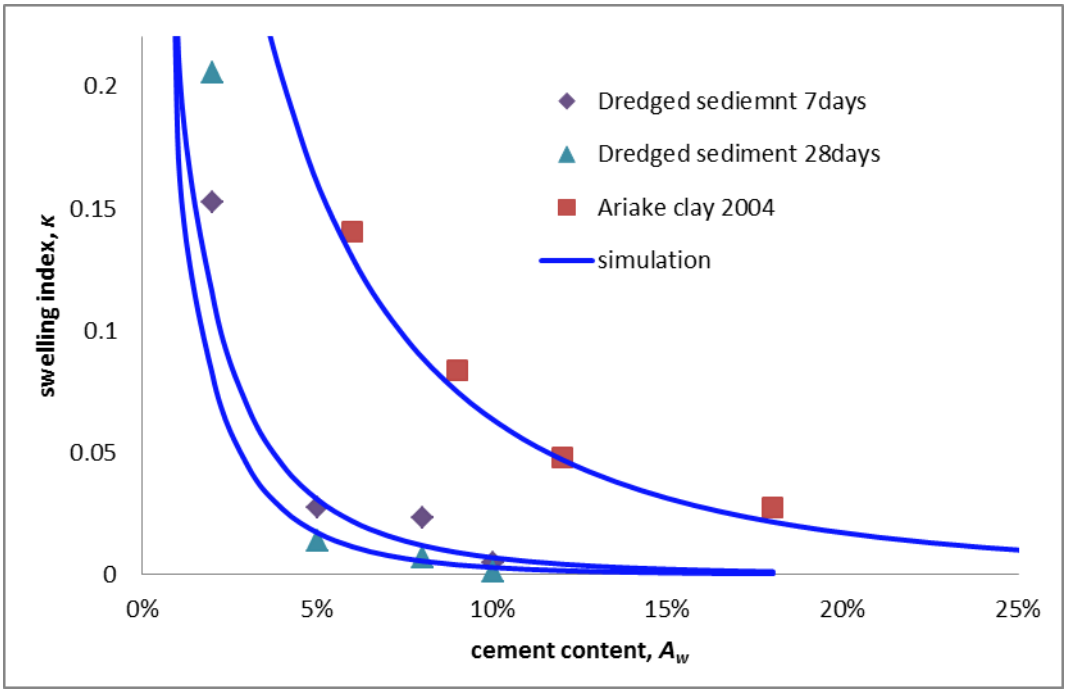

Fig 5.16 Cement content and swelling index simulation

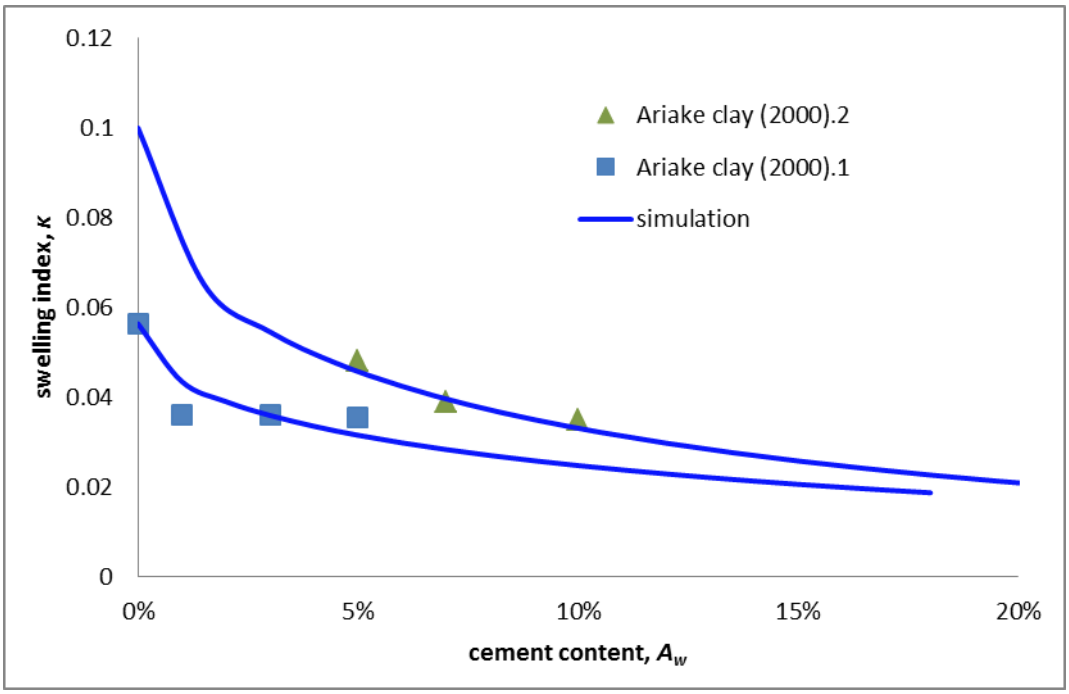

Fig 5.17 Cement content and swelling index simulation

5.3 Summary

Cementation in soil leads changes in soil mechanical characters. In terms of SCC model, it also changes cohesion parameter and swelling index. The increase of cohesion directly increases soil strength. As a result, from the strength of soil at peak stress state it is possible to calculate cohesion value from varied cement content tests. Through the strength, it is found that cohesion increases with cement content in a genarally constant rate. The rate is varied from one soil to another and sand tends to increase in larger rate with cement content than clay.

Although swelling index is proposed as structure independent parameter in SCC, it is found in tests data that cement content is able to change swelling index and this influence is studied in detail in this work. The swelling index values are captured from elastic behaviour of structured soil in compression tests. Swelling index decreases with

cement content significantly in low cement content range but slightly in high cement content range. An experimental equation is proposed to capture this relationship.

Chapter 6 The behaviour of loess

Loess is widely distributed in China, USA and many other countries. It has been proven to be responsible for cracks in constructions (Edward et al., 2009). Natural loess has a structured soil character, but this structure will be removed when the natural loess is disturbed, loaded or wetted. Cementation, water and friction are the main factors that affect the intrinsic structure of natural loess and the first two of these are unstable variables which can result in the collapse of natural loess. Very few laboratory and theoretical studies on loess behaviour have achieved acceptable results due to its special cementation and structure (Shao et al., 2006). In this paper, the possibility of using SCC to simulate loess behavior will be investigated and the special parameters of loess will be defined.

6.1 Mechanical properties of natural loess

Loess has different structural features compared to cemented clay. Cohesion contributes mainly to loess strength rather than soil structure (Hu et al., 2004). Cementation in loess can be dissolved in water which leads to diminishing cohesion. Therefore, saturated loess represents the situation whereby only soil structure contributes to loess strength as cohesion is totally removed. Shao and Deng (2008) concluded from experimental data that cementation in loess changes its strength as does crushing soil structure. Cohesion reaches a peak when shear strain is at a very low level (1%), followed by a cementation decrease as shear strain grows. When soil structure is completely crushed, cohesion tends to be zero. As confining stress increases, loess in the same water ratio retains a larger shear strength, meanwhile, stress-strain behaviour tends to shift from a softening

pattern to hardening one due to increases in destructuring and a rise in preconsolidation stress (Shao et al., 2006).

Fig 6.1 illustrates three compression behaviours: reconstructed loess, saturated natural loess and natural loess, with the same base soil for creating soil structure comparison. Both saturated natural loess and natural loess show higher voids ratios than reconstituted loess. This implies both of these two situations could be simulated by SCC. Saturated natural soil (no cohesion) shows the degree that loess structure contributes to the sustainability of the voids ratio. Natural loess indicates the contribution of both structure and cohesion to sustainability of the voids ratio. It reflects the fact that cohesion can support a greter voids ratio than structure and therefore the difference between the initial yield mean effective stress.

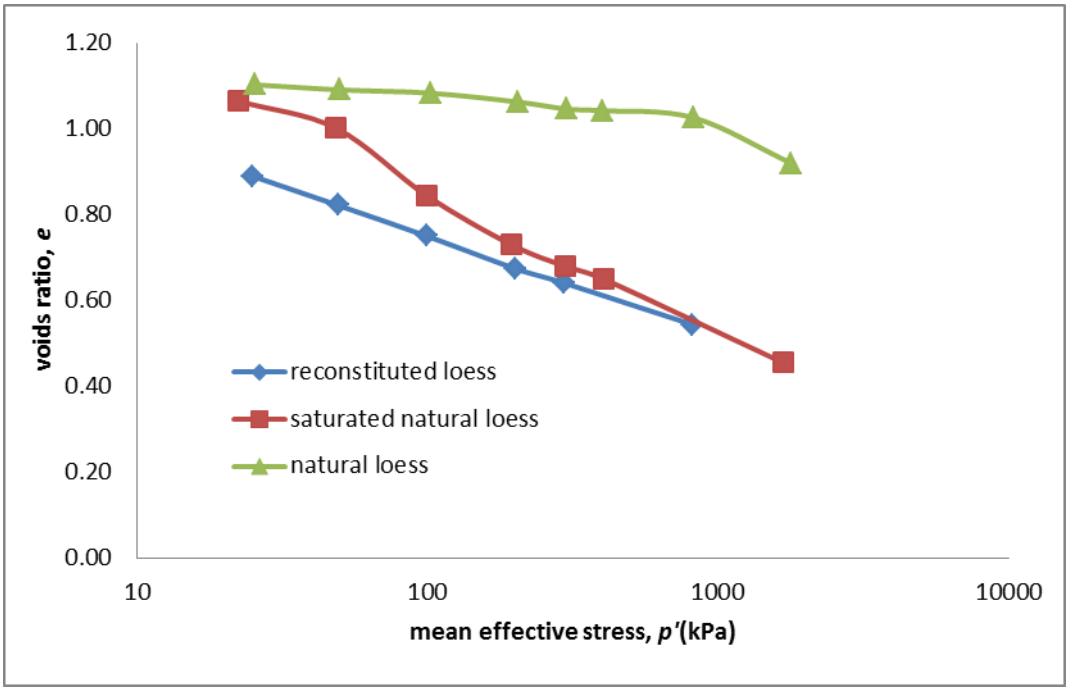

Fig 6.1 Consolidation curves of natural loess (10.8%) (Shao et al., 2006)

6.2 Ma Lan loess behavior simulation

Based on the previous discussion, SCC was extended to cemented soil and used to simulate Ma Lan Loess (Li and Yao, 2010). All selected Ma Lan loess specimens are from the same soil layer in Xi'an China, which is below the water table. The specific gravity of specimen soil is 2.71 with a water moisture content of 25.3%-32.9% and natural voids ratio of 0.725%-0.98%. Both drained and undrained experiments were performed on saturated specimens. Compression lines and stress paths therefore are plotted. Some parameters can be identified through the compression model and the parameters for simulations are listed in Table 6.1.

Table 6.1 Values of model parameters of Ma Lan loess

λ^*	κ^*	M^*	$e_{IC}{}^*$	ν^*	b	C (kPa)	ω	γ
0.122	0.03	0.98	1.403	0.3	1	30	1	1

Because of the yield surface distortion, virgin mean effective yield stress must be magnified to match the pear shaped stress path. The following equation is used to identify $p_{y,i}$ for SCC:

$$p_{y,i} = \frac{1.85 q_{peak}}{M^*} \qquad 6.1$$

q_{peak} is the peak value on the stress path and the unit of $p_{y,i}$ in this equation is MPa.

The simulation of effective stress paths for Ma Lan loess in undrained conventional triaxial tests is shown in Fig 6.2 and the predictions of deviatoric stress strain relationships are given by Fig 6.3. The compression behavior test data and simulation are indicated in Fig 6.4. Generally, the values defined in the compression behavior simulation could apply to SCC for undrained soil behavior simulations.

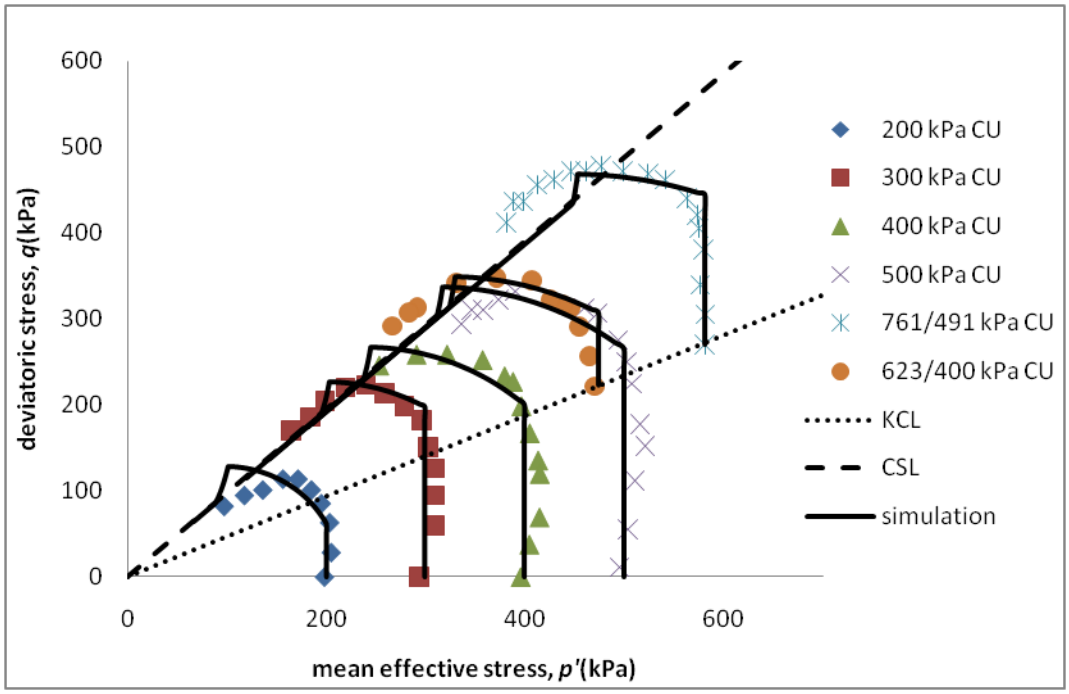

Fig 6.2 Effective stress paths for Ma Lan loess in undrained conventional triaxial tests (Li and Yao, 2010)

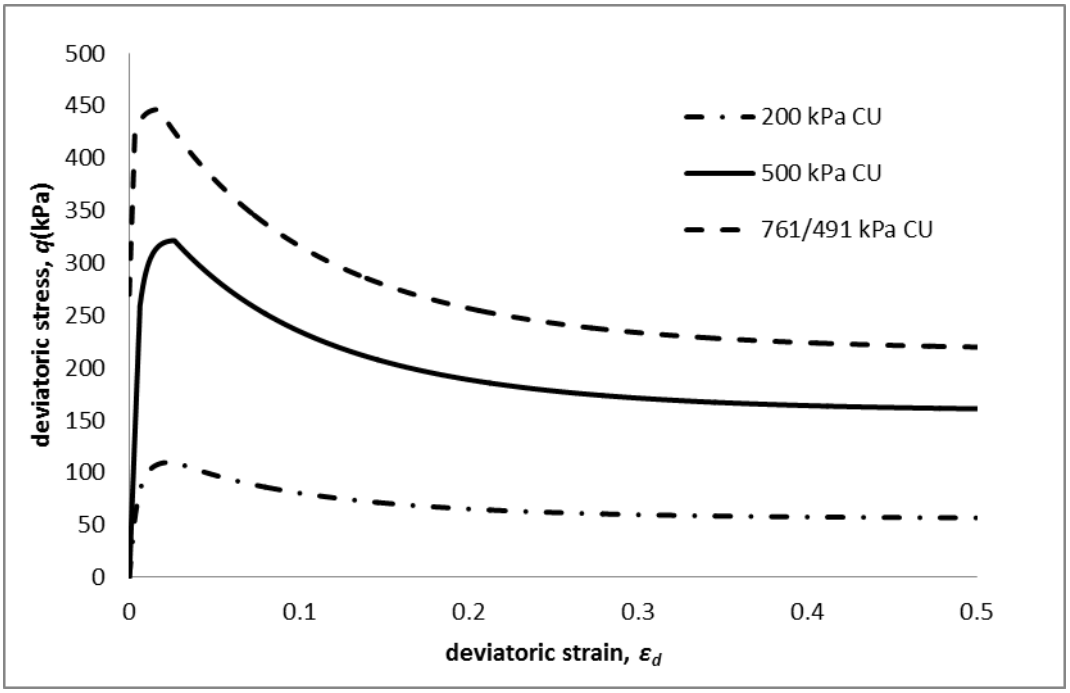

Fig 6.3 Ma Lan loess deviatoric stress and strain relationship prediction

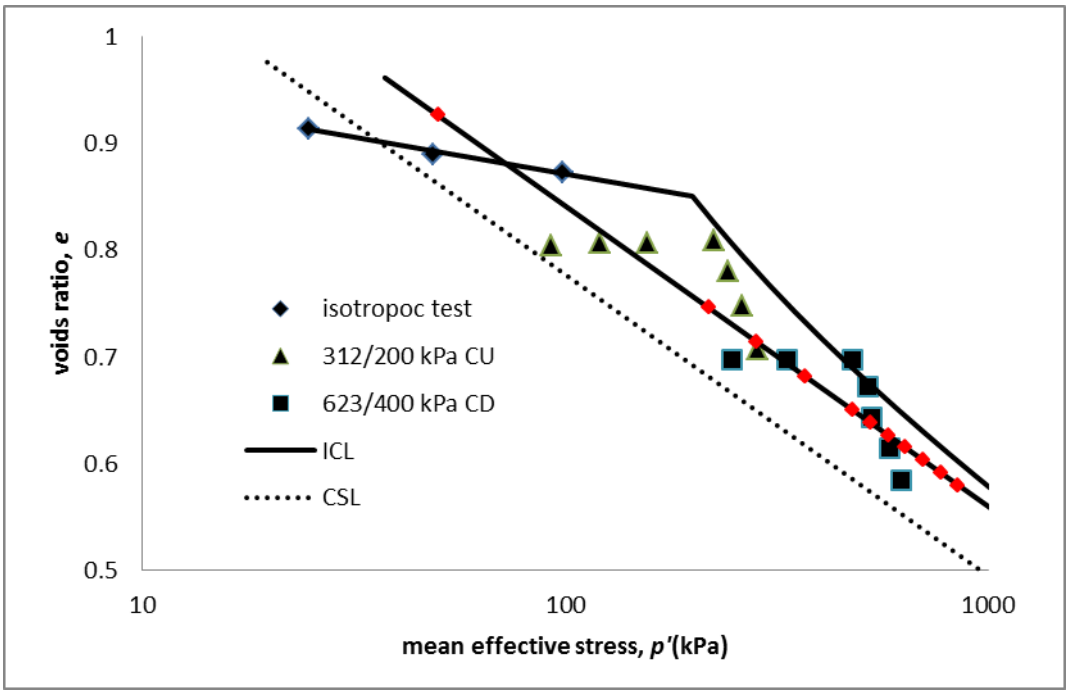

Fig 6.4 Compression line of Ma Lan loess (Li and Yao, 2010)

6.3 Analysis of loess behaviour

These are some of characteristics found in the test data.

1. The experimental data in *p'*-*q* space illustrates the critical state line and stress path. Studies found that the yield surface is 'pear shaped' but elliptical, being round in the right tip side but sharp at the tip origin (Li and Yao, 2010).

2. The virgin yielding stress from compression behaviour is not suitable for simulating the stress path. The method used to simulate the loess stress path is the enlargement of the real size of the virgin yielding surface and the introduction of some elastic behaviour to incorporate the pear shape of the loess yield surface. According to the real virgin yield stress, the specimens in stress path tests are either on the virgin yield surface or about to reach the virgin yield surface at the initial stress state.

3. Unlike traditional softening, there are two factors which induce softening for loess. (1) Crushing of soil structure: stress paths must maintain the same stress ratio at M^* and move downward along the failure envelope. (2) Decementation: a decrease and ultimate removal of cementation allows the stress path to approach and follow the critical state line downwards. The softening of loess is largely influenced by decementation. Therefore, cement breaks down before the soil reaches the structure cracking stage. This goes against the assumption that cementation only starts to break down at the stage of soil cracking. The generation of substructure and breakdown of cementation could be responsible for yield surface distortion.

4. Since all the specimens are taken from the same soil layer, they should be regarded as the same samples. This SCC simulation assumes the same C value of 300kPa. However, the stress path of those samples in different initial stress states shows different cohesion. In test data, cohesion in low confining stress tests of 200kPa, 300kPa and 400kPa is nearly 0, but it emerges and grows once preconsolidations are 623/400 and 761/491 (30kPa and 70kPa), respectively. These two preconsolidation stresses are simulated in the stress state in the field. Azman et al. (1994) concluded that cemented clay failure patterns are "friction-dominated" at very high confining stress, "cementation-plus-friction" at medium confining stress and "cementation-dominated" at low confining stresses. When confining stress is small, cementation mostly sustains the stress, so the yielding of soil mainly represents the process of decementation. Thus, cementation is likely to fully or mainly break down before the stress path meets CSL. This might explain one of the causes of loess yield surface distortion and the reason it shows no cohesion. However, this conclusion is not obvious for loess. There is the possibility that the process of loading is able to affect decementation. Only two stress paths overtake CSL and have cohesion. Loading from large deviatoric stress with high

confining stress cuts down the length of the stress path. Also, high confining stress causes “friction-dominated” failure. As a result, cementation in loess contributes little to soil strength when it is under high confining stress. In addition, despite confining stress of 200kPa, tests with very little “cementation-dominated” failure show no cohesion. Only both preconsolidation and confining stress conditions can show cohesion in SCC.

6.4 Summary

The glutinous ingredient in loess produces cementation force in the soil. According to the experiment data and simulation, the behaviour of loess seems stand between cement structure and nature soil structure features. An attempt is made to simulate the behaviouyr of loess by SCC. An equation is proposed especially for modifying virgin yield stress to catch stress path. The deviatoric stress strain relationship is predicted based on the parameters defined from compression tests and stress path.

Chapter 7 The behaviour of cemented soils

In this section, three cemented clays and one cemented sand were simulated via SCC extended for cemented soils. The complexity of cement treated soil challenges the SCC framework both parametrically and in terms of computation. It is also noted that Cam Clay frameworks are originally proposed for simulating the behaviour of clay while sand was not discussed.

7.1 Cemented clays

7.1.1 Ariake clay

Horpibulsuk et al. (2004) performed triaxial tests on Ariake clay to understand undrained shear behaviour of cemented admixed clay. Ariake clay was sampled from a depth of 2 m in Saga, Japan. This grey silty clay was treated with cement to attain proportions of 6%, 9% and 12%. The base soil properties are listed in Table 5.4.

Generally speaking, the Ariake clay with the lowest cement content of 6% demonstrates a less irregular stress path and fits the elliptical stress path better than the high cement content samples. Furthermore, the simulation of soil structure breakdown matches the test data reasonably well. In the 9% cement treated soil simulations, very few experimental stress path results follow the elliptical yield surface. The size of yield surface for this specimen varied with confining stress, which changes the stress path in a different way. Firstly, the entire stress path for most in this group shows an increase in the height width ratio. In this respect, the yield surfaces could raise the height width ratio by increasing the values of parameter M^*. Secondly, with the large confining stress of 600kPa, distortion emerges. It leads to yield surface turning with the original side of the yield surface acting as a pivot. This phenomenon only occurs at high levels of

confining stress and begins to emerge at the medium confining stress of 400kPa. Simulation for 12% cemented Ariake clay is more difficult. The high cement content combined with the large scale confining stress complicates soil behaviour. The height width ratio of the yield surface in the 600kPa and 1000kPa tests reaches a value that the elliptical yield surface is unable to predict. The simulated deviatoric strength could not measure up to the real data. All these three groups of experimental data and their associated simulations are indicated in Fig 7.1, Fig 7.2 and Fig 7.3, respectively, and parameters of SCC for those experiments and simulations are given in Table 7.1 and Table 7.2. Some points which can be concluded are as follows:

1) Generally, cement treated clay behavior can be simulated by SCC extended to cemented soil. However, the low cement content soil with low confining stress seems to follow Cam Clay model theory better than large cement content soil specimens or large confining stress test groups. Because its stress path is similar and elliptical, the decementation process fits the model.

2) As the data shows, 200kPa tests on 9% specimens and 400kPa tests on 12% specimens represent sub-yielding when at the elastic behaviour stress state. Compared with simulation, it was not merely elastic deformation that was shown in both of these two groups at an early stress state. The stress path should move straight up in the yield surface as the corresponding simulation does. Therefore, the model idealization in this aspect does not fit this test.

3) The simulation on 9% specimens gives the value of 2 for M^* which is larger than that for the remaining groups which have a value of 1.85. This could be responsible for cementation increasing the friction angle of soil. In SCC, parameter M^* and cohesion C have similar effects on yield surface in that they increase deviatoric strength although the scale of their influence is different. Theoretically, cohesion increases the effective friction angle by introducing an interlocking force. In this theory, cohesion can transform soil by causing an increase in the soil original friction angle. Based on both SCC frame work and soil mechanical theory, the cohesion parameter and the value of M^* are correlated. This explains why the value of M^* adopted in simulation varies and does not correspond to the value found in Fig 5.3.

4) Model parameters, identified through compression behaviour tests in Fig 5.12, are suitable for SCC simulation. The values of Δe_i, c, κ^* and $p'_{y,i}$ are varied from one cement content group to another according to the compression model. For swelling index κ^*, the value adopted in SCC simulation is calculated from Equation 5.7.

The parameters are listed in Table 7.1 and Table 7.2.

Table 7.1 The common parameters for Ariake cemented clay

λ^*	${e_{IC}}^*$	ν^*	b	ω	γ
0.44	4.37	0.3	1	1	1

Table 7.2 The parameters for different cemented Ariake clay

	6%	9%	12%
κ^*	0.13	0.08	0.04
Δe_i	1.72	2.25	2.44
M^*	1.85	2	1.85
$p'_{y,i}$ (kPa)	78	210	490
C (kPa)	25	80	245
c	1.6	2	2

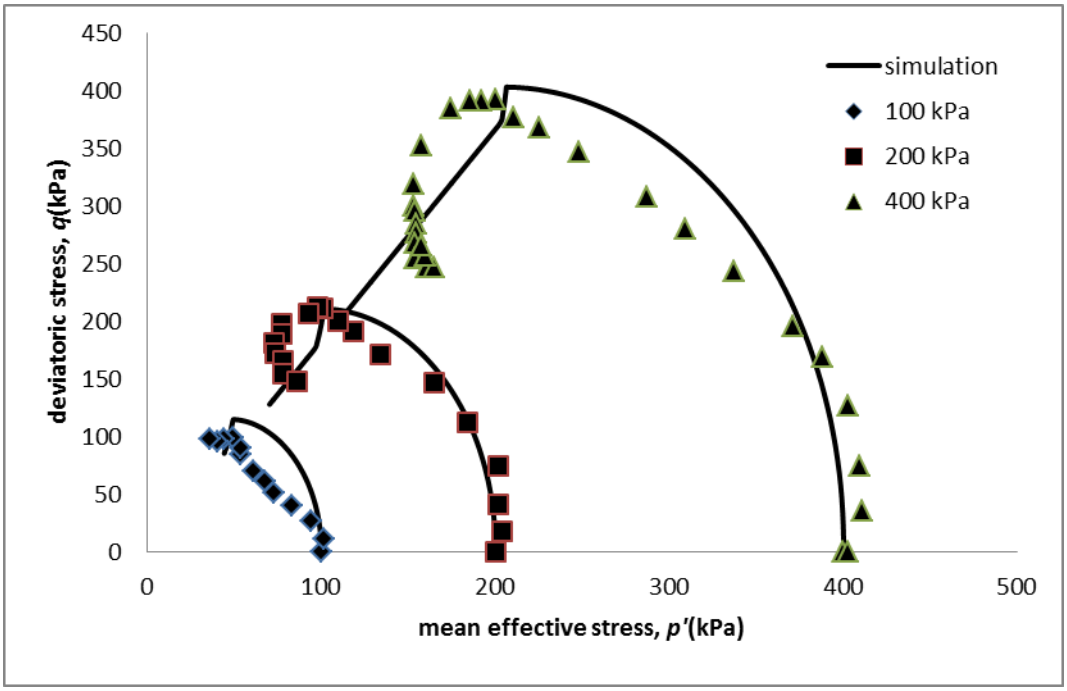

(a) Stress path

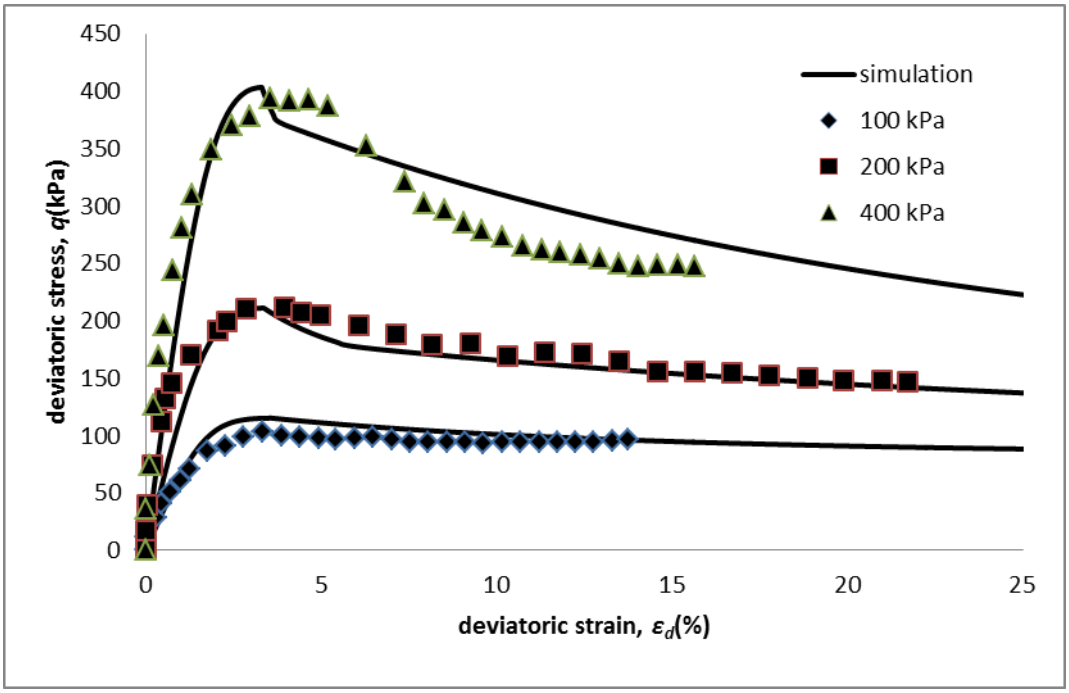

(b) Deviatoric stress and deviatoric strain

Fig 7.1 Undrained triaxial tests on 6% cemented Ariake clay (Horpibulsuk et al., 2004)

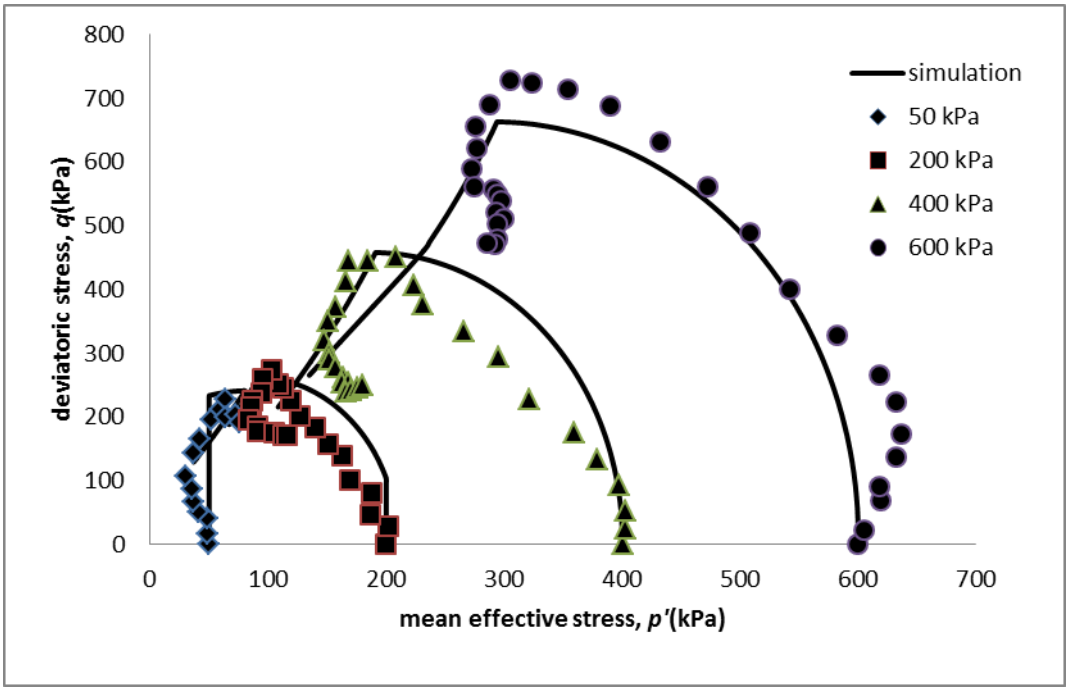

(a) Stress path

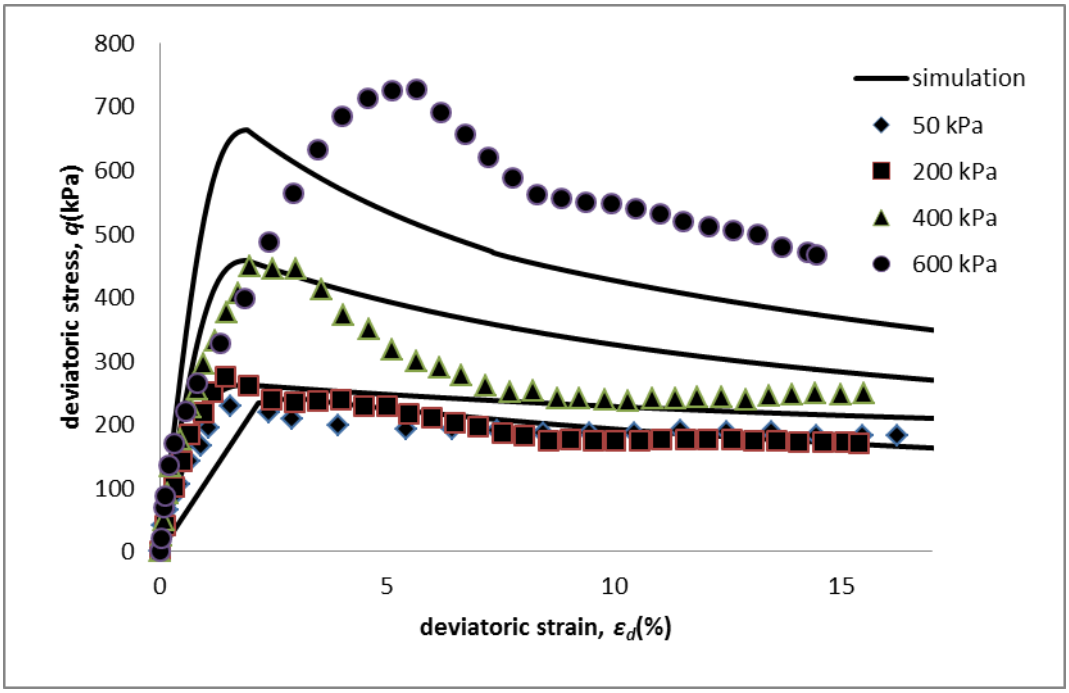

(b) Deviatoric stress and deviatoric strain

Fig 7.2 Undrained triaxial tests on 9% cemented Ariake clay (Horpibulsuk et al., 2004)

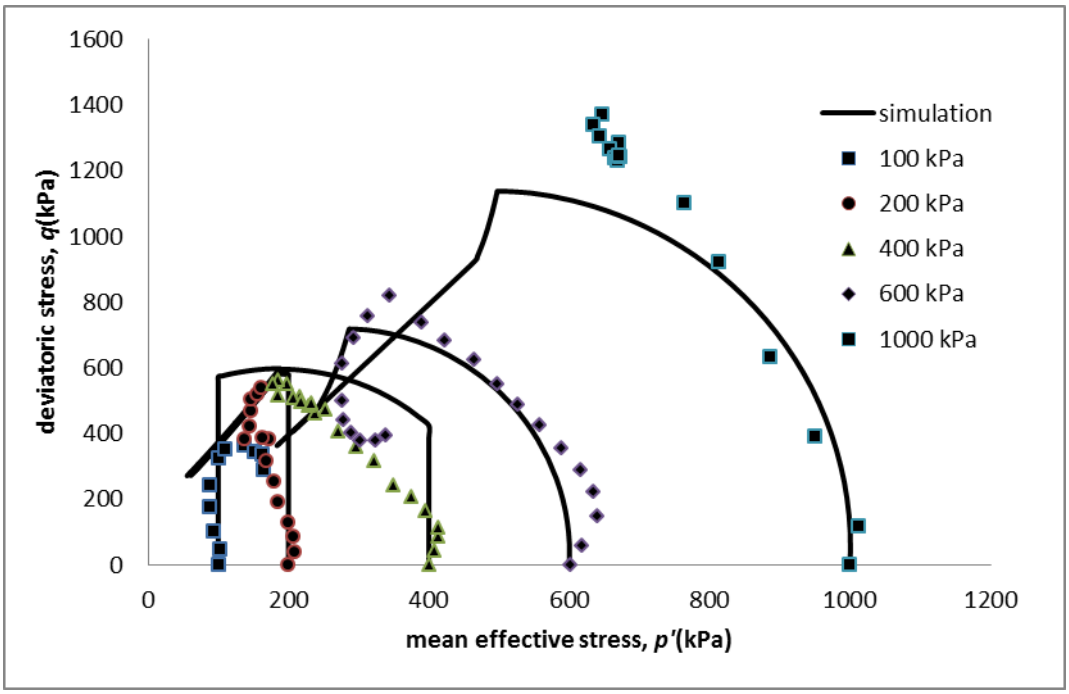

(a) Stress path

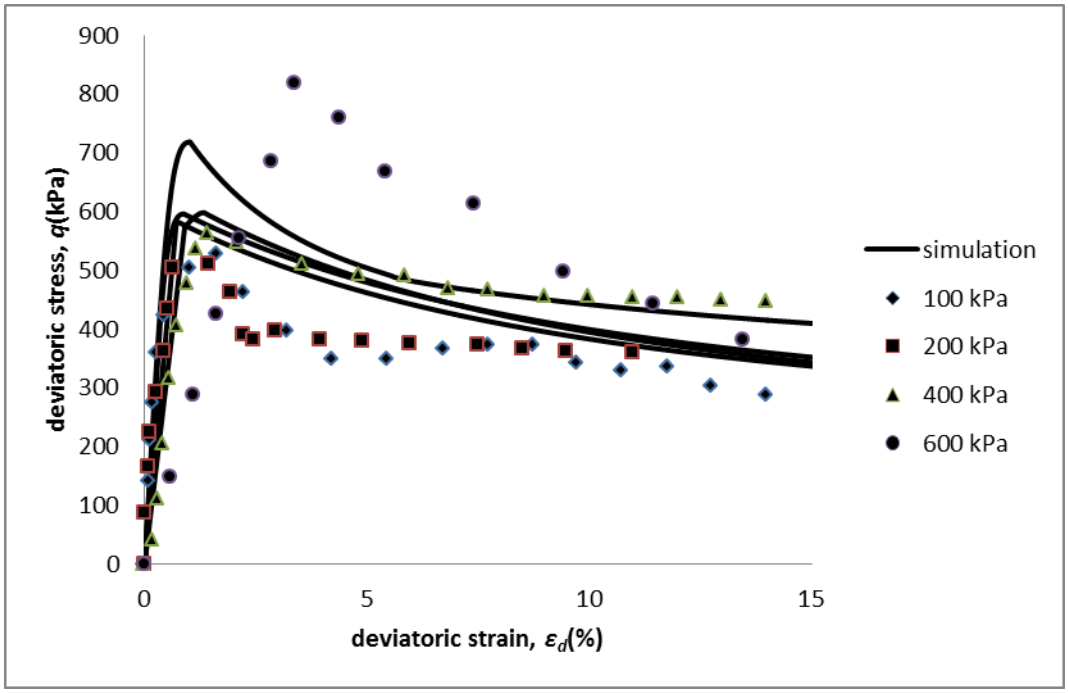

(b) Deviatoric stress and deviatoric strain

Fig 7.3 Undrained triaxial tests on 12% cemented Ariake clay (Horpibulsuk et al., 2004)

7.1.2 Singapore marine clay

The soil base of Singapore marine clay has already been introduced. The noticeable character of this cemented clay is the high M^* value as deduced via Fig 5.5.

Cemented Singapore marine clay is an extreme case with quite remarkable parameters. In addition to the value of M^*, the cement content of the specimens is huge and ranges from 10% to 50%. The specimen of simulated data has 100% water content and employ no loading during curing. In this group of data, the entire yield surface presented is extremely large with a large height width ratio. This phenomenon is caused not just by its high M^* value but also by subyielding in elastic behaviour. That is why the stress path simulations all pass through elastic behaviour to yielding so that the height increases to catch the peak deviatoric stress. The simulation is illustrated in Fig 7.4, Fig 7.5 and Fig 7.6. As the stress path characteristics are not simulated appropriately, a group of simulations, which are based on the stress path, are illustrated in Fig 7.7, Fig 7.8 and Fig 7.9. It is obvious that the stress path based simulation fails to fit both the peak deviatoric stress and the stress path correctly. The model parameters are listed in Table 7.3 and Table 7.4. The following points were discovered through this simulation.

1) Swelling index for this simulation is a constant. The minor change with cement content is also reflected in the experimental equation simulation in Fig 5.15. The values of swelling index are all around 0.01 both in terms of experiment and simulation.

2) The parameter M^* value of 3 is not the original M^* value of base soil, which should be 0.9. But the value is increased by cementation. By substituting an M^* value of 3 in Equation 4.1, the friction angle will be infinitely large. In this simulation, the parameter M^* is substituted with 2.9. The gap between the real value of 3 and the assumed value of 2.9 is small and is adjusted with slight cohesion (see Table 7.4).

3) Comparing experimental data and simulation, once again, the existence of subyielding and decementation in elastic behaviour is proven. In fact, it is even more obvious in these cases. The stress path reaches a peak strength then seems to move in a straight line towards the peak stress. This behaviour shows a huge difference with the combination of vertically straight elastic behaviour and elliptical plastic behaviour.

4) Although the figures do not show this, the stress path of test groups in low confining stress tends to move up along the critical state line after it goes straight up and reaches CSL. This does not follow the theory that the stress path should surpass the failure envelope until reaching the yield surface and softening takes place.

The model parameters are listed in Table 7.3 and Table 7.4.

Table 7.3 The common parameters for Singapore marine clay

λ^*	κ^*	Δe_i	$e_{IC}{}^*$	ν^*	b	γ	c	M^*
0.08	0.01	0.15	1.3	0.25	1	0.5	0	2.9

Table 7.4 The parameters for different cemented Singapore marine clay

	$p'_{y,i}$ q_{peak} *based* (kPa)	$p'_{y,i}$ *stress path based* (kPa)	C (kPa)	ω
10%	140	120	40	1.2
15%	240	200	50	0.3
30%	400	350	70	0.3

Furthermore, the comparison between SCC and MCC is also performed in this simulation. The MCC simulations are shown in Fig 7.10, Fig 7.11 and Fig 7.12. The

SCC simulation compared with MCC simulation is illustrated in Fig 7.13, Fig 7.14 and Fig 7.15.

It can be seen that MCC barely describes soil behaviour even with the same parameters of peak stress based on the simulation from SCC. The stress path of MCC stops when it reaches the summit of the yield surface. There is no further movement along the critical state line due to its representation of reconstituted soil. As a result, no softening shows in stress strain behaviour. On the contrary, the stress path of SCC will move along the critical state line after the peak as long as the structure is not fully removed. This behaviour of SCC reflects the character of structured soil and cemented soil.

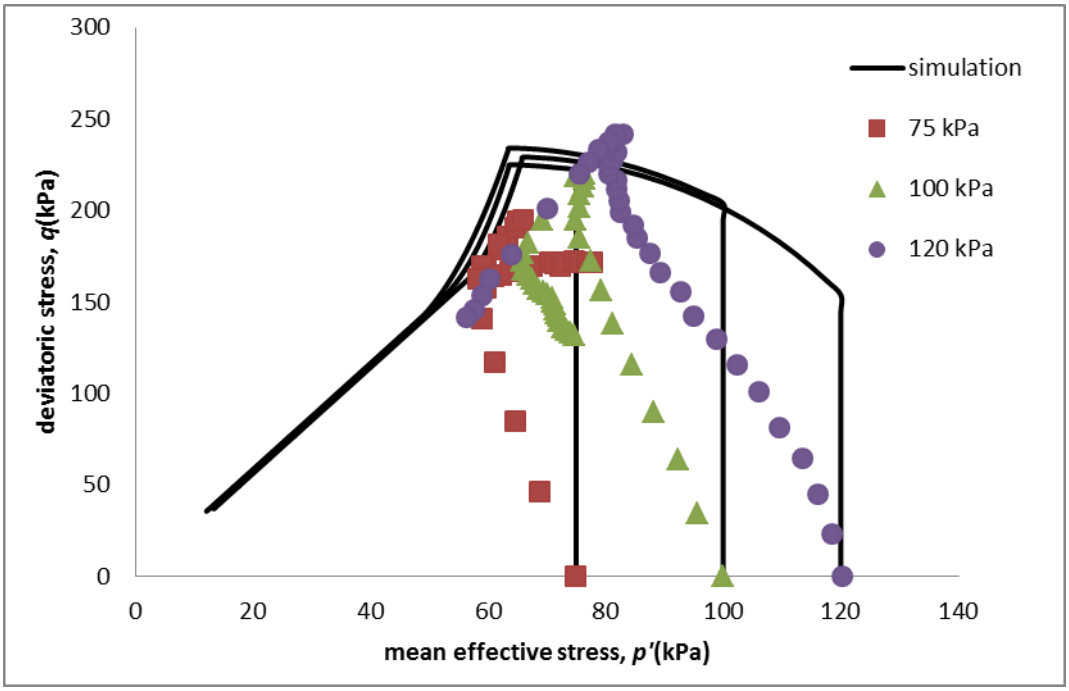

(a) Stress path

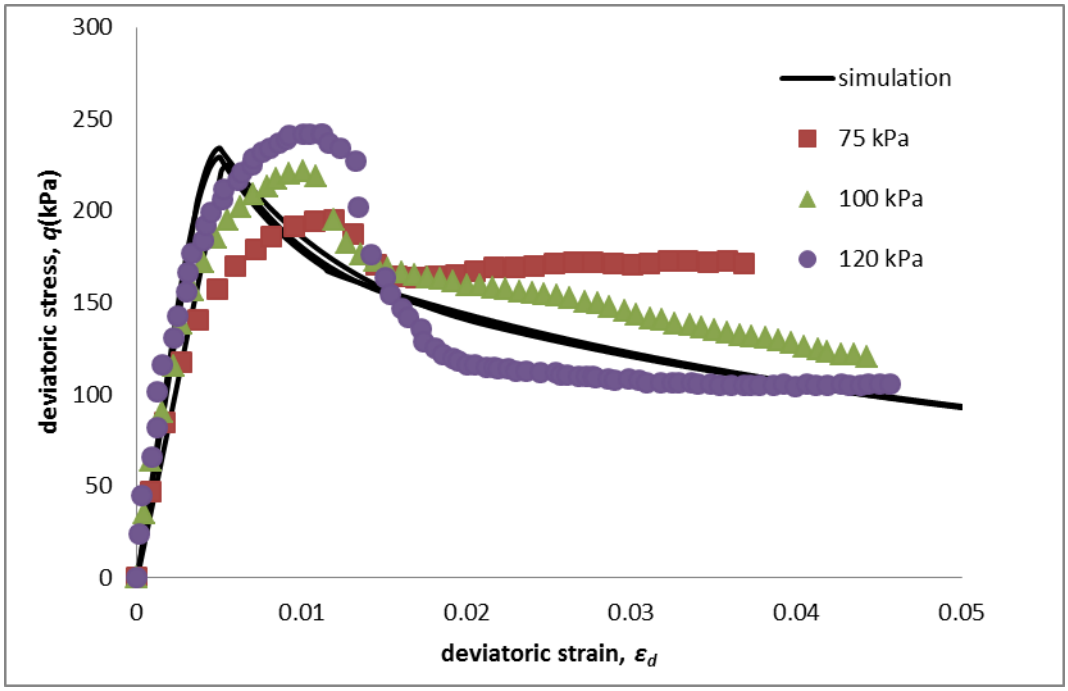

(b) Devaitoric stress and deviatoric strain

Fig 7.4 Undrained triaxial tests on 10% cemented Singapore marine clay-q_{peak} based simulation (Huawen, 2009)

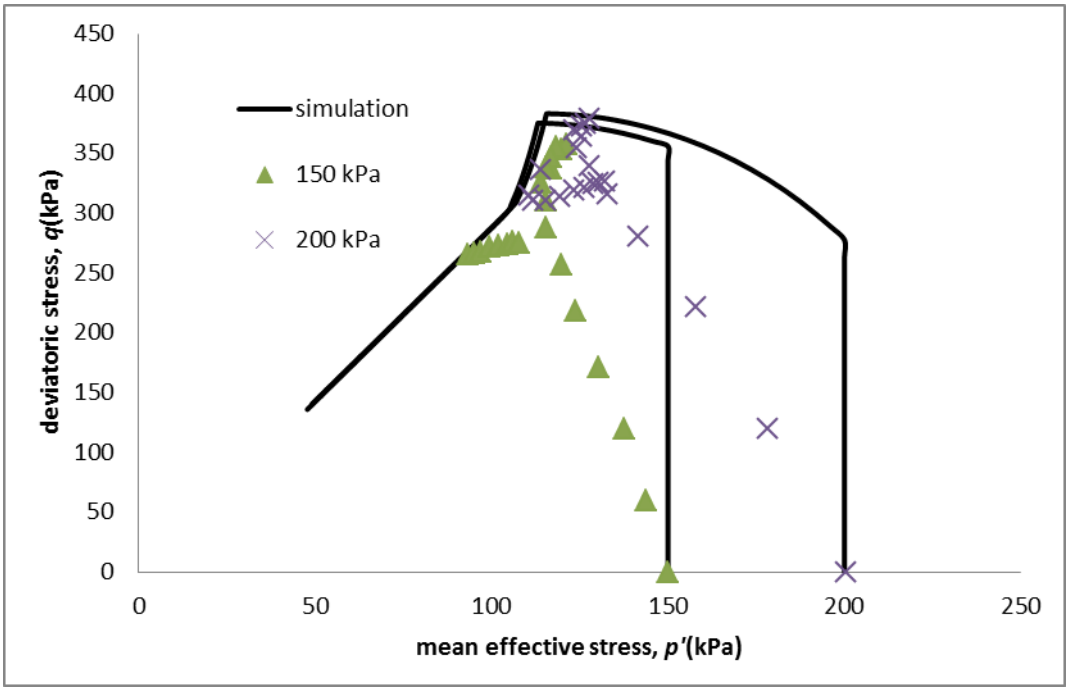

(a) Stress path

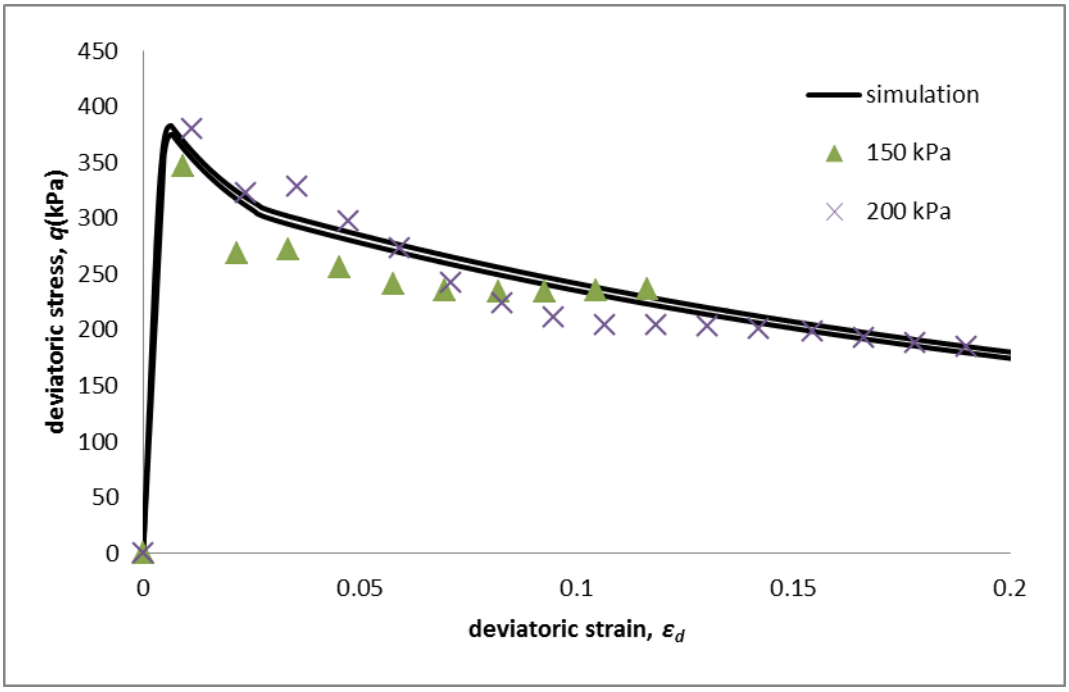

(b) Devaitoric stress and deviatoric strain

Fig 7.5 Undrained triaxial tests on 15% cemented Singapore marine clay-q_{peak} based simulation (Huawen, 2009)

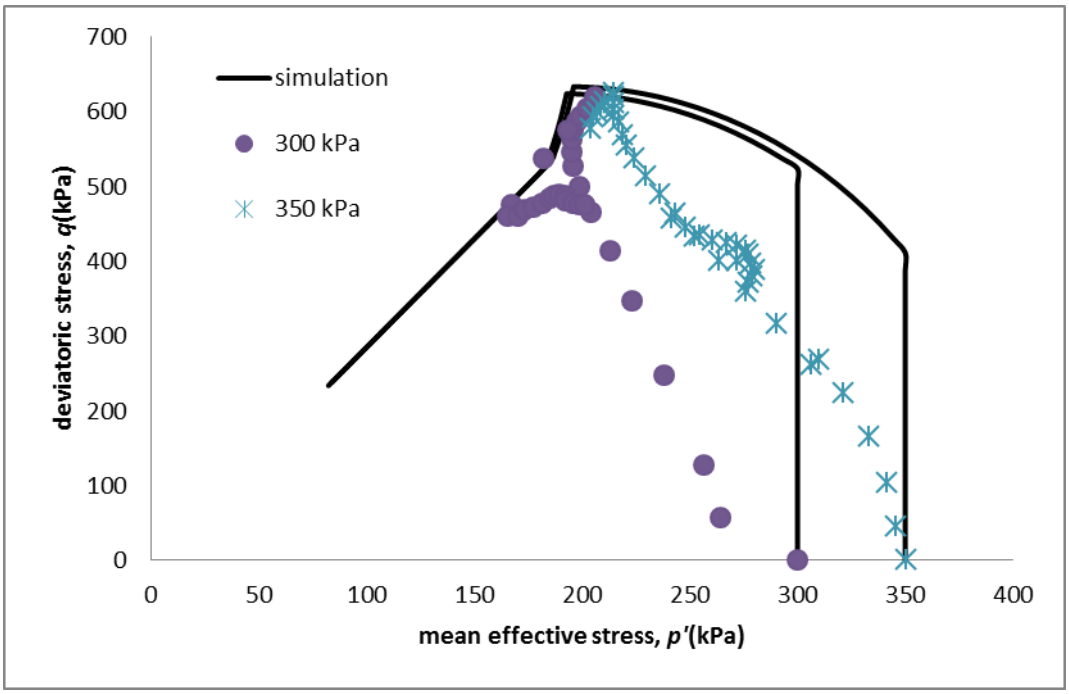

(a) Stress path

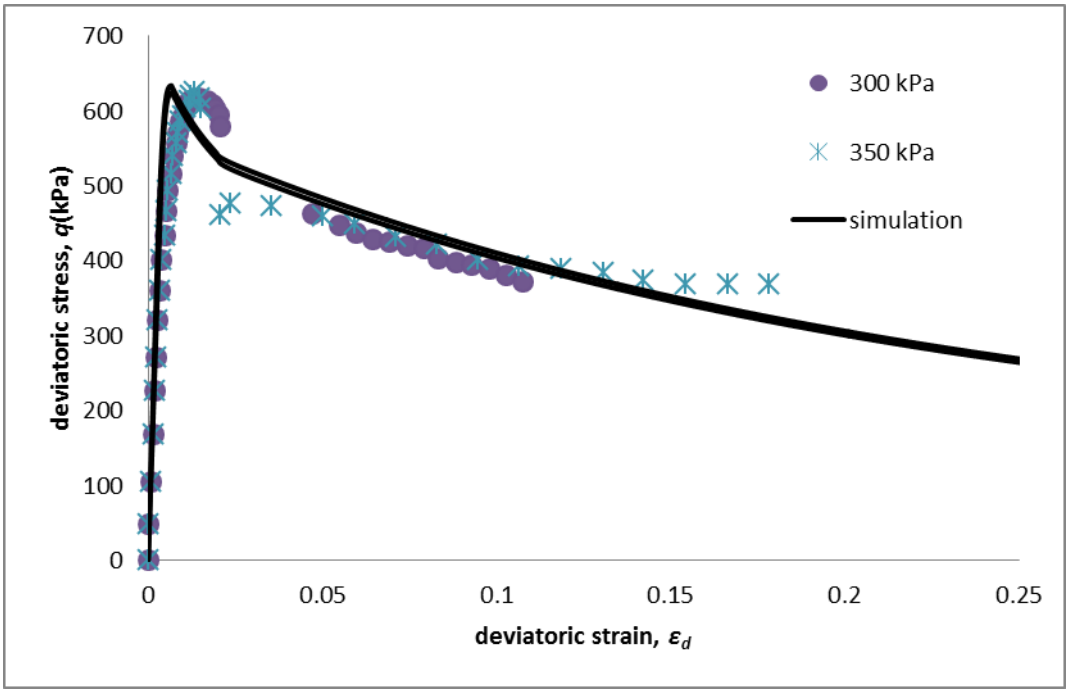

(b) Devaitoric stress and deviatoric strain

Fig 7.6 Undrained triaxial tests on 30% cemented Singapore marine clay-q_{peak} based simulation (Huawen, 2009)

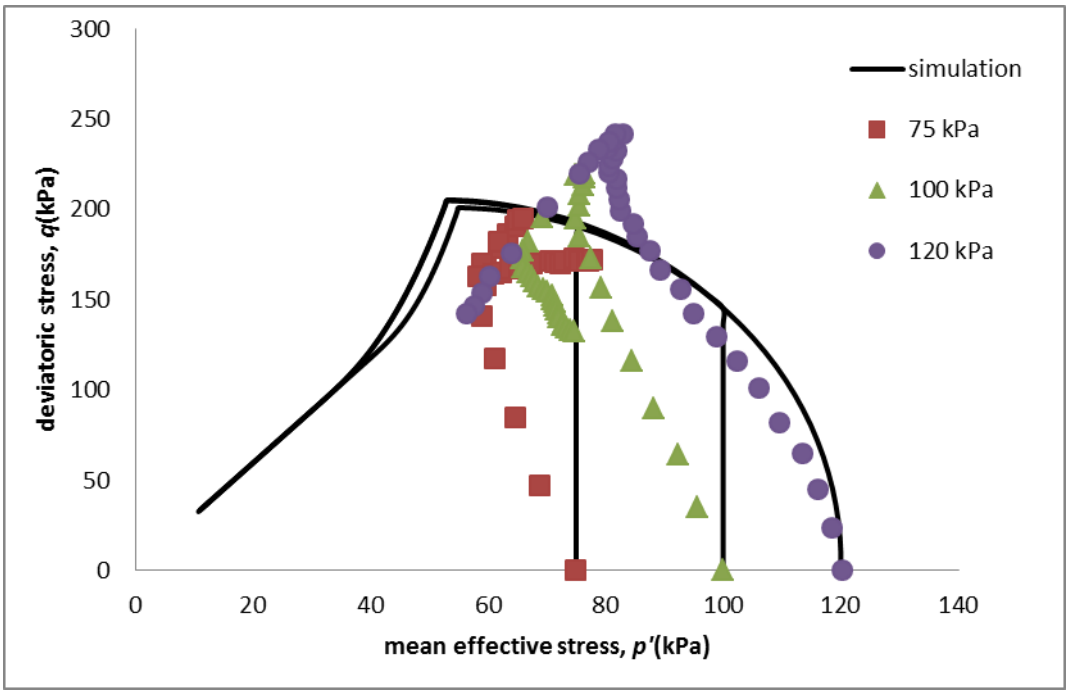

(a) Stress path

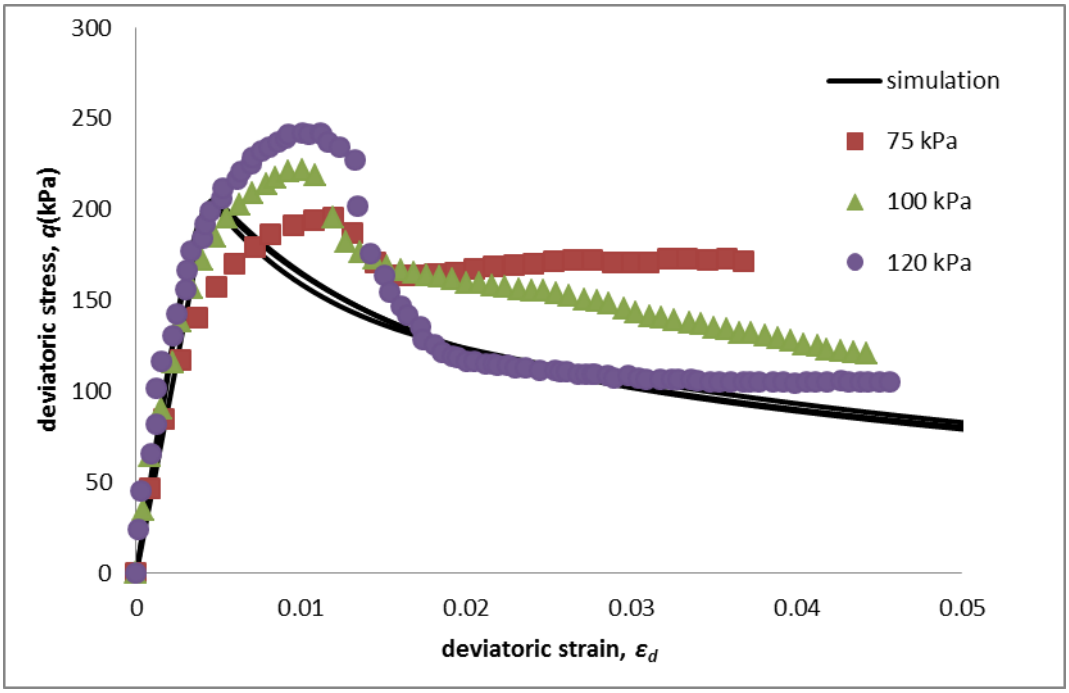

(b) Devaitoric stress and deviatoric strain

Fig 7.7 Undrained triaxial tests on 10% cemented Singapore marine clay-stress path based simulation (Huawen, 2009)

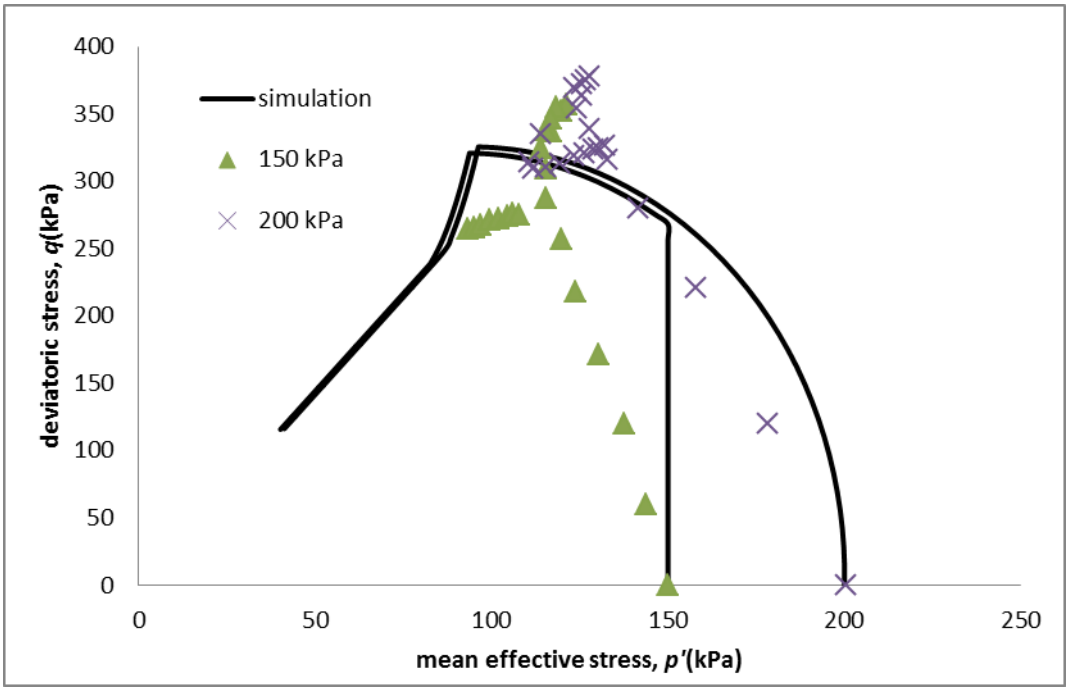

(a) Stress path

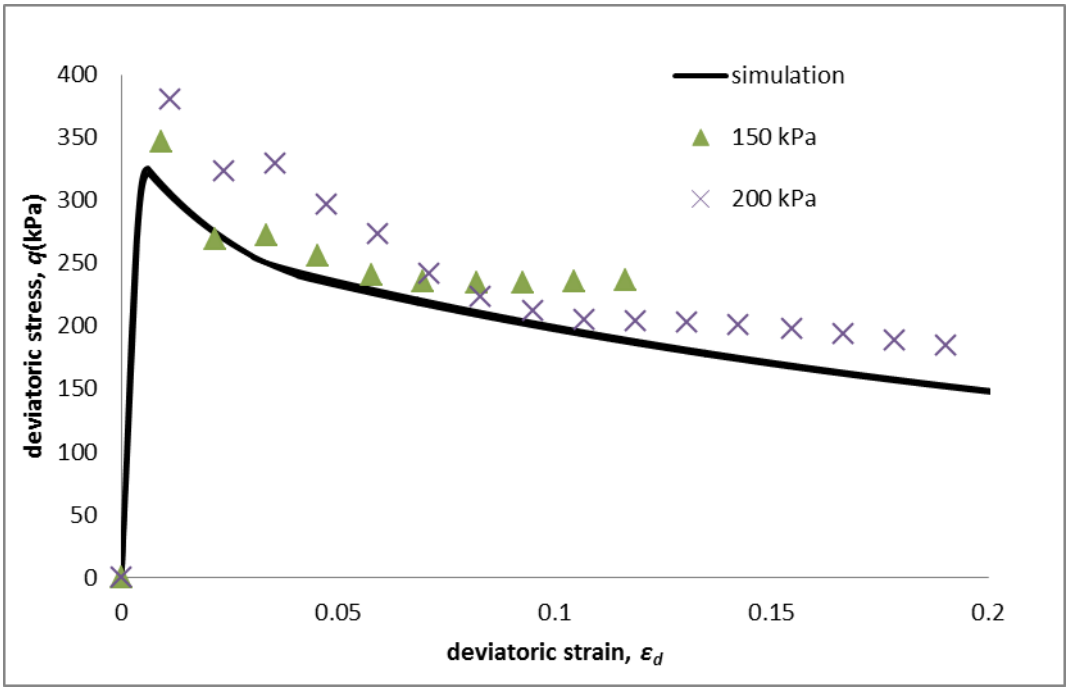

(b) Devaitoric stress and deviatoric strain

Fig 7.8 Undrained triaxial tests on 15% cemented Singapore marine clay-stress path based simulation (Huawen, 2009)

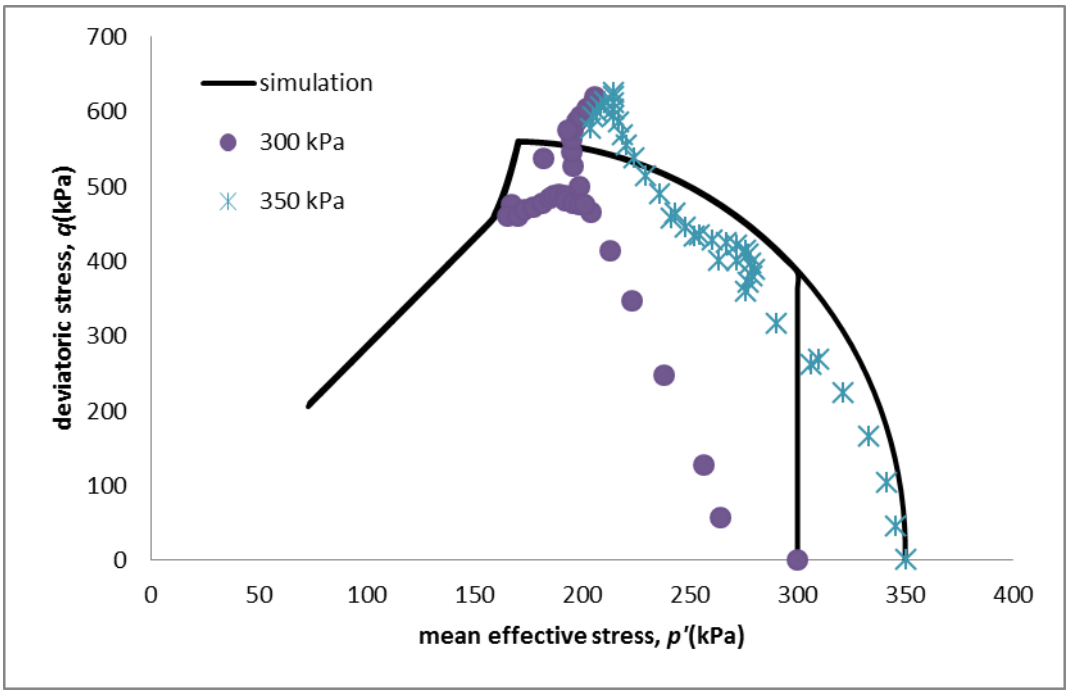

(a) Stress path

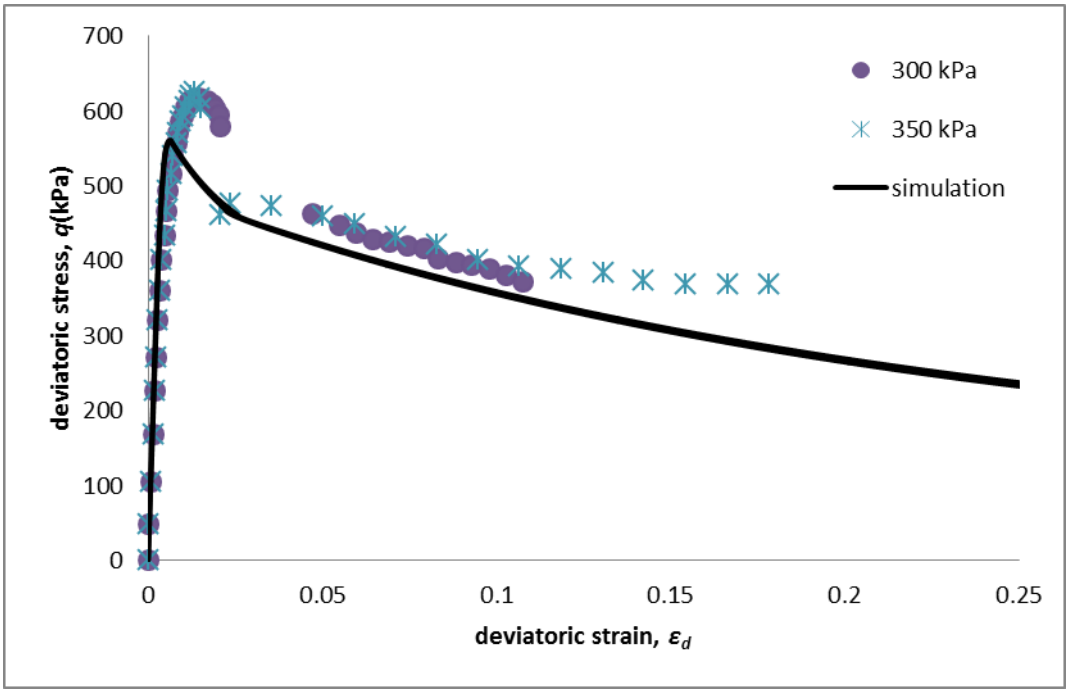

(b) Devaitoric stress and deviatoric strain

Fig 7.9 Undrained triaxial tests on 30% cemented Singapore marine clay-stress path based simulation (Huawen, 2009)

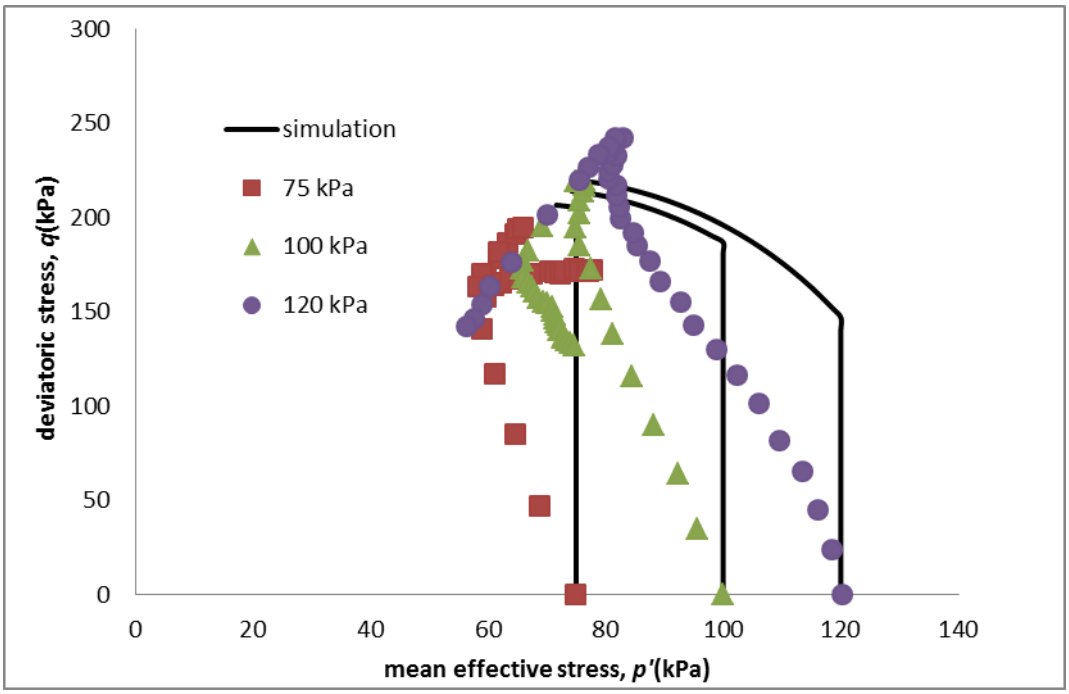

(a) Stress path

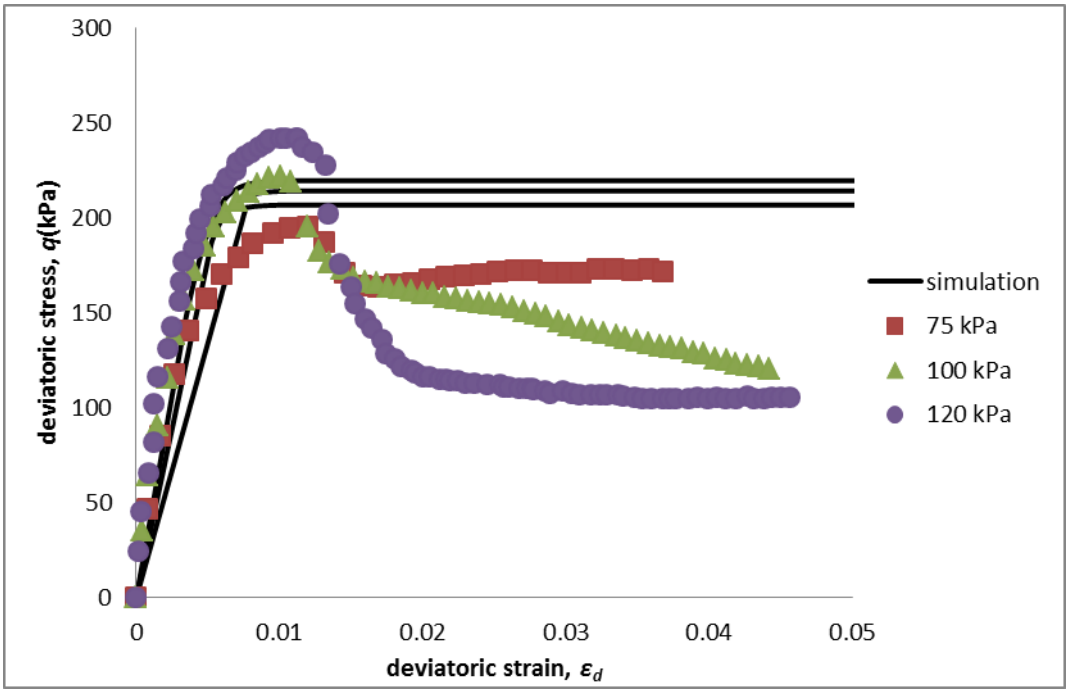

(b) Devaitoric stress and deviatoric strain

Fig 7.10 Undrained triaxial tests on 10% cemented Singapore marine clay-MCC simulation (Huawen, 2009)

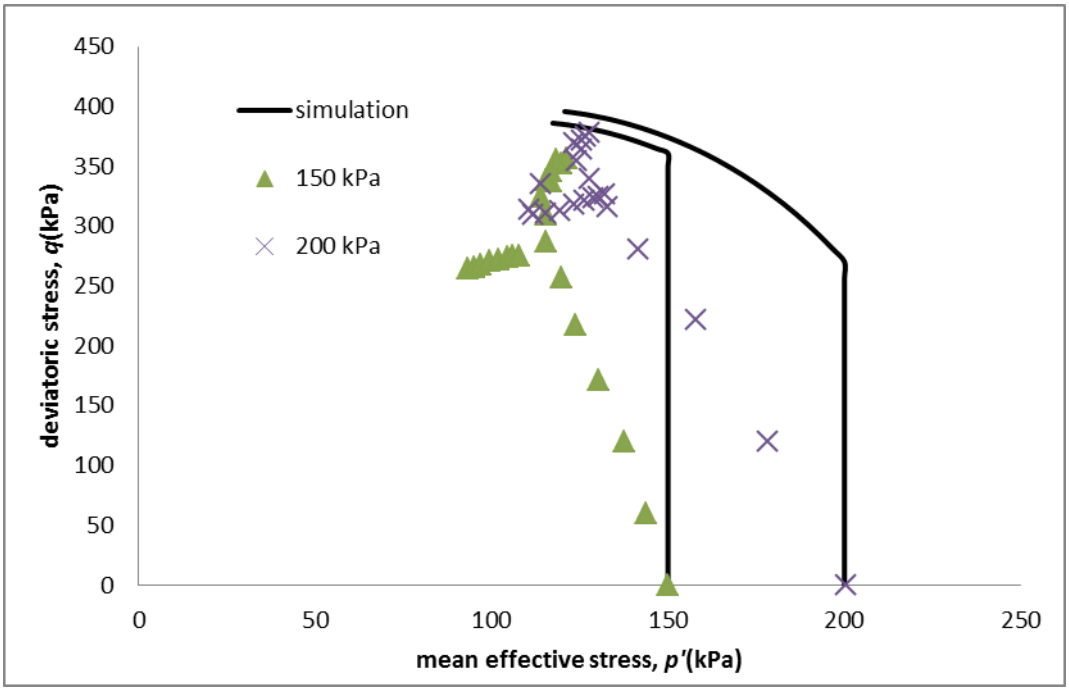

(a) Stress path

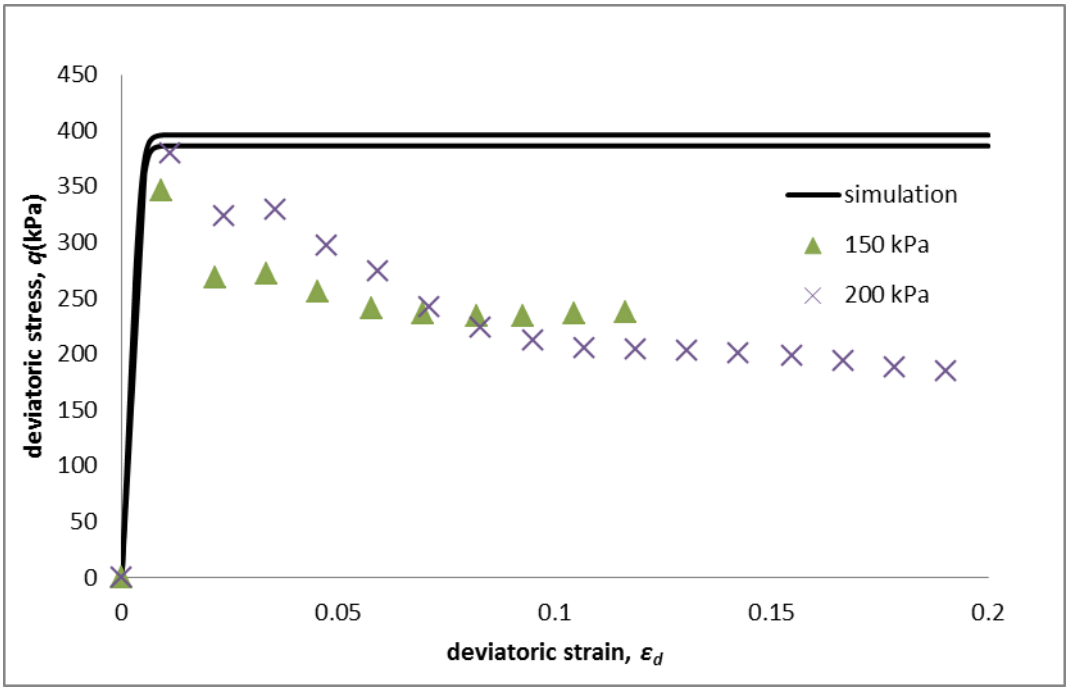

(b) Devaitoric stress and deviatoric strain

Fig 7.11 Undrained triaxial tests on 15% cemented Singapore marine clay-MCC simulation (Huawen, 2009)

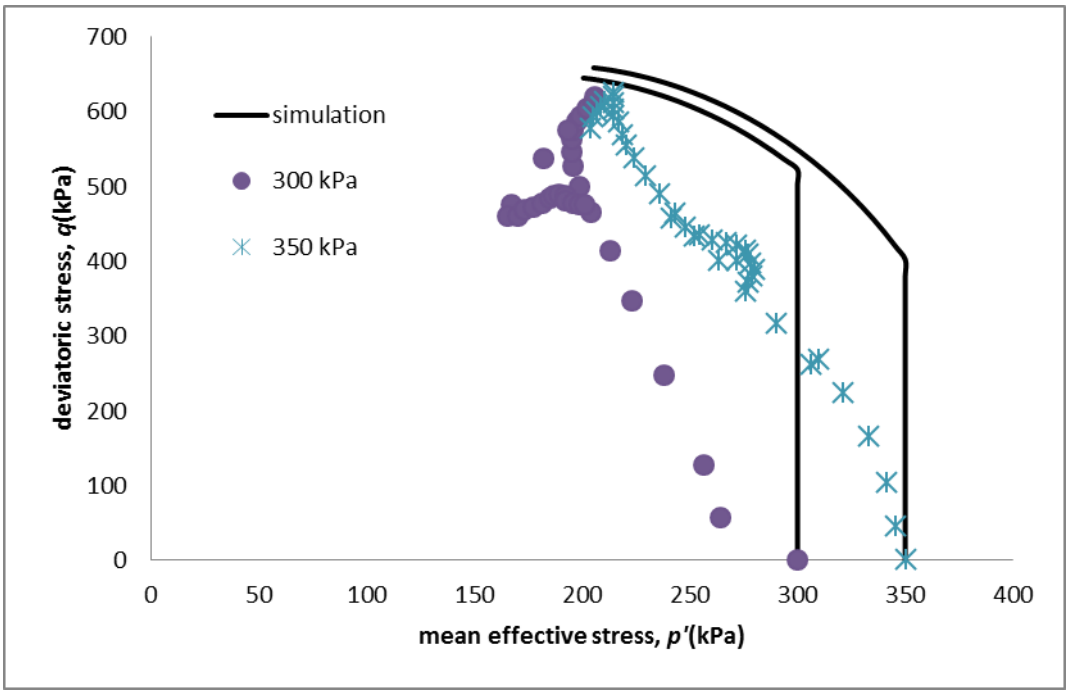

(a) Stress path

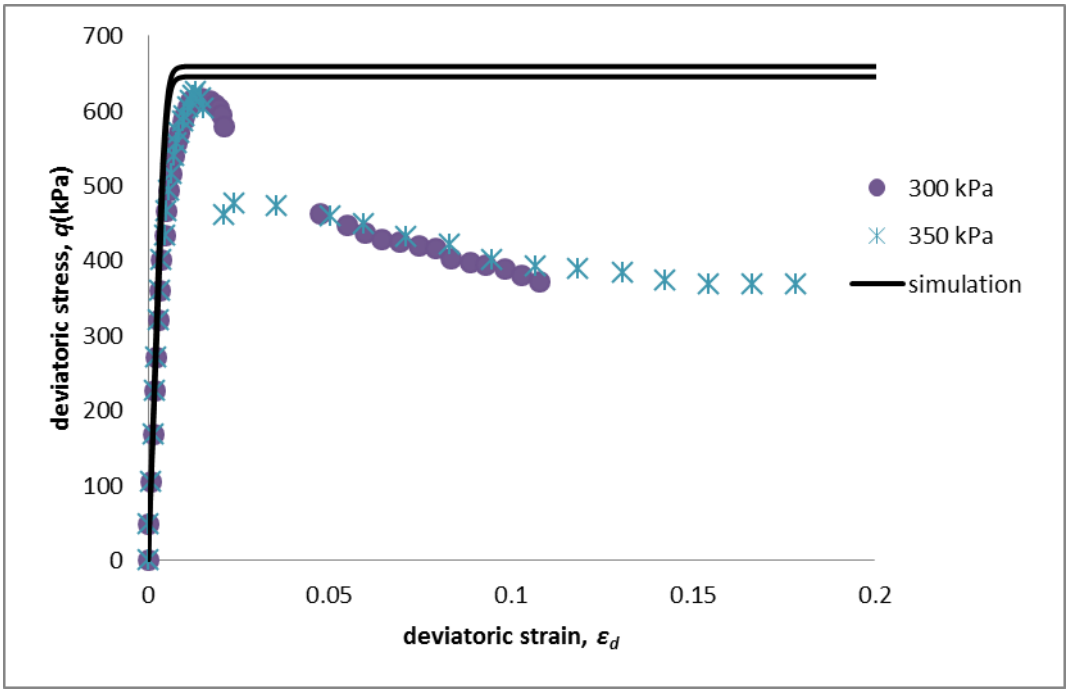

(b) Devaitoric stress and deviatoric strain

Fig 7.12 Undrained triaxial tests on 30% cemented Singapore marine clay-MCC simulation (Huawen, 2009)

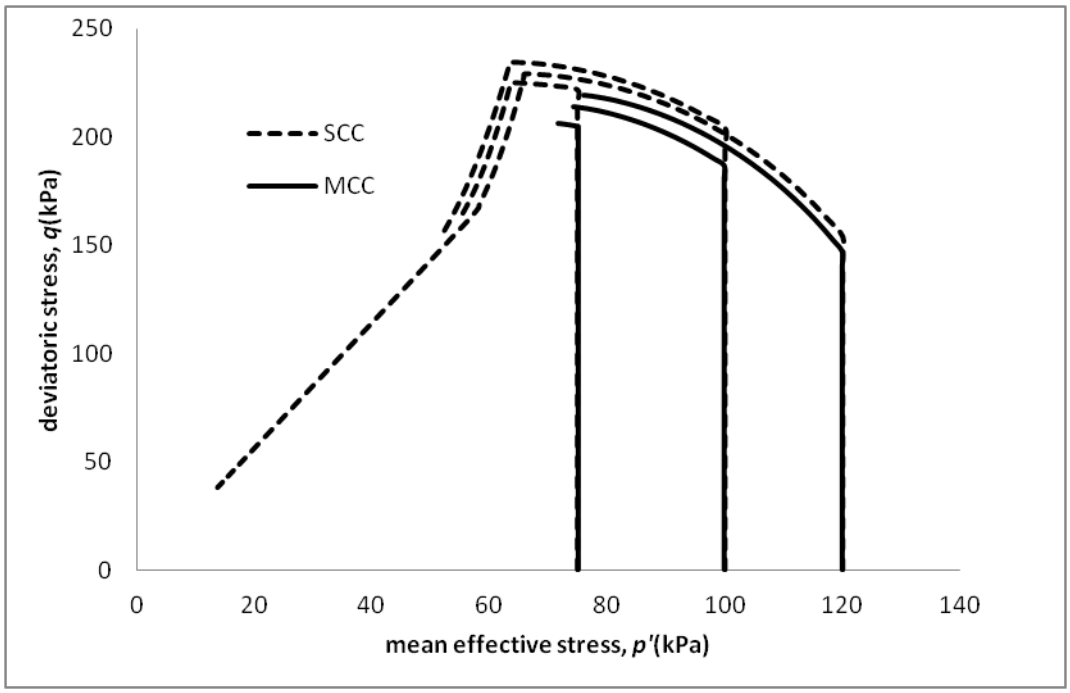

(a) Stress path

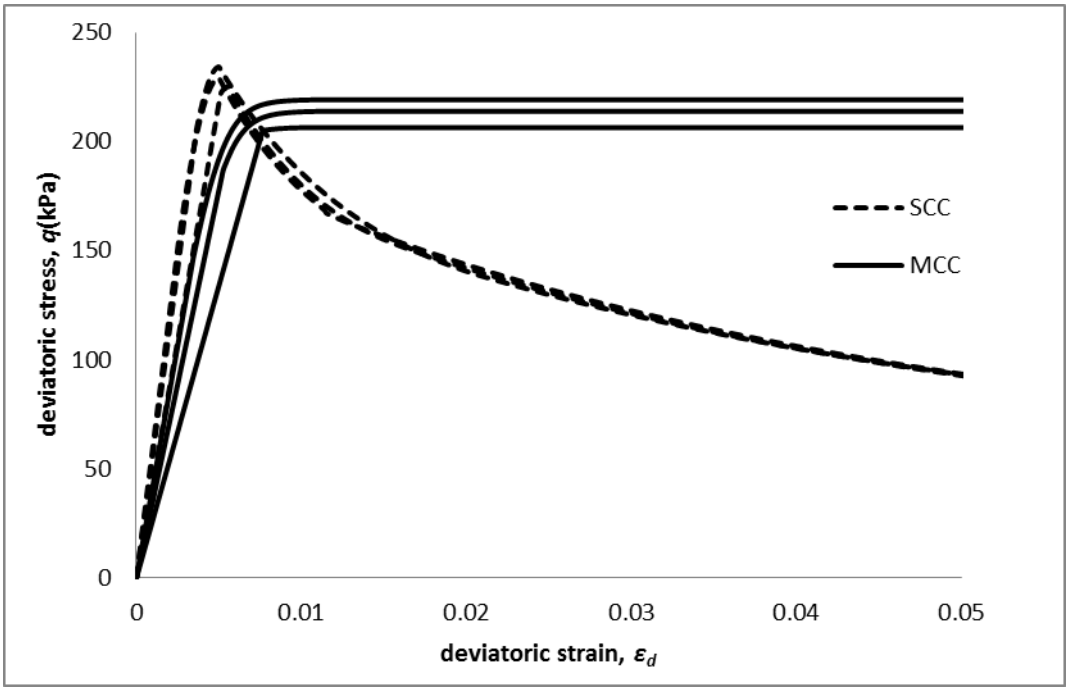

(b) Devaitoric stress and deviatoric strain

Fig 7.13 Undrained triaxial tests on 10% cemented Singapore marine clay-SCC vs. MCC simulation (Huawen, 2009)

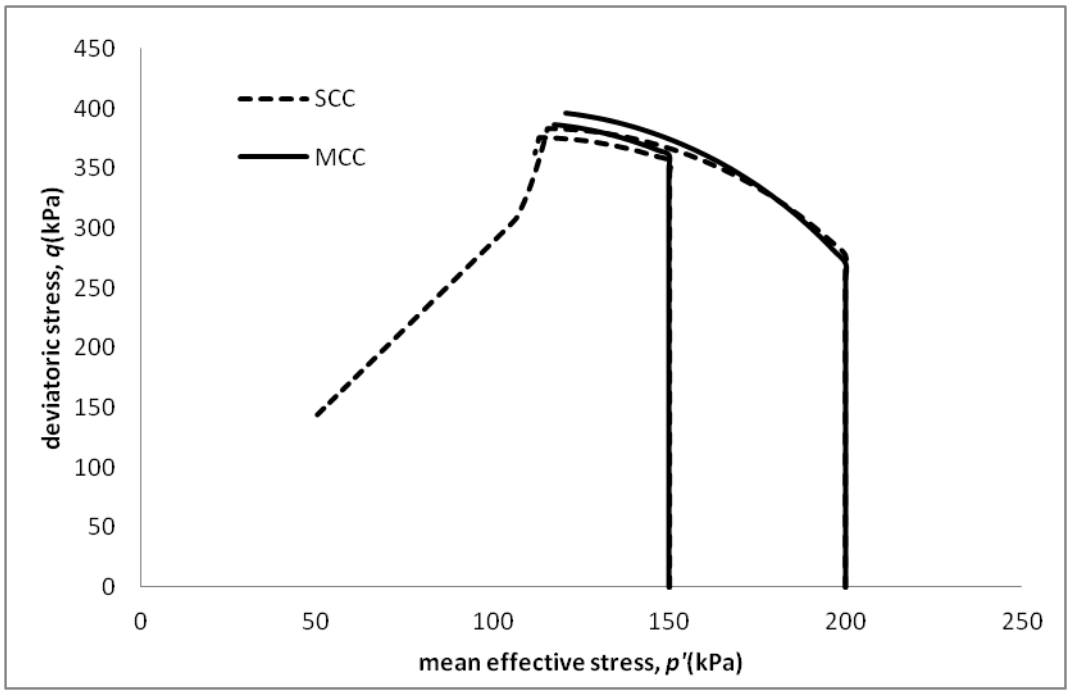

(a) Stress path

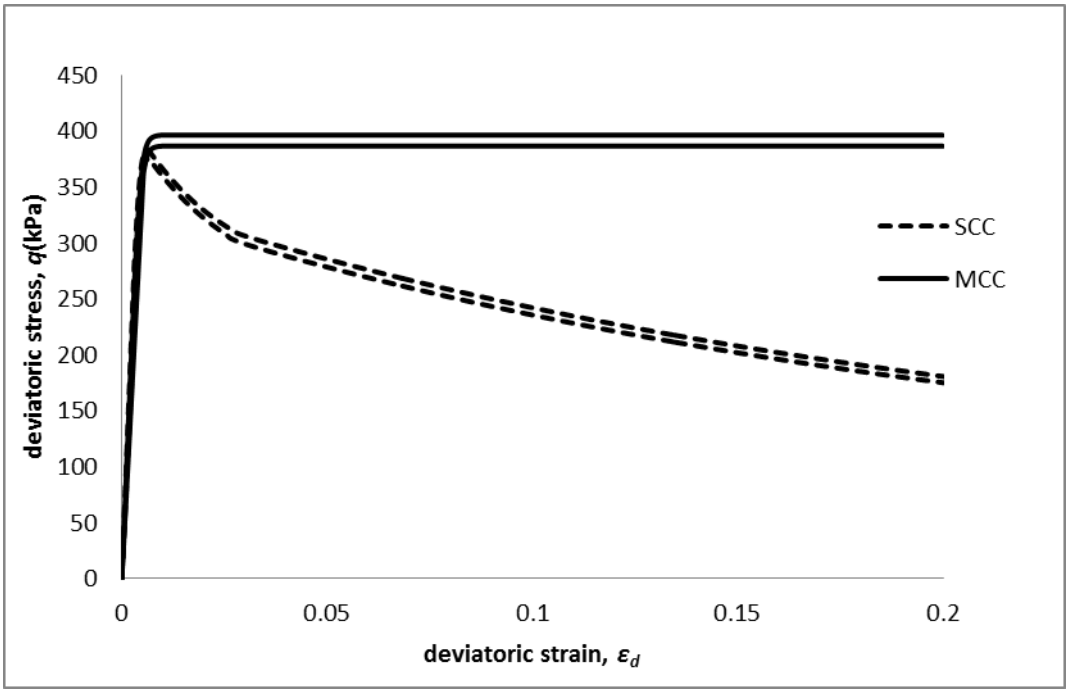

(b) Devaitoric stress and deviatoric strain

Fig 7.14 Undrained triaxial tests on 15% cemented Singapore marine clay-SCC vs. MCC simulation (Huawen, 2009)

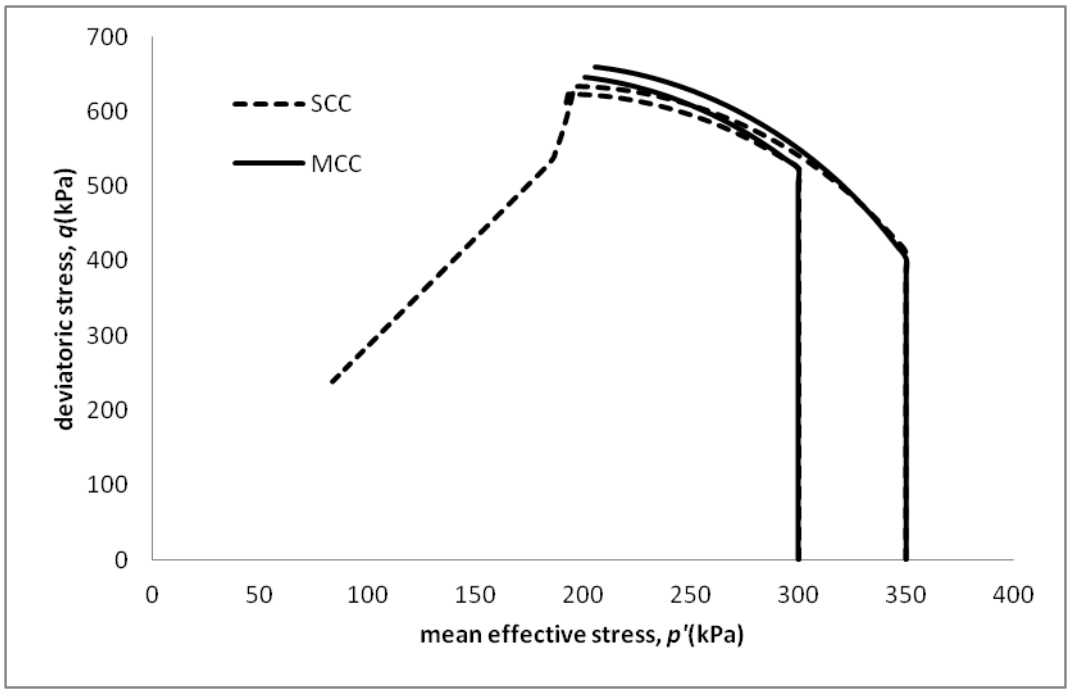

(a) Stress path

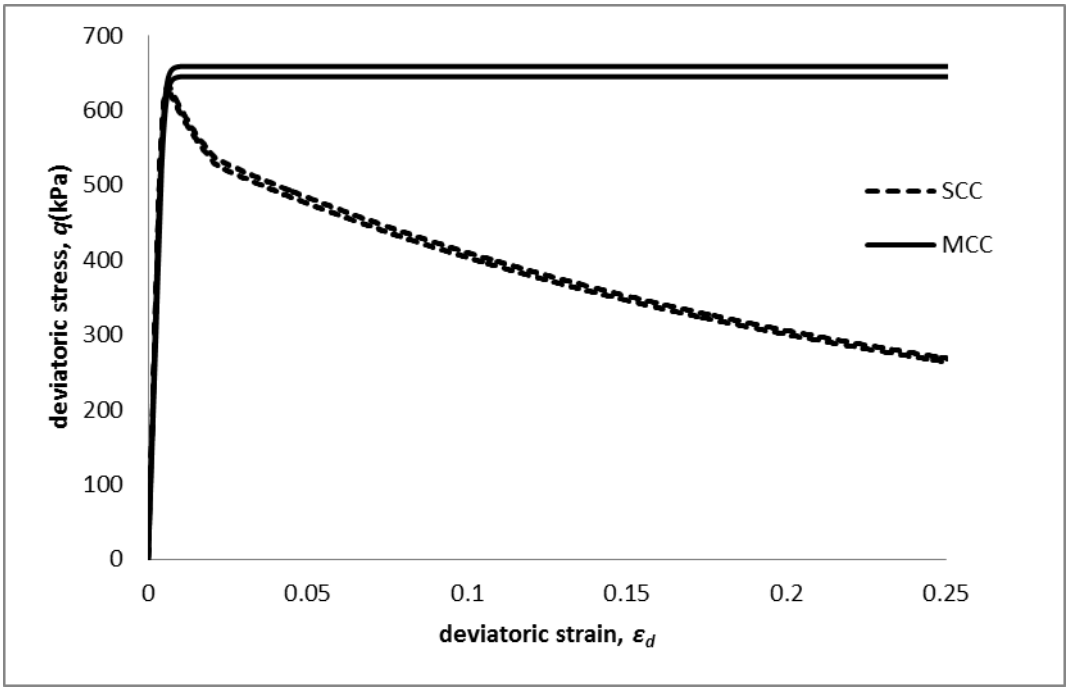

(b) Devaitoric stress and deviatoric strain

Fig 7.15 Undrained triaxial tests on 30% cemented Singapore marine clay-SCC vs. MCC simulation (Huawen, 2009)

7.1.3 Marine clay

A series of tests on marine clay were conducted by Rakesh et al. (2012). Soil base is excavated from Ennore, Chennai, India. The air dried and crushed soil, with liquid limit of 56% and plastic limit of 25%, mixed with 5% of 52 grade ordinary Portland cement. The water content was controlled in 0.8 times of liquid limit. Different tests including Constant Rate of Strain (CSR) Test and Consolidated Undrained (CIU) Triaxial Tests were conducted to identify model parameters. The simulation parameters are listed in table 7.5. The simulation is shown in Fig 7.16.

The simulation is able to match experiment data both in terms of stress path and critical state strength. The stress path for initial confing stress being 200 kPa tests have obviously sub yielding as Singapore marine clay tests. The paths for the rest two tests followed the elliptic yield surface boundary theory.

Table 7.5 The parameters for 5% cemented marine clay

λ^*	κ^*	Δe_i	${e_{IC}}^*$	ν^*	b
0.5	0.02	0.12	2	0.25	1
γ	c	M^*	$p'_{y,i}$ (kPa)	C (kPa)	ω
0.8	0	1.3	280	70	0.7

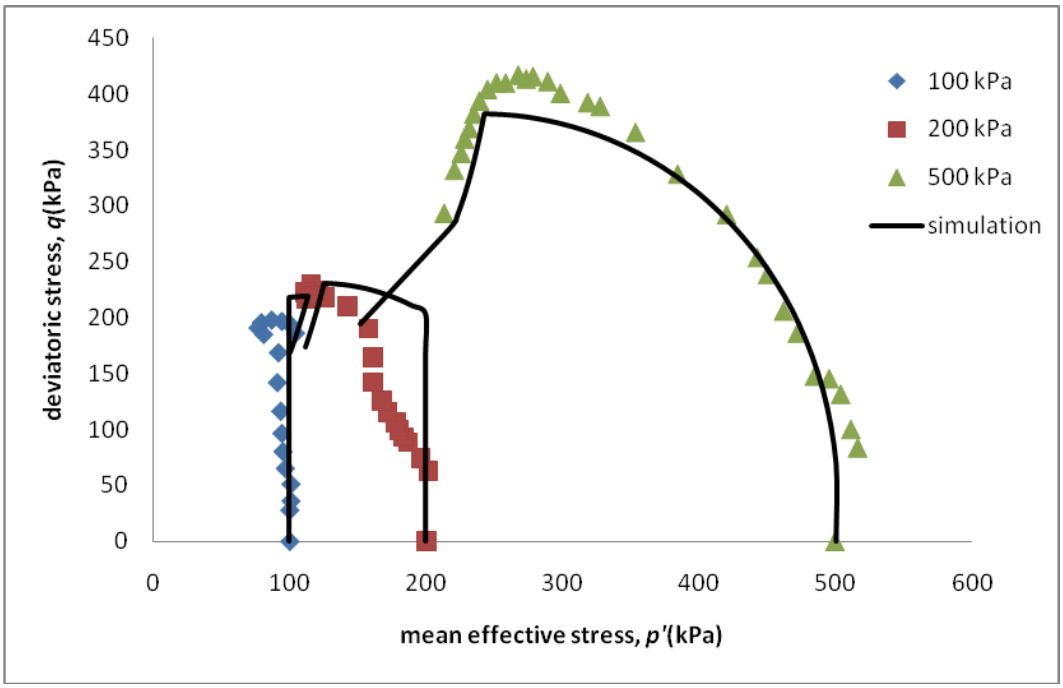

(a) Stress path

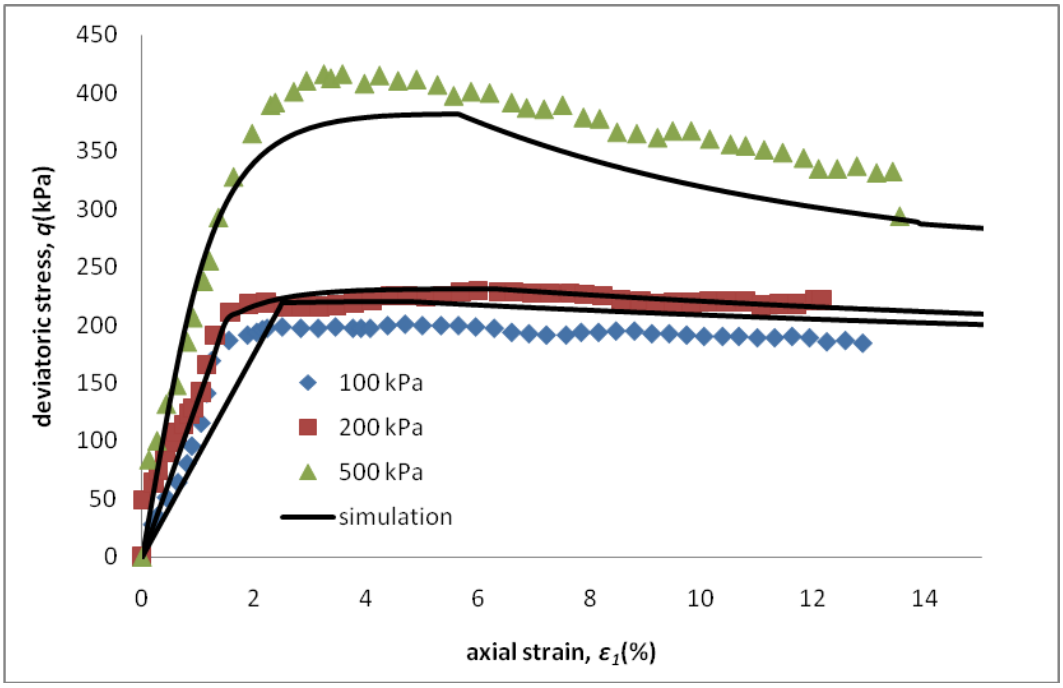

(b) Deviatoric stress and deviatoric strain

Fig 7.16 Undrained triaxial tests on cemented marine clay (Rakesh et al., 2012)

7.1.4 Summary of cemented clay simulations

The main features of soil behaviour can be captured by SCC for both of the clays. But the overall performance and general trends of simulation for the Ariake clay are better than that for Singapore marine clay. The accuracy and details of these two simulations need to be improved. The consideration of plastic deformation and breakdown of cementation during the elastic stress state would be the key to improving the simulation.

7.2 Cemented gravel sand

The Cam Clay frame work was proposed in order to simulate clayey soil and is applied to describe the behaviour of cemented sand. Because the behaviour of clay and sand is very different and is usually modelled separately (e.g., Scot, 1985; Muir Wood, 1990; Yao et al, 2004; Khalili et al, 2005), some problems can be found in this sandy soil simulation. In addition, the cemented soil undrained behaviour is even more challenging for SCC. Gravel sand from Asghari et al. (2003) is used in simulation. The soil base is introduced in section 5.1.2 and its parameters are listed in Table 5.2.

SCC extended to cemented clay was only used to consider the undrained behaviour. For this simulation, drained behaviour simulation should also extend to cemented soil. The new proposal is adopted in the same way for cohesion and extended yield surface but different for the decementation process. A simple equation for the breakdown of cementation is proposed. No additional parameter is added and an improvement is made in the new equation. Complete breakdown of the cementation will be achieved when the soil reaches a final state of deformation, the critical state of deformation, even when the state is approached via dp'=0.

$$dC = -2\left(\frac{C}{C_{in}}\right)\frac{d\varepsilon_d^p}{(\lambda^*-\kappa^*)} * \frac{e}{\sqrt{(^q/_{p'}-M^*)}} \qquad 7.1$$

Equation 7.1 is close to the undrained cementation break down behaviour (Equation 3.28). The proposed equation is correlated with plastic deviatoric strain but not mean effective stress. The simulation parameters are listed in Table 7.6 and Table 7.7 and simulation are shown in Fig 7.17 and Fig 7.18.

As seen in in Fig 7.18(b), the simulations show a volume shrinking, because soil is elastic behaviour and the volume decreases with the increment in mean effective stress. Then the softening occurs as the stress reaches the yield surface on the dry side and volume expansion is seen. At the end where stress state is close to critical state, the volume shrink again. This implies that positive additional voids ratio is being removed completely before a critical state of deformation is reached. Thus the volume deformation is positive again.

It seems that the peak stress in the simulation for cemented sand is higher than that of test data (Fig 7.18, 300kPa). Specifically, test data demonstrates less softening in stress strain behaviour than simulation even when the critical state tend occurs at the same level. This could be the inaccuracy of the shape of the yield surface causing the peak stress state difference. Cementation of sand tends to distort the elliptical yield surface to a "pear shaped" yield surface as for the yield surface of loess. This test reveals 'dry behaviour', which takes place on the left hand side of the yield surface. Due to the shear stress of the elliptical yield surface being higher than the corresponding part of the "pear shaped" yield surface on the left side, the simulated peak stress will be higher than test data (see Fig 7.19).

Table 7.6 The common parameters for gravel sand

λ^*	κ^*	${e_{IC}}^*$	ν^*	M^*	c
0.08	0.01	2.5	0.3	1.5	0

Table 7.7 The parameters for different cemented gravel sand

	Δe_i	$p'_{y,i}$ (kPa)	C (kPa)	b	ω	γ
0%	0.03	500	0	0.2	1	1
1.5%	0.05	2600	100	0.5	0.1	0.05

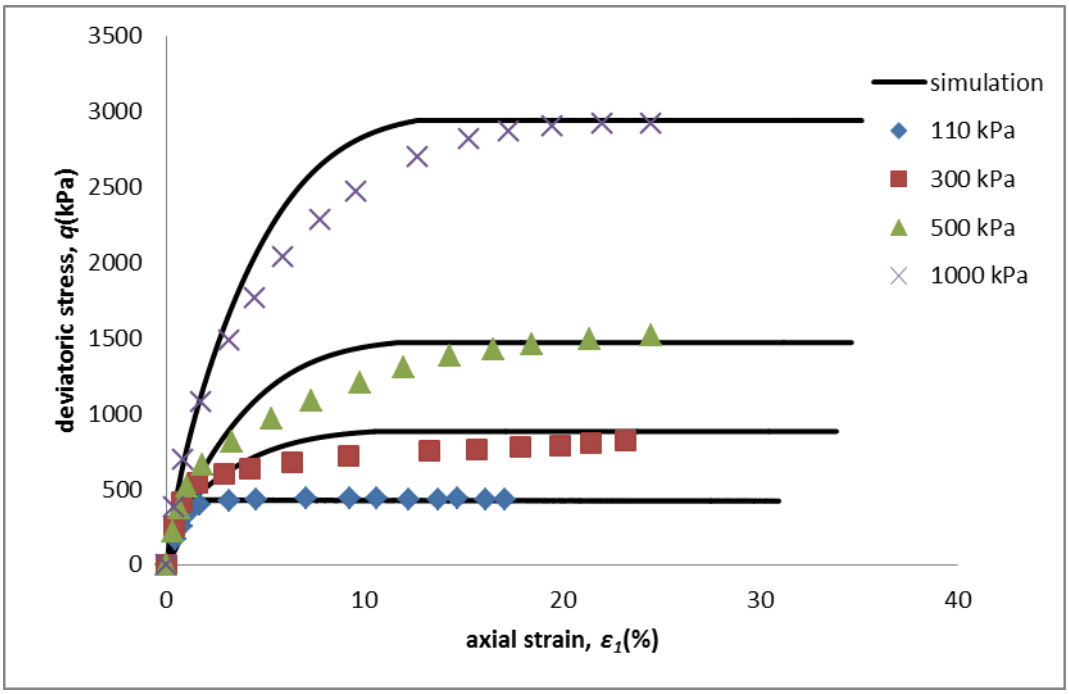

(a) Deviatoric stress and axial strain

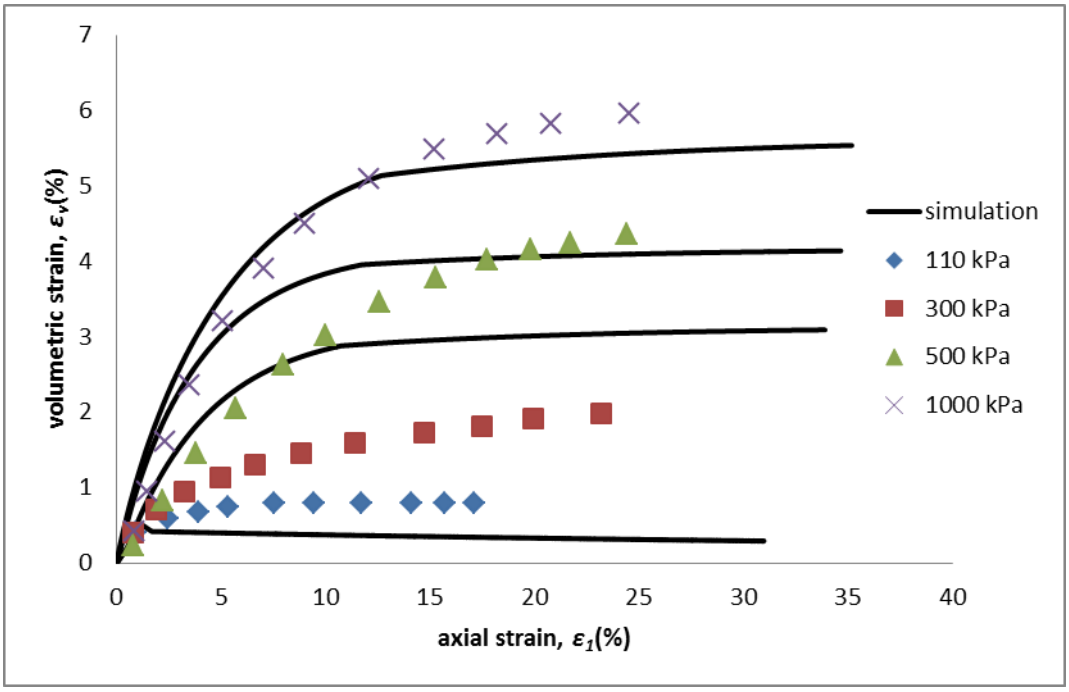

(b) Volumetric strain and axial strain

Fig 7.17 Drained triaxial tests on 0% cemented gravel sand (Asghari et al., 2003)

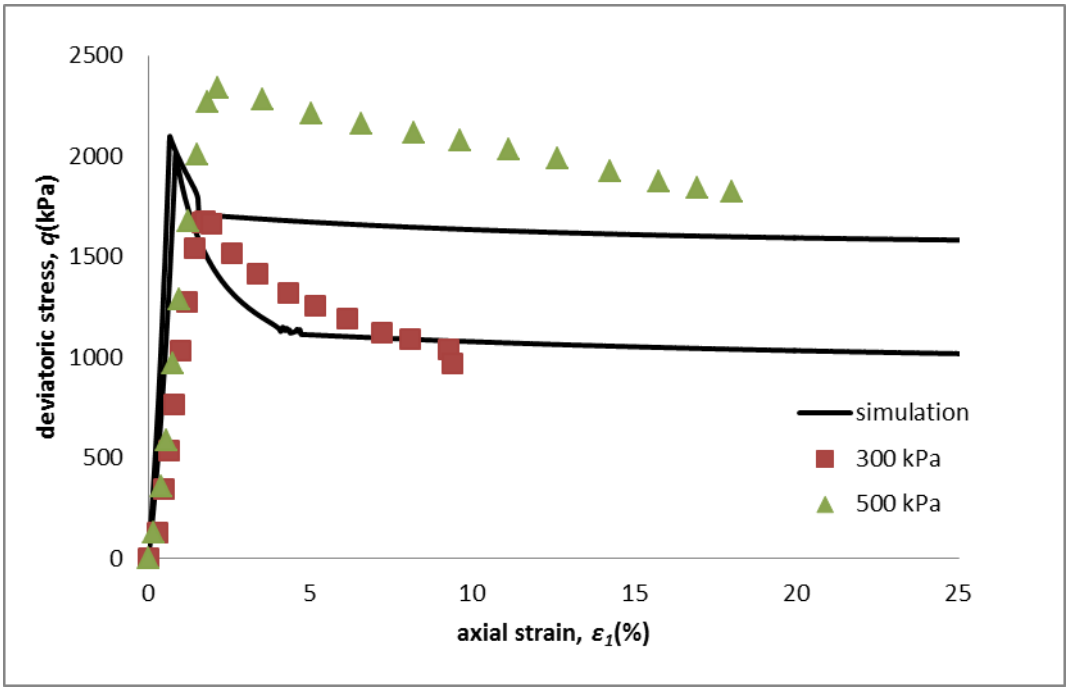

(a) Deviatoric stress and axial strain

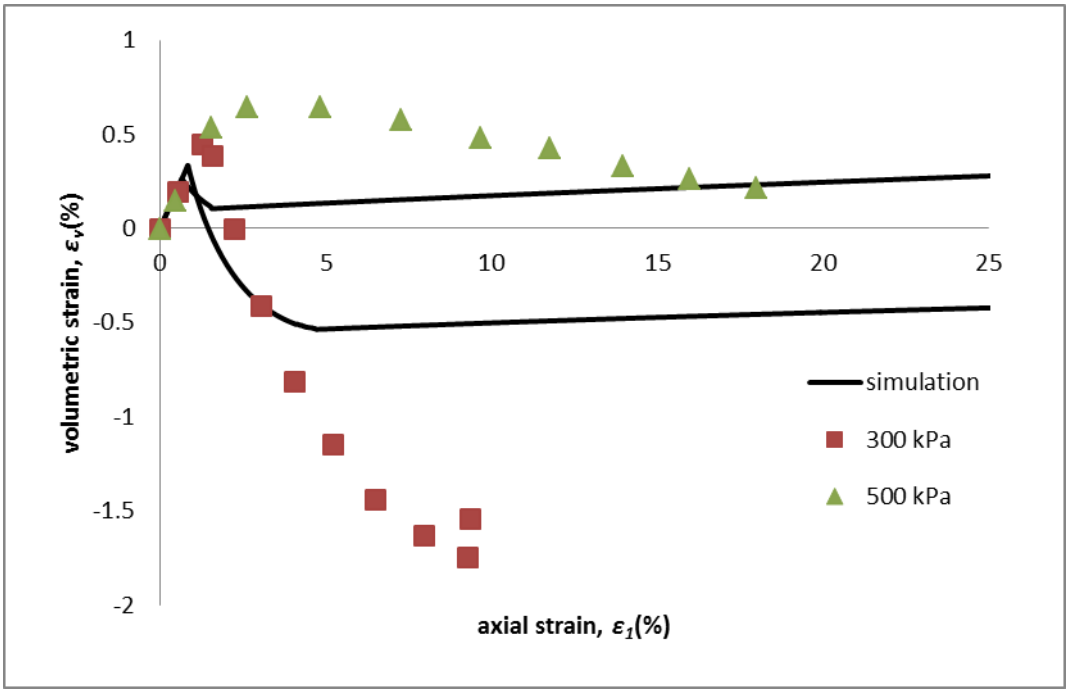

(b) Volumetric strain and axial strain

Fig 7.18 Drained triaxial tests on 1.5% cemented gravel sand (Asghari et al., 2003)

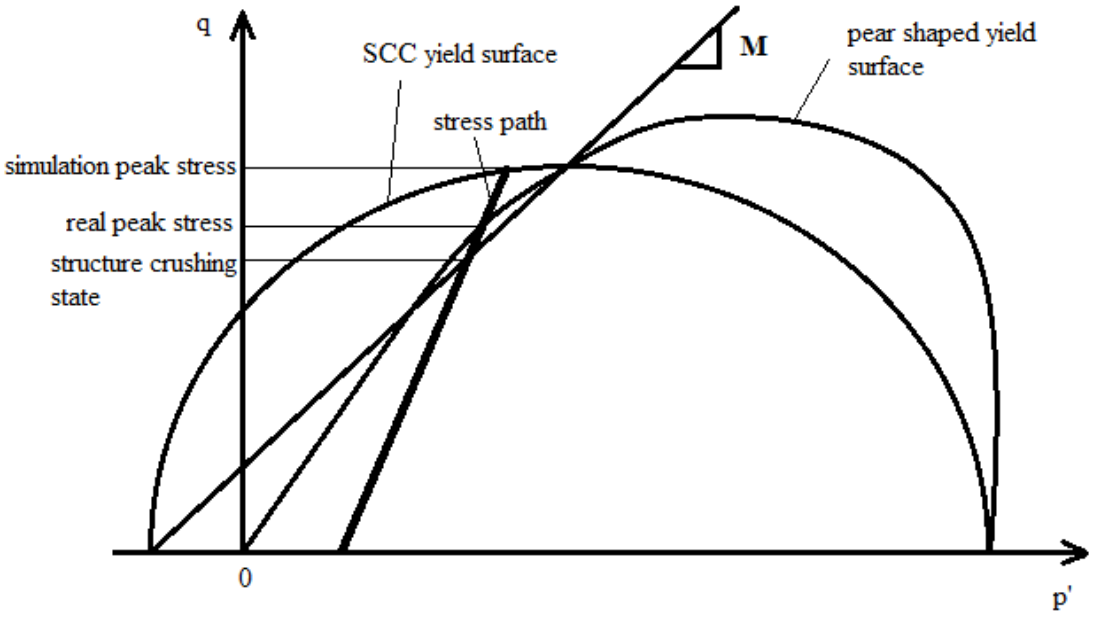

Fig 7.19 Simulation and test data peak stress comparison

7.3 Proposed equation assessment

7.3.1 Swelling index relating to cement content

All the simulation in this chapter adopts the experimental equation proposed in chapter 5. Equation 5.7 gives the relationship between cement content and swelling index κ^*. In this case, swelling index, which is independent of soil structure, will change with cementation. In order to demonstrate the improvement of the equation, the former simulated experimental data will be used again to carry out additional simulations without the influence of Equation 5.7. The comparative simulations are shown in Fig 7.20 and Fig 7.21.

Simulation 2 (represented by dashed lines), with the original swelling index shows less stiffness than the simulation with modified swelling index in elastic behaviour. Generally, this is the case. Some behaviour in Simulation 2 fits the experimental data better than the modified κ^* simulation as illustrated by Fig 7.20(b). However, the modification of κ^* reflects the real data better. Owing to the inaccurate assumption that

only elastic deformation takes place inside the yield surface and by ignoring the subyielding, the simulation is supposed to be less flexible than experimental data. For this reason, the simulation should be as stiff as or stiffer than experimental data and the modified κ^* simulation reflects this character.

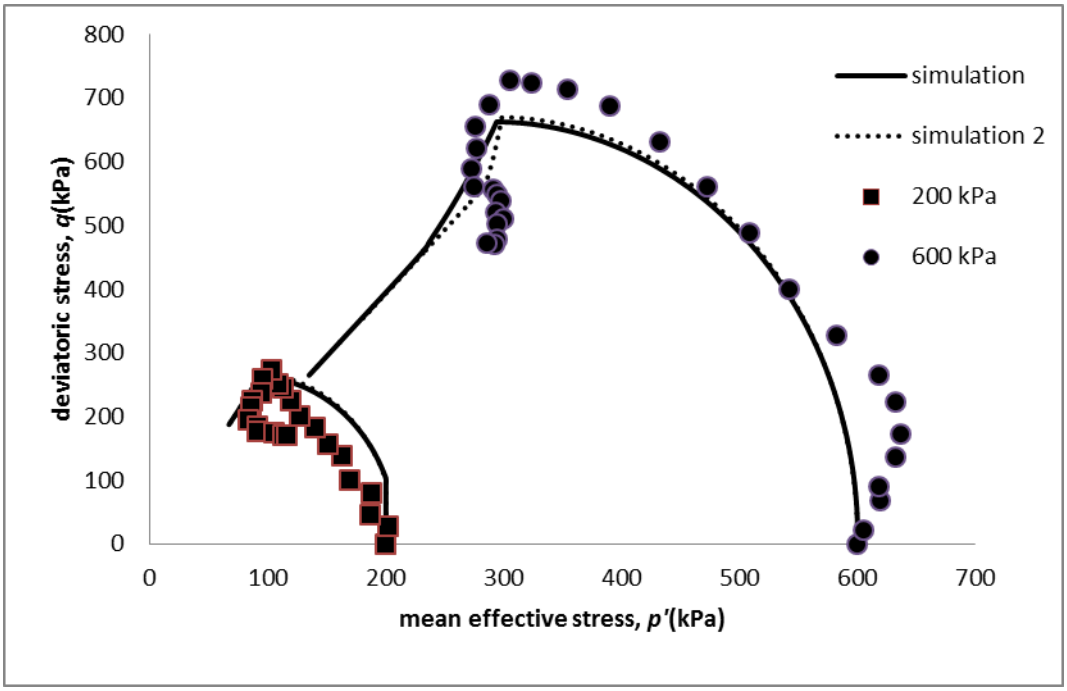

(a) Stress path

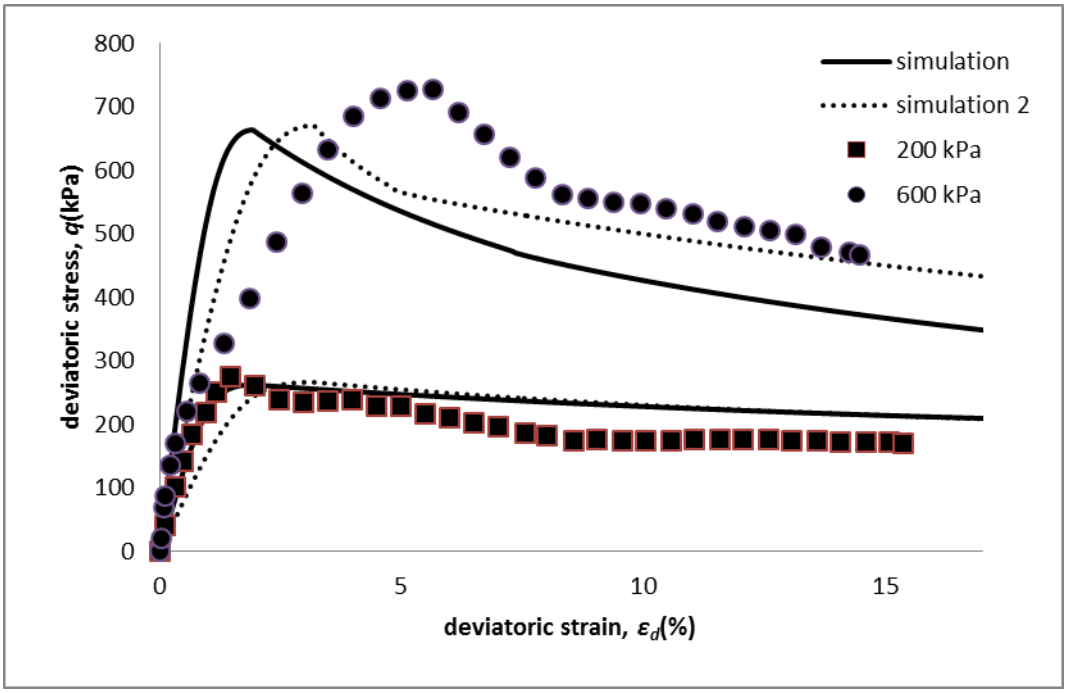

(b) Deviatioric stress and deviatoric strain

Fig 7.20 Undrained triaxial test simulation comparison on 9% cemented Ariake clay (Horpibulsuk et al., 2004)

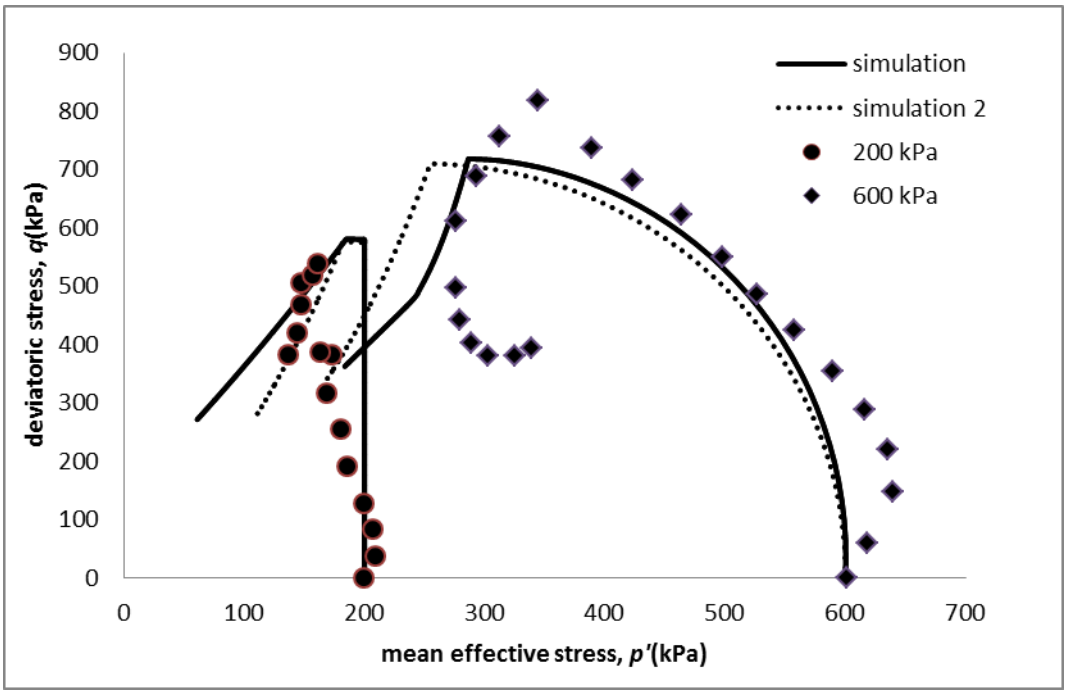

(a) Stress path

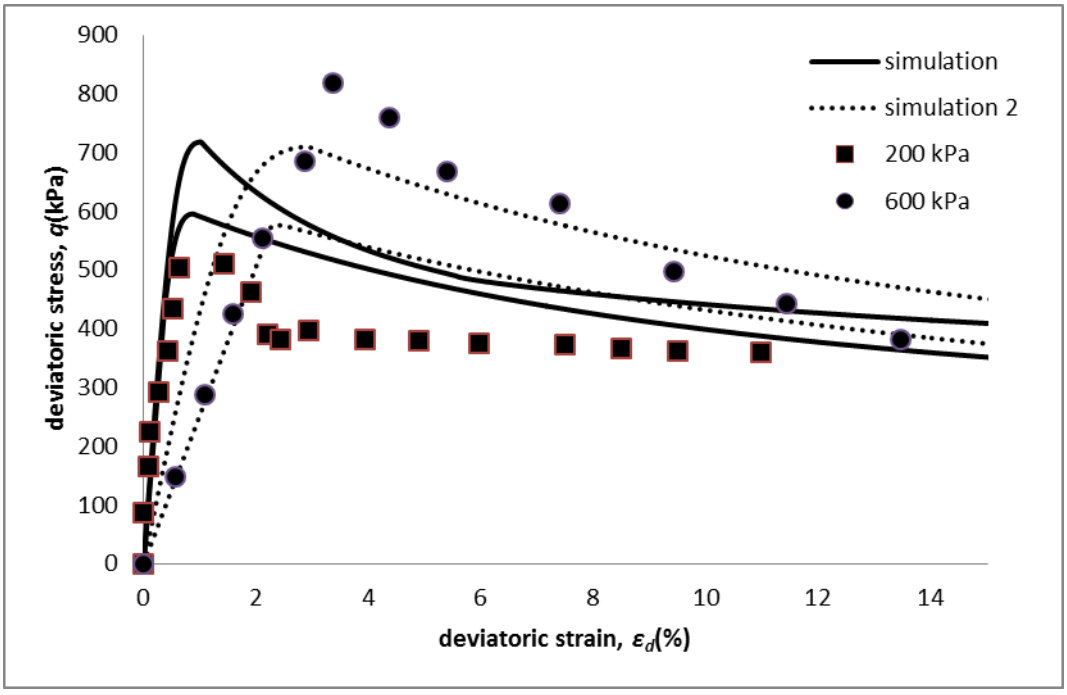

(b) Deviatoric stress and deviatoric strain

Fig 7.21 Undrained triaxial test simulation comparison on 12% cemented Ariake clay (Horpibulsuk et al., 2004)

7.3.2 Decementation in drained behavior

The simulation in gravel sand drained behaviour considered the influence of Equation 7.1. Fig 7.22 implies the influence of Equation 7.1 on the relationship between deviatoric strain and cementation. Also, the simulations with and without decementation in undrained behaviour are illustrated in Fig 7.23. Although they adopt the same parameters, the non-decemented simulation could not describe the soil structure behaviour appropriately. In Fig 7.23(a) at the beginning soil is elastic behaviour and then followed by softening behaviour. Therefore, the shear stress increases firstly and the decreases. There is a stable increase at the end in not decemented simulation. The reason of this phenomenon may be due to the fact that cementation force can not been removed completed in drained situations. It is mainly due to the type of problems, a new equation for the breakdown of cementation, i.e., equation 7.1, was suggested. Therefore, in the stress strain space, decementation ensures the stress would not behave inflexibly in the critical stress state. This reflects the definition of critical state correctly. However, the decementation has little effect on axial strain and volumetric strain behaviour.

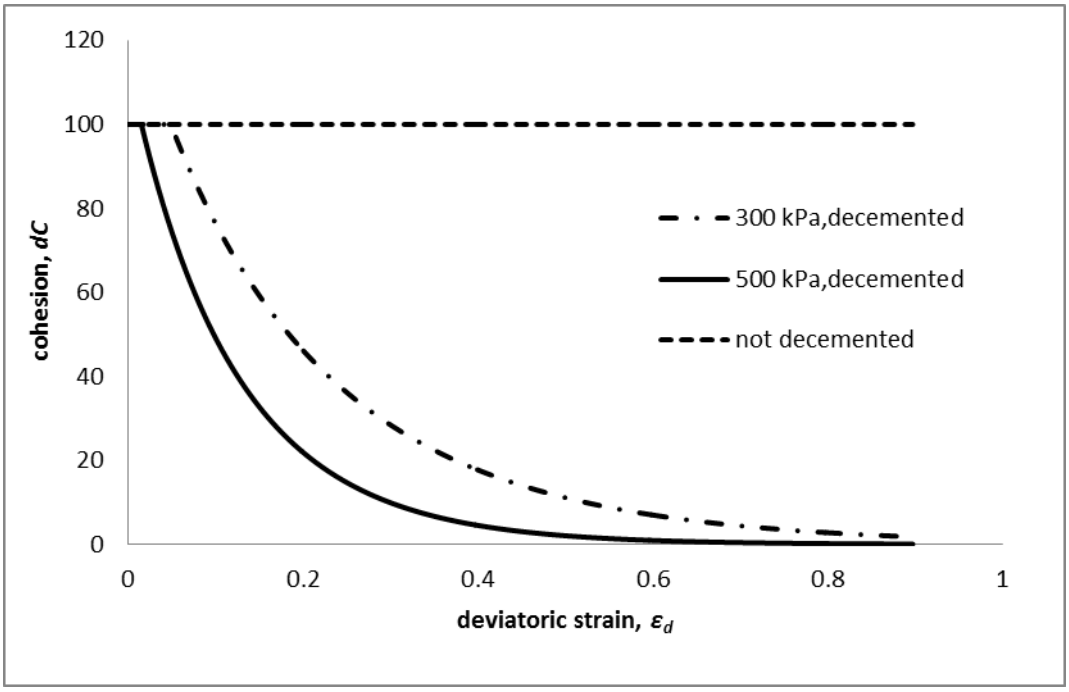

Fig 7.22 Devaitoric strain and current cementation for decemented and not decemented simulation

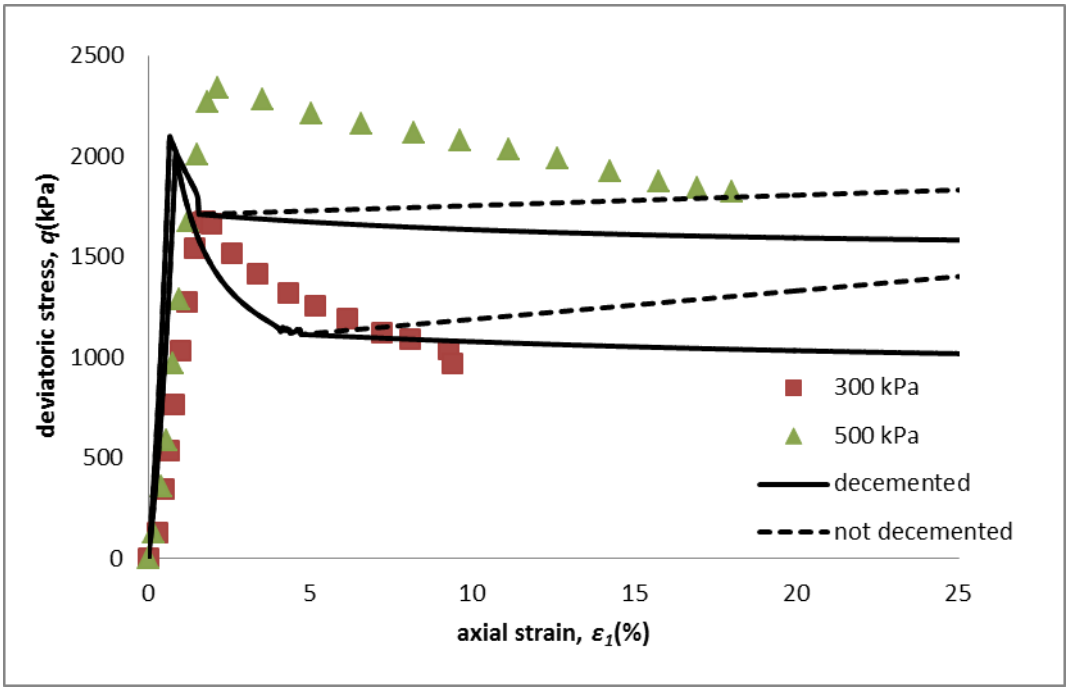

(a) Deviatoric stress and axial strain

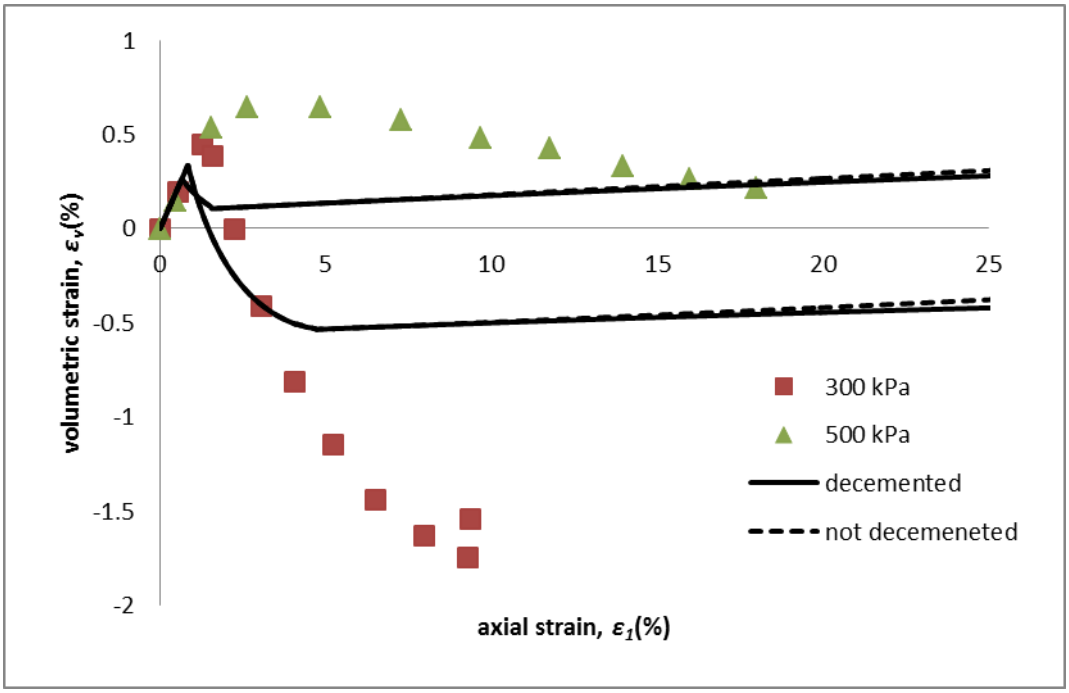

(b) Volumetric strain and axial strain

Fig 7.23 Drained triaxial test simulation comparison on 1.5% cemented Gravel sand (Asghari et al., 2003)

7.4 Summary

SCC extended to cemented soil is applied to describe the behaviour of three cemented clays and one cemented sand. The simulations include: drained and undrained conditions, sand and clay soils, and different cement contents. As compared with experimental data, soil behaviour in all the tests are all been reasonably captured. Some improvements in this model are also showed in simulations. firstly, the advantages of SCC over MCC is illustrated in simulation of Singapore marine clay. SCC is introduced softening at the end of tests based on MCC. The undrained simulations in cemented sand help detected a problem in SCC. Decementation is not well considered in drained behaviour and shows stiffness in cemented sand at the end of the test. Therefore, a new equation for decementation is proposed and assessed with simulations. Secondly, the advantage of proposed experimental equation which describe the relationship between swelling index and cement content has been assessed by simulation comparison. Significant improvement of model simulations are seen from the modification.

Chapter 8 A study on the yield surface

Literature review and simulations indicate that yield surface is so variable that elliptical yield surface could not describe all cases. By summarizing the variants of yielding surface, the possibility of a modification of the yield surface is studied. A new failure envelope is deduced and a new yield surface is proposed separately. Simulations on cemented soil stress paths and yield surfaces by the new yield surface are performed, leading to the study of the two introduced parameters of the new yield surface.

8.1 Summary of yield surface

As plenty of experiment data are investigated and many tests cases are simulated, some phenomenon can be found as follows:

1) Even if the cement rate in soil is very high, the soil stress path is unlikely to cross the stress ratio of 3. In other words, the failure envelope of 3 can cover the stress path for any case. There is no theory to explain or even clarify this phenomenon. This was, however, the experience in this case.

2) Soil with cohesion tends to produce a yield surface other than an elliptical one. When considering simulated cement treated soil, none follow the elliptical yield surface. This was particularly so for the high cemented specimens.

3) Subyielding is very common during elastic deformation. Stress paths tend to follow those of virgin yielding from inside the virgin yield surface at beginning. It is unlikely to expect an obvious virgin yielding point that divides elastic behaviour and plastic behaviour on the stress path.

4) The friction angle might be affected by cohesion. As a result, both cementation and decementation are able to change the M^* value. As decementation occurs during the whole process of testing in the real cases, the virgin yield surface is not stable, owing to changes in M^* throughout the test.

8.2 Deductions on the failure envelope

The scale at which the cementation increases the friction angle (or M^* value) is hard to identify. There are cases where the M^* value changes from 1.85 to 2.0 and even from 0.9 to 3.0 in the former simulation. An attempt is made in this section to determine the influence of cohesion on the stress ratio applicable to a cohesive soil.

Assuming cohesion is the only reason to increase the friction angle and no decementation occurs before the peak stress state, cohesion could be fully transferred to the extra friction angle. According to Coulomb theory, shear strength is written as:

$$\tau = C + \sigma tan\varphi \qquad 8.1$$

For cohesionless soil like sand, C=0. So, to transfer cohesion soil to cohesionless soil and find the effective friction angle, Equation 8.1 should be written as:

$$\tau = \sigma tan\varphi(C) \quad C \neq 0 \qquad 8.2$$

If Equation 8.1 is equal to Equation 8.2, the effective friction angle becomes a value that considers both the effect of cohesion and the intrinsic friction angle.

$$\tau = C + \sigma tan\varphi = \sigma tan\varphi(C) \qquad 8.3$$

$$\varphi(C) = tan^{-1}(\frac{C}{\sigma} + tan\varphi) \qquad 8.4$$

The effective friction angle, referred as φ(C) is a function of the variable parameter of cohesion. φ is the intrinsic friction angle. σ is the normal stress.

For

$$\sigma = \frac{1}{2}(\sigma_1 + \sigma_3) + \frac{1}{2}(\sigma_1 - \sigma_3)cos2\alpha \qquad 8.5$$

Where

σ_1 is the largest main stress of uncemented soil when the stress state reaches a peak without cohesion affecting the friction angle. The peak of the stress path of base soil can be deduced from the value of σ_1 in Equation 8.5.

$$q_{peak} = \sigma_{1peak} - \sigma_3 \quad 8.6$$

$$\sigma_1 = q_{peak} + \sigma_3 \quad 8.7$$

α is the angle between the direction of σ_3 and the stress cross section. In this case, the friction angle is adopted.

Substitute Equation 8.7 into Equation 8.5

$$\sigma = \frac{1}{2}\left(q_{peak} + 2\sigma_3\right) + \frac{1}{2}\left(q_{peak} - 2\sigma_3\right)cos2\varphi \quad 8.8$$

Combine Equation 8.4 and Equation 8.8

$$\varphi(C) = tan^{-1}\left(\frac{C}{\frac{1}{2}(q_{peak}+2\sigma_3)+\frac{1}{2}(q_{peak}-2\sigma_3)cos2\varphi} + tan\varphi\right) \quad 8.9$$

$$\varphi(C) = tan^{-1}\left(\frac{C}{q_{peak}cos^2\varphi+2\sigma_3 sin^2\varphi} + tan\varphi\right) \quad 8.10$$

For

$$M^* = \frac{6sin\varphi}{3 - sin\varphi}$$

Then the effective critical state strength parameter is:

$$M(C) = \frac{6sin\varphi(C)}{3-sin\varphi(C)} \quad 8.11$$

$$M(C) = \frac{6\,sin\,tan^{-1}\left(\frac{C}{q_{peak}cos^2\varphi+2\sigma_3 sin^2\varphi}+tan\varphi\right)}{3-sin\,tan^{-1}\left(\frac{C}{q_{peak}cos^2\varphi+2\sigma_3 sin^2\varphi}+tan\varphi\right)} \quad 8.12$$

In this equation, the only unknown variable is cohesion. The effective critical state stress ratio Equation 8.12 adopts the same frame work as the original equation. Therefore, Equation 8.12 still retains 3 as the maximum value. The value can only be

amplified by cohesion. As discovered previously, subyielding, accompanied by decementation, tends to take place in elastic behaviour and is hard to quantify. This equation is based on the assumption that decementation would not occur before the peak deviatoric stress is reached, which is the same as the assumption for SCC extended to cemented soil.

Although a way to transfer cohesion to critical state stress ratios is being sought, it is not easily adopted into SCC. It was found that cohesion and the friction angle are mutually correlated and both affect soil strength. The scale that each of them influences soil is hard to define. Whether it is a "friction-dominated", "cementation-plus-friction" or "cementation-dominated" failure pattern, there should be a failure envelope to cover all of the stress states for each soil. This envelop is a combination of the section of CSL from Equation 5.1 and *M(C)* from 8.12 (Fig 8.1).

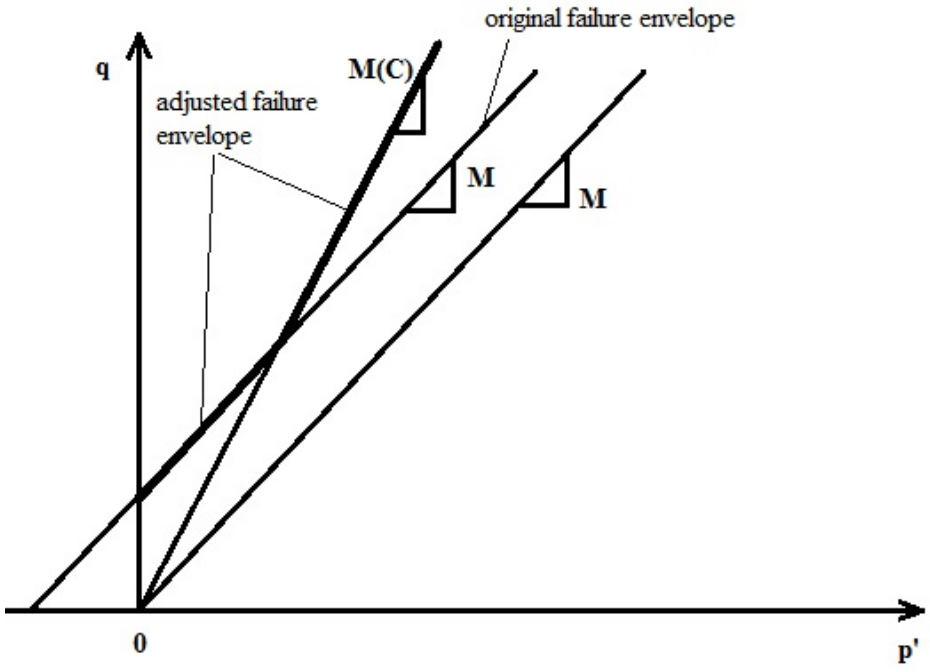

Fig 8.1 New failure envelope for cemented soil

8.3 New yield surface

Based on the former investigation, the original elliptical yield surface is unable to adequately describe the complex yield surface. There are some characteristics that should be included in yield surface experiments.

1) The value of the critical state parameter should be adjustable so that it reflects the influence of cohesion. Fig 8.2 indicates the adjusted M^* value in simulating increased height width ratio of the yield surface. However, this adjustment alone could not ideally model the two types of yield surface in Fig 8.2.

2) The inclination of yield surface should be altered to take into consideration the inclination of stress path test data. Here, although the value of M^* can change the height width ratio of the yield surface, the stress path is unlikely to follow the elliptical tendency exactly. It usually moves to the right or left from the elliptical yield surface before reaching CSL. In this case, even peak deviatoric stress might not locate to the critical state line (see two types of stress path in Fig 8.2).

To meet all the requirements, the new yield surface is proposed as:

$$q = A * M^* * p' * [\ln(\frac{p_0}{p'})]^N \qquad 8.13$$

A is the aspect ratio index. It determines the height of the yield surface. This parameter works in the same way as in Equation 8.12 but this equation has a simpler pattern.

Parameter N determines the inclination of the yield surface. It can distort the yield surface diagonally.

The CSL might not exceed the peak deviatoric stress and the mean effective stress of the peak is not necessarily located on the centre of the yield surface. Meanwhile, the new yield surface is less likely to surpass the stress ratio of 3 than the elliptical yield

surface. These characteristics suggest the yield surface could simulate a “pear shaped” stress path.

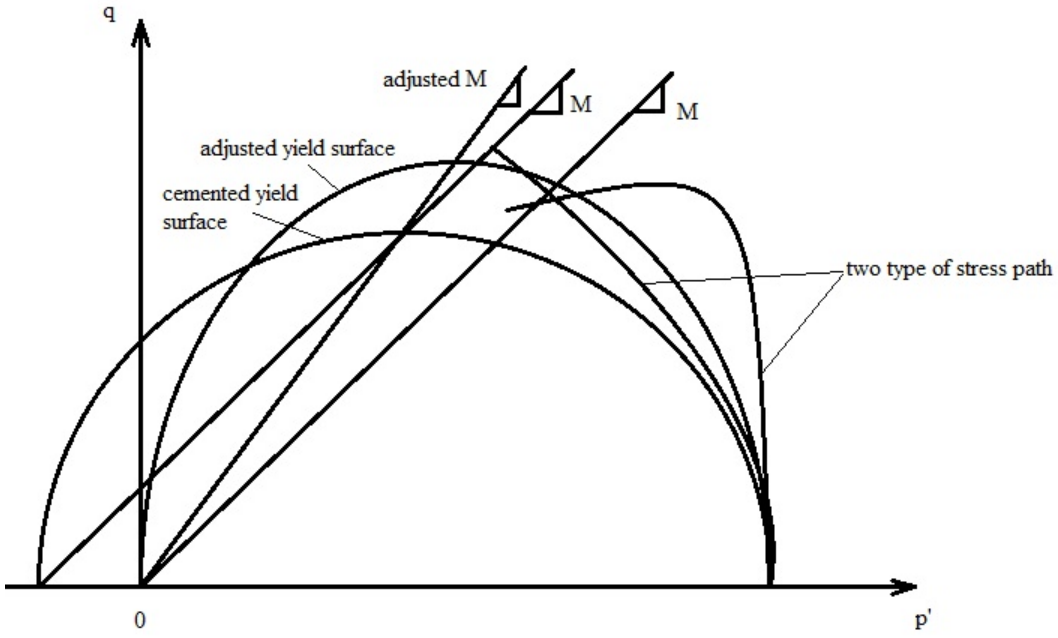

Fig 8.2 Stress path and elliptical yield surface for cemented soil

8.4 Yield surface simulation

Three cemented soil yield surfaces are simulated by the new yield surface equation which implies that the new yield surface parameters are meaningful for simulation.

Fig 8.3 includes a group of unified yield surface data from Huang (1994). The same base soils with different cement contents all follow the irregular yield surface “pear shape”. Still, the new yield surface describes the shape appropriately. Looking at the two parameters in this yield surface, parameter N has no change in this case while the aspect ratio index A increases with the cement content. None of the A values is less than 1, which implies the earlier conclusion that cohesion amplifies the effective friction angle and increases soil strength. The simulation parameters are listed in Table 8.1.

As predicted in Fig 8.2, the capacity of the new yield surface is seen to represent the yield surfaces for various cement rates. SCC yield surface is able to capture the yield surface of 0% in this simulation. But it can not matches the yield surfaces with cementation, particularly for the high cement content tests (see Fig 8.4).

Table 8.1 Parameters of yield surface from Huang (1994)

	P_0	M^*	A	N
0%	1.25	0.85	1.2	0.5
5%	1.35	0.85	1.5	0.5
10%	1.43	0.85	1.85	0.5
20%	1.7	0.85	2.65	0.5

The second simulation concerns the stress path of Ariake clay. This simulation applies stress paths as an indication of the shape of the yield surface. It is obvious that the new yield surface captures the stress path better than the elliptical yield surface. The test groups with elastic stress state at the beginning are not simulated to avoid the complication of subyielding. The simulation parameters are listed in Table 8.2 and the simulation results are shown in Fig 8.5, Fig 8.6 and Fig 8.7.

Table 8.2 Parameters of yield surface from Horpibulsuk et al. (2004)

	P_0 (kPa)	M^*	A	N
6%	100	1.85	1.4	0.75
	200	1.85	1.5	0.75
	400	1.85	1.4	0.75
9%	200	1.85	2	0.8
	400	1.85	1.6	0.8
	600	1.85	1.65	0.65
12%	400	1.85	1.95	0.75
	600	1.85	1.8	0.6
	1000	1.85	2	0.7

Yield surfaces are also plotted and simulated based on the research data of Huawen (2009). Two of the tests are used to simulate with the new yield surfaces. Their cement content is 10% and 30% respectively. Both of the samples for these tests are prepared in 100% water content. The simulation parameters and results are showed in Table 8.3, Fig 8.8 and Fig 8.9.

The new yield surface is successfully to describe the yield locus with the same value of *M*. With the slight irregular yield surface reshape as the preconsolidate stress change, the new yield surface still able to catch the shape. The parameter A and N brought flexibility to yield surface.

Table 8.3 Parameters of yield surface from Huawen (2009)

	P_0 (kPa)	M^*	A	N
10%	130	0.85	4.5	0.45
	300	0.85	3	0.5
	500	0.85	3	0.75
	1000	0.85	2.7	0.7
	1500	0.85	2.6	0.76
	2000	0.85	2.45	0.7
	2500	0.85	2.4	0.73
30%	355	0.85	5	0.5
	500	0.85	4.3	0.7
	1000	0.85	3.3	0.7
	1500	0.85	3	0.7
	2000	0.85	3	0.68
	2500	0.85	2.9	0.68

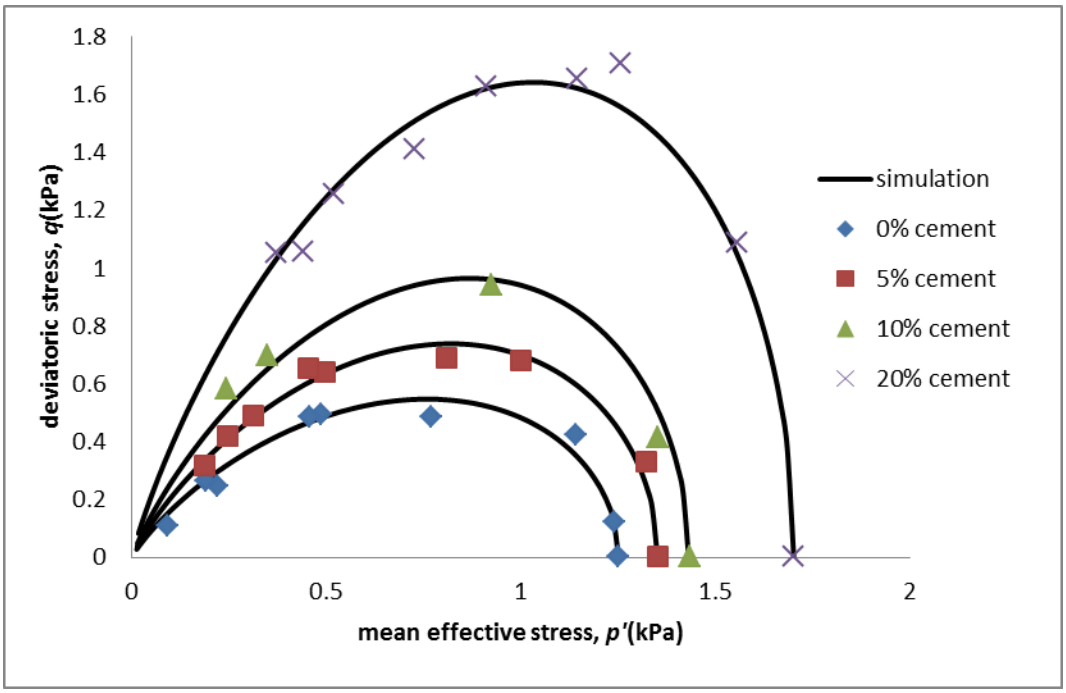

Fig 8.3 New yield surface simulation (Huang, 1994)

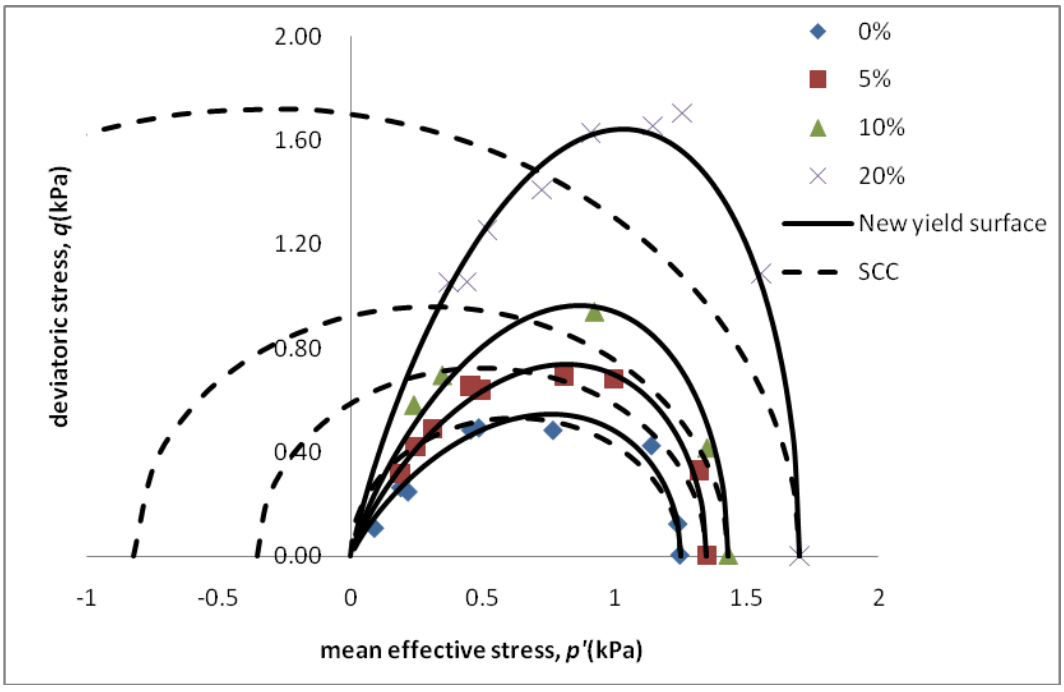

Fig 8.4 Yield surface simulation comparison (Huang, 1994)

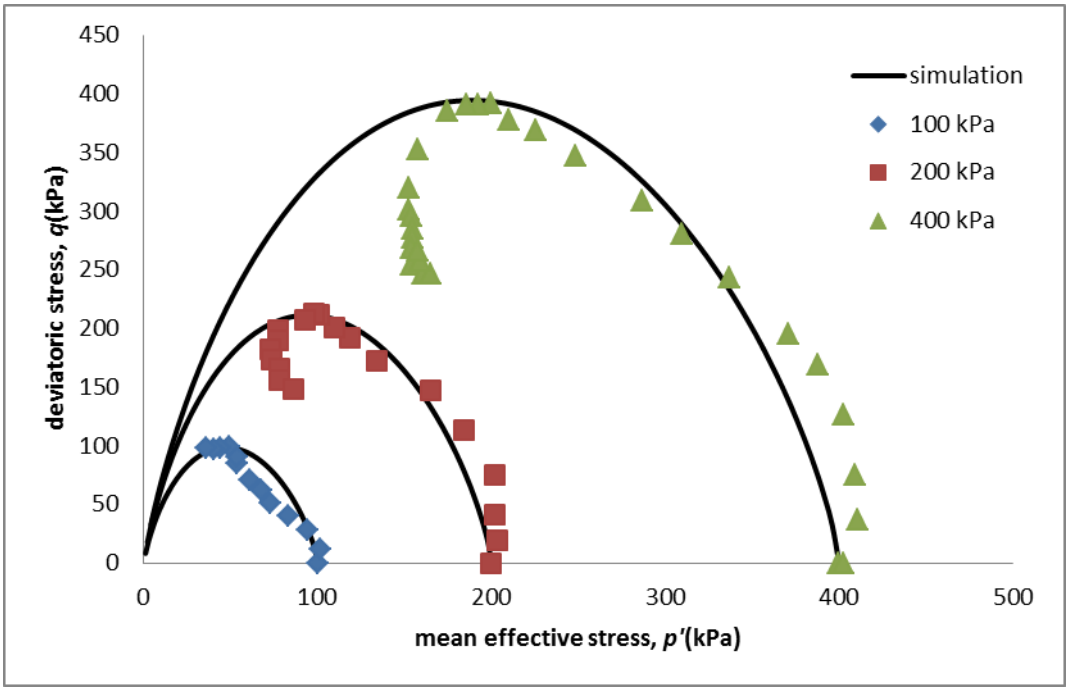

Fig 8.5 New yield surface simulation of 6% cemented Ariake clay (Horpibulsuk et al., 2004)

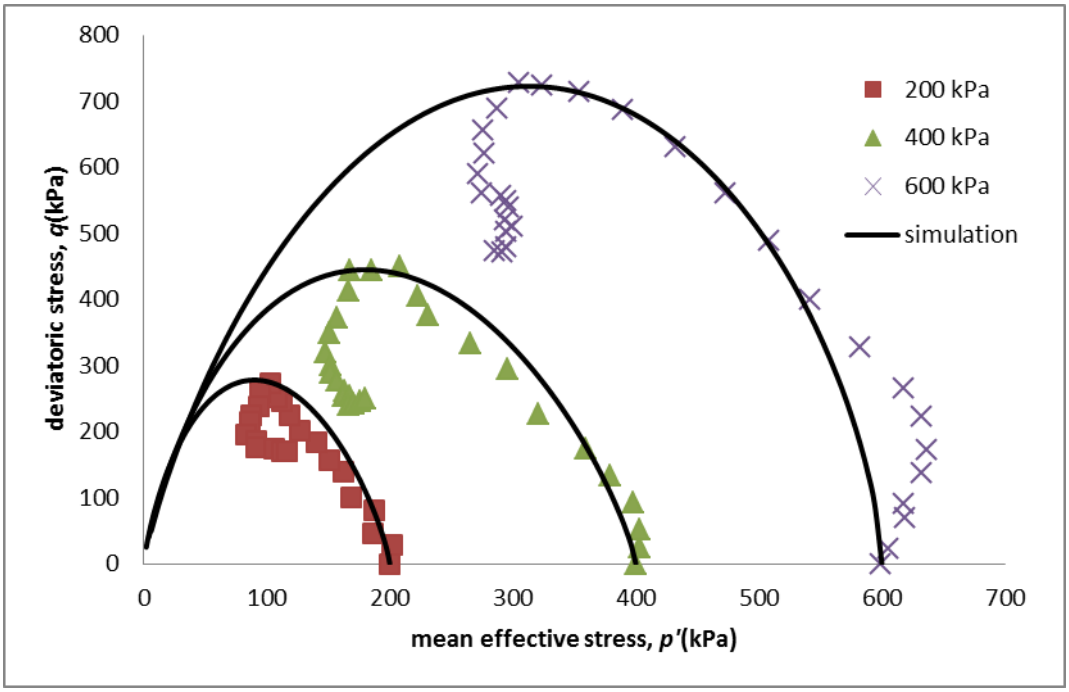

Fig 8.6 New yield surface simulation of 9% cemented Ariake clay (Horpibulsuk et al., 2004)

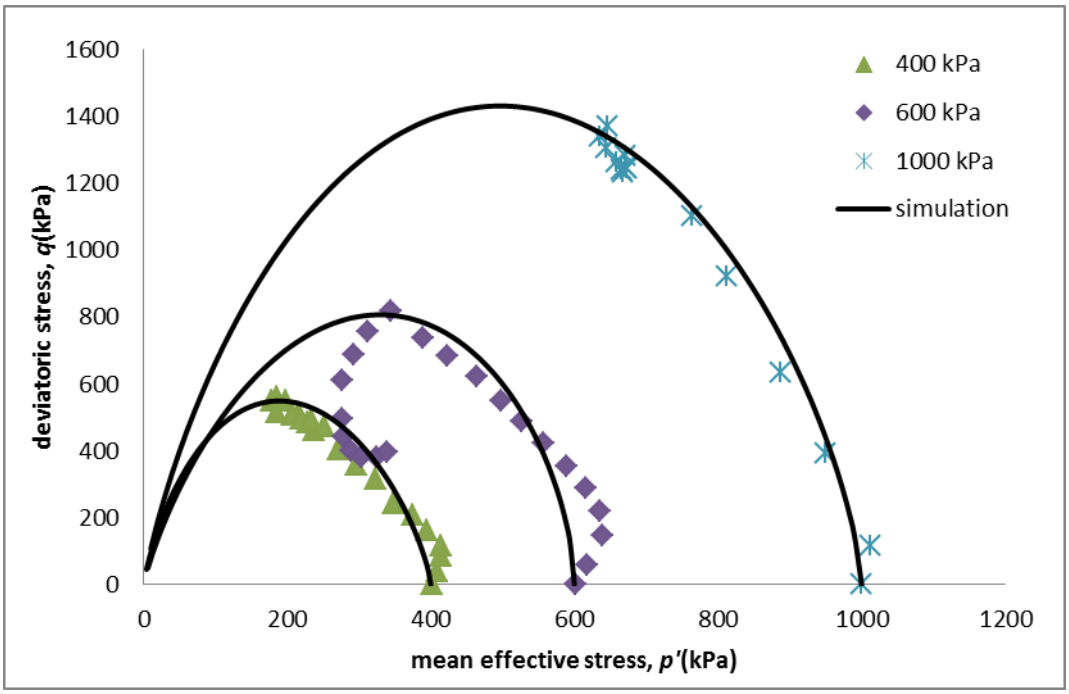

Fig 8.7 New yield surface simulation of 12% cemented Ariake clay (Horpibulsuk et al., 2004)

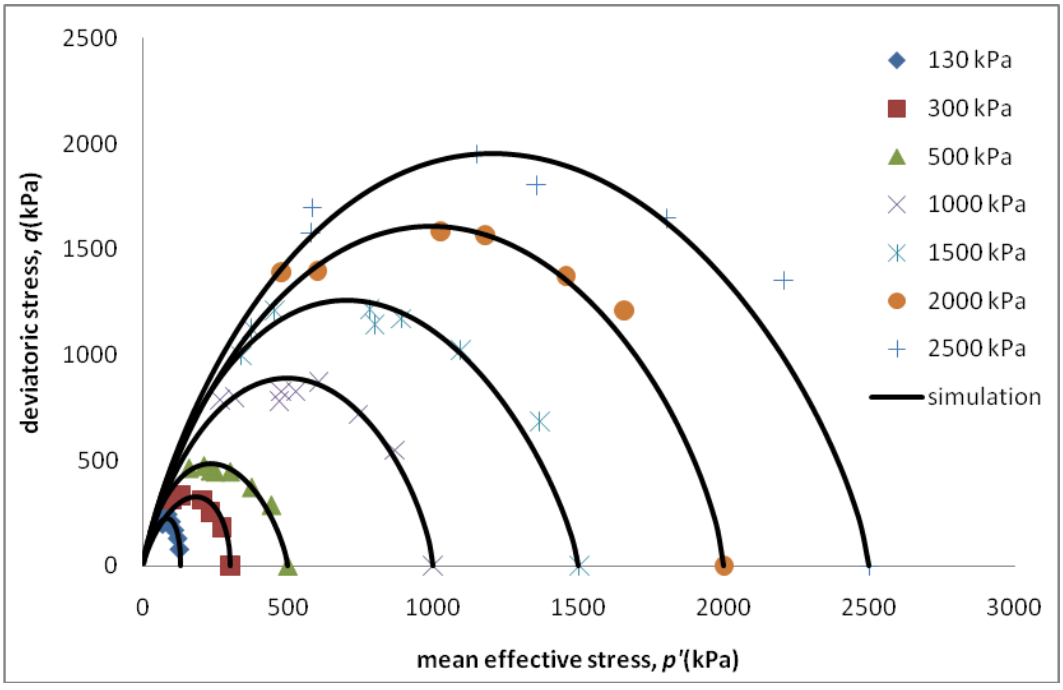

Fig 8.8 New yield surface simulation of 10% cemented Singapore marine clay (Huawen, 2009)

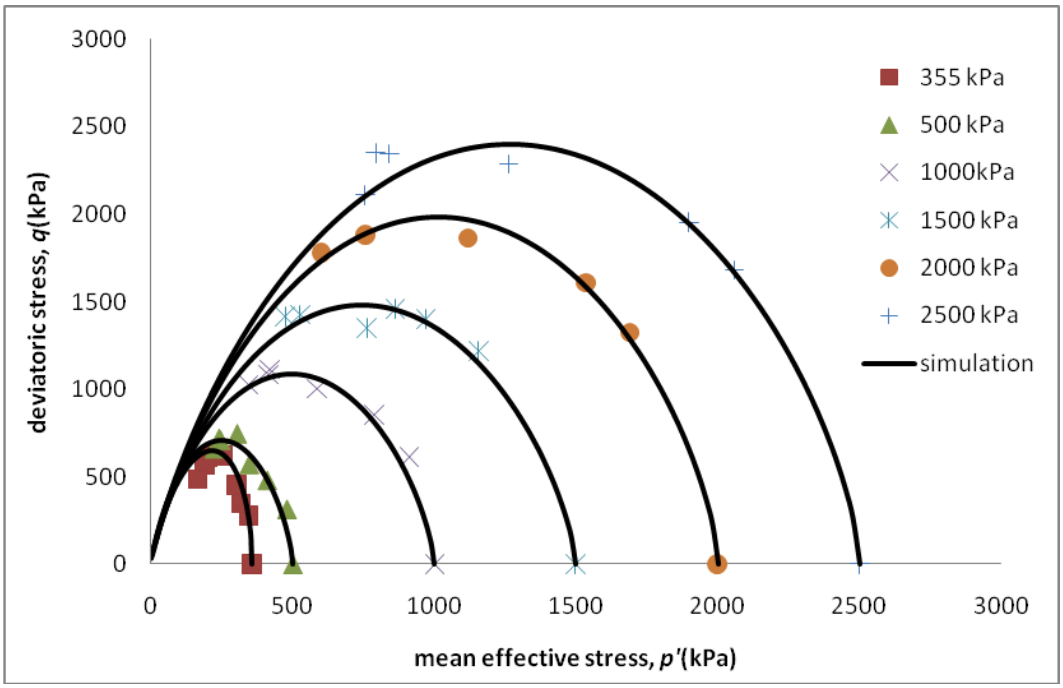

Fig 8.9 New yield surface simulation of 30% cemented Singapore marine clay (Huawen, 2009)

8.5 Summary

Based on the character of soil stress paths, some problems of traditional yield surface are discussed. A new yield surface is suggested and two new parameters are introduced to the original Cam Clay yield surface. Some initial study of the new yield surface is made and it appears to be useful. The distortion of the yield surface associated with cementation is complicated, and a rational description of anisotropic distortion of the yield surface is highly challenging. In this study a very limited work on mathematical representation of the shape of the surface is made. However, the new yield surface allows isotropic model simulate complex soil behaviour.

Chapter 9 Conclusions and suggestions for further studies

SCC for cemented soils has been presented. Parameters in SCC are discussed with respect to their significance in this model, the origination of these parameters, identification methods and the effects parameters have on soil behaviour. The main work is on investigating the behaviour of cemented soil. The following are the useful conclusions based on this study.

1. An empirical equation for the relationship between cementation and swelling index is proposed. This equation is based on the study of eight groups of experimental data. It is found that sand obeys the equation better than clay.
2. Cemented Ariake clay, Singapore marine clay and cemented gravel sand are simulated via SCC. Generally, SCC simulates cemented soil well. Among these cases, Ariake clay and Singapore marine clay show a distorted yield surface with a magnified height width ratio on the right hand side. This is partly attributed to subyielding and decementation at the virgin yielding stage and elastic behaviour state. As anisotropic behaviour is not considered in SCC, the method to improve the model to predict cemented soil behaviour includes adjusting parameters and yield surface. For Ariake clay, when the change of swelling index with cement content is considered, better simulations of the soil behaviour are obtained. For Singapore marine clay, two types of simulations have been made. The first is based on the peak strength measure, and the second is on the stress path. It is obvious that none of the simulations can capture the characteristics of cemented soil completely. A comparison between SCC simulations and MCC simulations is also made. The performance of the SCC is significantly better than that of the MCC.
3. A problem in SCC was found during the drained behaviour of cemented gravel sand simulation. SCC does not give good description of decementation in drained tests. A

new equation for the breakdown of cementation during drained test simulation is proposed. Thus, SCC can simulate both drained and undrained tests.

4. The mechanical properties of loess are reviewed. Simulations of the stress and strain behaviour of Ma Lan Loess are made via the theoretical framework of SCC, with the added effect of a glutinous ingredient in loess to be modeled as a cementation effect. It is seen that the SCC can provide an approximate estimation of the behaviour of the loess. Therefore loess is essentially a frictional material, and its behaviour can be represented by conventional elastoplastic models.
5. Based on the problems encountered in simulations, a new yield surface is proposed. Two parameters are introduced in the new yield surface and the surface is assessed. Different soils have different height width ratios of yield surface and the distortion of the stress path may be captured. It is highly promising that the proposed equation and the new yield surface could be adopted in the constitutive model.

Further study of SCC is required on the following aspects.

1. SCC only considers isotropic deformation. More work should be carried out in anisotropic deformation of soils.
2. Subyielding and decementation before virgin yielding should be included in SCC. It is proved in this thesis that these two factors can influence soil behaviour significantly.
3. Updating the yield surface could be a good direction for more Cam Clay study. A better yield surface should be proposed with fewer new parameters. Then the yield surface can replace the elliptical one in SCC and achieve a more accurate simulation of cemented soil.

References

Ahnberg H. (2007), "On yield stresses and the influence of curing stresses on stress paths and strength measured in triaxial testing of stabilized soils", *Can. Geotech. J*, Vol.44, pp.54-66.

Asghari E., Toll D.G. and Haeri S.M. (2003), "Triaxial behaviour of a cemented gravely sand, Tehran alluvium", *Geotechnical and Geological Engineering*, Vol.21, pp.1–28.

Bobet A., Hwang J., Johnston C.T., and Santagata M. (2011), "One-demensional consolidation behaviour of cement-treated organic soil", *Can. Geotech. J*, Vol.48, pp.1100-1115.

Carter J.P. and Liu M.D. (2005), "Review of the Structured Cam Clay model", *Soil constitutive models: evaluation, selection, and calibration*, ASCE, Geotechnical special publication, No.128, pp.99-132.

Chen C., Zhu Z. and Gao P. (2006), "Research on relationship between structure and deformation property of intact loess", *Rock and Soil Mechanics*, Vol.27, No.11, pp.1892-1896.

Chen H., Yan H. and Zhang J. (2011), "Study on strength forming process of cement stabilized soil", *Advanced Materials Research*, Vol. 250-253, pp.1707-1710.

Chiu C.F., Zhu W. and Zhang C.L. (2008), "Yielding and shear behaviour of cement-treated dredged materials", *Engineering Geology*, Vol.103, pp.1-12.

Clough, G.W., Sitar, N., Bachus, R.C. and Rad, N.S. (1981), "Cemented sands under static loading", *Journal of the Geotechnical Engineering Division*, ASCE, Vol.107, No.6, pp.799-817.

Consoli N.C., Rosa A.D., Corte M.B., da Silva Lopes Jr. L. and Consoli B.S. (2011), "Porosity-Cement Ratio Controlling Strength of Artificially Cemented Clays", *Journal of Material in Civil Engineering*, ASCE, Vol. 23, No. 8, pp.1249-1254.

Edward D.P., Joseph A. and Waxse, P.E., (2009), "Know more about loess", *Geo-Strata*, July/August 2009, pp.31-35.

Horpibulsuk S., Liu M.D., Liyanapathirana D.S. and Suebsuk J. (2010), "Behaviour of cemented clay simulated via the theoretical framework of the Structured Cam Clay model", *Computers and Geotechnics*, Vol.37, pp.1–9.

Horpibulsuk S., Suebsook J., Liu M.D. and Carter J.P., "Simulation of undrained shear behaviour of cemented clay with the modified Structured Cam Clay model".

Hu Z., Shen Z. and Xie D. (2004), "Deformation properties of structural loess", *Chinese Journal of Rock Mechanics and Engineering*, Vol.23, No.24, pp.4143-4145.

Huang M., Liu Y. and Sheng D. (2011), "Simulation of yielding and stress–stain behavior of shanghai soft clay", *Computers and Geotechnics*, Vol.38, pp.341–353.

Juarez-Badillo E. (2012), "Discussion of 'One-dimensional consolidation behaviour of cement-treated organic soil'", *Can. Geotech. J*, Vol.49, pp.743-745.

Kasama K., Ochiai H. and Yasufuku N. (2000), "On the stress-strain behaviour of lightly cemented clay based on an extended critical state concept", *Soils and Foundations*, Vol.40, No.5, pp.37-47.

Kasama K., Zen K. and Iwataki K. (2006), "Undrained shear strength of cement-treated soils", *Soil and Foundations*, Vol. 46, No. 2, pp.221-232.

Khalili N., Habte M.A. and Valliappan S. (2005), "A bounding surface plasticity model for cyclic loading of granular soils", *Int. J. Meth. Engng*, Vol. 63, pp.1939-1960.

Li J.L. and Yao Y.P. (2009), "Critical state model of K_0-comsolidated structure loess", *J.Xi'an Univ. of Arch. & Tech. (Natural Science Edition)*, Vol.42, No.4, pp.533-537.

Liu M.D. and Carter J.P. (1999), "Virgin compression of structured soils", *Géotechnique*, Vol. 49, No.1, pp.43-57.

Liu M.D. and Carter J.P. (2002), "On the volumetric deformation of reconstituted soils", *International journal for numerical and analytical methods in geomechanics*, Int. J. Numer. Anal. Meth. *Geomech*, Vol.24, pp.101-133.

Liu M.D. and Carter J.P. (2002), "Structured Cam Clay Model", *Canadian Geotechnical Journal*, Vol.39, No.6, pp.1313-1332.

Liu M.D. and Carter J.P. (2003), "The volumetric deformation of natural clays", *International Journal of Geomechanics*, ASCE, Vol 3, No.3/4, pp.236-252.

Liu, M.D. and Carter, J.P. (2000), "Modeling the destructuring of soils during virgin compression", *Geotechnique*, Vol.50, No.4, pp.479-483.

Liu, M.D., Carter, J., and Dasai, C.S. (2003), "Modeling compression behavior of structured geomaterials", *International Journal of Geomechanics*, ASCE, Vol.3, No.2, pp.191-204.

Lorenzo G.A. and Bergado D.T. (2004), "Fundamental parameters of cement-admixed clay-new approach", *Journal of geotechnical and geoenvironmental engineering*, ASCE, Vol.130, No.10, pp.1042-1050.

Lorenzo G.A. and Bergado D.T. (2006), "Fundamental characteristics of cement-admixed clay in deep mixing", *Journal of materials in civil engineering*, ASCE, Vol.18, No. 2, pp.161-174.

Moses G.G., Rao S.N. and Rao P.N. (2003), "Undrained strength behaviour of a cemented marine clay under monotonic and cyclic loading", *Ocean Engineering,* Vol.30 pp.1765–1789.

Pekau O.A. and Gocevski V. (1989), "Elastro-plastic model for cemented and pure sand deposits", *Computers and Geotechnics,* Vol.7, pp.155-187.

Pillai R.J., Bushra I. and Robinson R.G. (2013), "Undrained triaxial behavior of cement treated marine clay", *Geotech Geol Eng,* Vol.31, pp 801-808.

Rekik B. and Boutouil M. (2009), "Geotechnical properties of dredged marine sediments treated at high water/cement ratio", *Geo-Mar Lett,* Vol.29, pp171-179.

Rouainia M. and Muir Wood D. (2000), "A kinematic hardening model for natural clays with loss of structure", *Géotechnique,* Vol.50, No.2, pp.153-164.

Sariosseiri F. and Muhunthan B. (2009), "Effect of cement treatment on geotechnical properties of some Washington State soils", *Engineering Geology,* Vol.104. pp.119-125.

Schmertmann J.H. (1991), "The mechanical aging of soils", *J. Geotechnical Engineering,* ASCE, Vol.117, No.9, pp.1288-1330.

Scott R.F. (1985), "Plasticity and constitutive relations in soil mechanics", *J. Geotechnical Engineering,* ASCE, Vol.111, No.5, pp.563-605.

Shao S.J. and Deng G.H. (2008), "The strength characteristics of loess with different structures and its application in application in analyzing the earth pressure on loess tunnel", *China civil engineering journal,* Vol.41, No.11, pp.93-98.

Shao S.J., Long J.Y., Yu Q.G. and Zhou F.F. (2006), "A constitutive model of collapsible loess with structural parameter", *Shuilixuebao,* Vol.37, No.11, pp.1316-1322.

Shao S.J., Luo A.Z., Yu Q.G. and Zhou F.F. (2006), "Structural damage properties of Q_3 loess under triaxial loading and moistening", *Chinese Journal of Geotechnical Engineering*, Vol.28, No.12, pp.2078-2081.

Tsuchida T., Tang Y.X. and Watabe Y. (2007), "Mechanical properties of lightweight treated soil cured in water pressure", *Soils and Foundations*, Vol. 47, No. 4, pp.731-748.

Whittle A.J. (1993), "Evaluation of a constitutive model for overconsolidated clays", *Géotechnique*, Vol. 43, No.2, pp.289-314.

Wood D.M. (1990), *Soil Behaviour and Critical State Soil Mechanics*, Cambridge University Press.

Xiao H.W. (2009), "Yielding and failure of cemented treated soil", Ph.D. dissertation, National university of Singapore.

Yao Y.P., Sun D.A. and Luo T. (2004), "A critical state model for sands dependent on stress and density". *International Journal for Numerical and Analytical Methods in Geomechanics*, Vol.28, pp. 323-337.

Yao Y.P.，Hou W. and Zhou A.N. (2009), "UH model：three-dimensional unified hardening model for overconsolidated clays". *Géotechnique*，Vol.59, No.5, pp451–469.

Yasufuku N., Ochiai H. and Kasama K. (1997), "The dissipated energy equation of lightly cemented clay in relation to the critical state model", *Proc. 9 th Int. Conf the International/ Association for Computer Methods and Advances in Geomechanics*, Vol.2, pp.917-922.

Appendix

SIMULATING THE STRESS AND STRAIN BEHAVIOR OF LOESS VIA SCC MODEL

M.D. LIU
Faculty of Engineering, University of Wollongong, Australia, martindl@uow.edu.au

J. LIU
Faculty of Engineering, University of Wollongong, Australia, jl370@uow.edu.au

S. HORPIBULSUK
Civil Engineering, Suranaree University of Technology, Thailand, suksun@g.sut.ac.th

W. HUANG
College of Mechanics and Materials, Hohai University, China, wh670@hhu.edu.cn

The behaviour of collapsible soils (loess) is studied in this paper. Simulations of the stress and strain behaviour of the soil are made via the theoretical framework of Structured Cam Clay, with the effect of glutinous ingredient in loess suggested to be modelled as cementation effect. Based on the simulations, the capacity of the model for representing the behaviour loess is investigated, and discussions on modelling the behaviour of collapsible soil in general are given.

INTRODUCTION

Loess, found in many parts of the world, has been proved to be engineering challenge because of its collapsible nature [e.g., 1, 2, 3]. The soil possesses features of structured soil, and undergoes dramatically destructuring when it is wetted, disturbed, or loaded. Compared with natural clays, the study on the collapsible nature of the mechanical properties of loess both laboratory tests and theoretical modelling are relatively less investigated. Recently, there have been useful advances in constitutive modelling of natural soft soils [e.g., 4, 5]. In this paper, the mechanical properties of loess are investigated. A primary study is performed on the capability of the Structured Cam Clay modified for cementation effect proposed by Horpibulsuk et al [6] for representing the behaviour of loess and some discussions on model parameters for loess are also made.

MECHANICAL PROPERTIES OF NATURAL LOESS

Loess is structured soil and frequently strongly structured. The original structure of loess may undergo dramatically destructuring when it is wetted, loaded or disturbed, normally leading to the reduction of the strength and stiffness of the soil. Based on the examination of some available experimental data [e.g., 1, 2, 3, 7, 8], some special mechanical properties of loess are found.

(1) The structural strength of loess is mainly contributed by cementation among soil. However, the cementation link can be dissolved in water; thus cohesion strength diminishes when the soil is fully saturated. The cementational strength can also be removed by loading. (2) Qualitative similarity in the mechanical behaviour between loess and natural clays can be seen as follows. Firstly, the voids ratio for a natural loess is higher than that of the reconstituted soil of the same mineralogy and the virgin yielding stress of the soil is also higher that of the corresponding reconstituted soil. Secondly, the stress and strain behaviour of the structured loess appear to be asymptotic to the curve for the reconstituted soil, *i.e.* the influence of soil structure tends to diminish with loading. (3) A basic feature of the behaviour of a loess is its dependence on the degree of saturation of the soil.

STRUCTURED CAM CLAY MODEL EXTENDED FOR CEMENTATION EFFECT

Because loess possesses both cementation structure and particle-arrangement structure, the Structured Cam Clay Model Extended for cementation effect is employed as a base to describe the soil. A brief introduction of the extended model is given below, and details of the model can be found in papers by Liu and Carter [9] and Horpibulsuk et al [6].

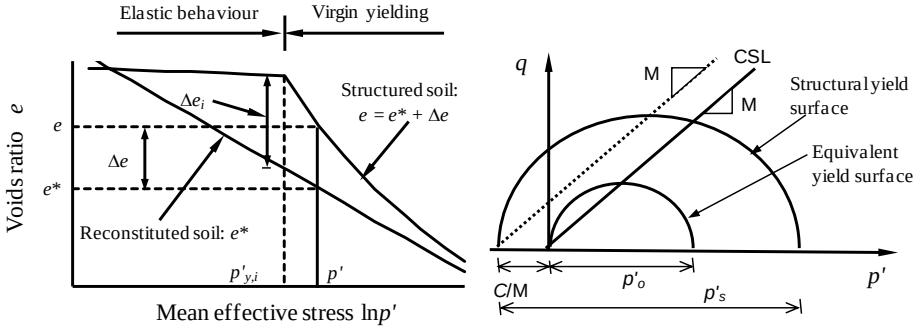

(a) Compression behaviour of structural soils (b) Structural and equivalent yield surfaces

Figure 1. Materialization for the Structured Cam Clay Model

Modification of the mean effective stress cementation

A fundamental assumption in the extending the SCC model for the effect of cementation is taken into consideration as the reinforcement of the confining mean effective stress; and a modified mean stress parameter is proposed as follows,

$$\bar{p}' = p' + C/\mathrm{M} \qquad \text{Eq. (1)}$$

where p' is the mean effective stress, M is the slope of the failure envelope of cemented clay, and C is a parameter related to the shear strength contributed by cementation. It should be pointed out that C is

generally not constant, but a function of soil structure. The cohesion strength of loess is strongly dependent the degree of saturation. In this study, the value for C for loess with a given saturation is identified. Then it is assumed that the value fo C remains constant before the peak strength. After peak failure state, C gradually decreases due to the crushing of soil structure, and finally $C = 0$ will be reached at a critical state of deformation.

Material idealization

In the extended SCC model, cemented clay is idealized as an isotropic material with elastic and virgin yielding behaviour. The yield surface varies isotropically with plastic volumetric deformation. Soil behaviour is assumed to be elastic for any stress excursion inside the current structural yield surface. Virgin yielding occurs for a stress variation originating on the structural yield surface and causing it to change. During virgin yielding, the current stress of a cemented clay stays on the structural yield surface. The idealization of the mechanical behaviour of cemented clays is illustrated in Figure 1. In this figure, e represents the voids ratio for a cemented clay, e^* is the voids ratio of the reconstituted clay at same stress state with the same yield surface, $p'_{y,i}$ is the mean effective stress at which virgin yielding of the cemented soil begins, and Δe, the additional voids ratio, is the difference in voids ratio between the cemented clay and the reconstituted clay at the same stress state. Hence, the virgin compression behaviour of a cemented soil can be expressed by the following equation proposed by Liu and Carter [11],

$$e = e^* + \Delta e = e^* + (\Delta e_i - c)\left(\frac{p'_{y,i} + C/\mathrm{M}}{\bar{p}'}\right)^b + c \qquad \text{Eq. (2)}$$

where b and c are soil parameters describing the additional voids ratio sustained by cementation. Δe_i is the value of the additional voids ratio at the start of virgin yielding (Figure 1a). Parameter c is that part of the additional voids ration that can not be removed completely by loading,

The yield surface of a cemented clay in p'-q space is also assumed to be elliptical and is described as (Figure 1b). The size of the yield surface is denoted as p'_s.

Elastic behaviour

For stress excursions within the yield surface, only elastic deformation occurs. For simplicity, elastic deformation of cemented clay is assumed to be described by Hooke's law, i.e.,

$$d\varepsilon_v^e = \frac{3(1-2\nu)}{E} dp', \quad d\varepsilon_d^e = \frac{2(1+\nu)}{3}\frac{dq}{E} \qquad \text{Eq. (3)}$$

where ν is the Poisson's ratio and E is the Young's modulus.

Virgin yielding behaviour

For stress states on the yield surface and with $dp'_s > 0$, virgin yielding occurs. The plastic volumetric strain increment for the original SCC model was derived from the assumption that both hardening and destructuring of clays are dependent on volumetric deformation, with a consideration of the destructuring associated with shearing [e.g., 9, 10]. The incremental stress and strain relationship of the Structured Cam Clay is

$$d\varepsilon_v = d\varepsilon_v^e + \left\{ \left(\lambda^* - \kappa\right) + b\left\langle \Delta e - c \right\rangle \left[1 + \frac{\gamma \bar{\eta}}{\mathrm{M} - \bar{\eta}} \right] \right\} \frac{dp'_s}{(1+e)p'_s} \qquad \text{Eq. (4)}$$

$$d\varepsilon_d = d\varepsilon_d^e + \frac{2\bar{\eta}}{\left|\mathrm{M}^2 - \bar{\eta}^2\right| + \omega\left|1 - \sqrt{p'_o / p'_s}\right|} \times \left\{ \left(\lambda^* - \kappa\right) + b\left\langle \Delta e - c \right\rangle \left[1 + \frac{\gamma \bar{\eta}}{\mathrm{M} - \bar{\eta}} \right] \right\} \frac{dp'_s}{(1+e)p'_s} \qquad \text{Eq. (5)}$$

where □* and □* are the compression and the swelling indices of reconstituted clay, respectively, γ is a soil parameter describing the destructuring associated with shearing, ω is a model parameter, and p'_o is the size of the equivalent yield surface with consideration of the influence of c, the part of the additional voids ration that can not be removed completely by loading [6].

Softening behavior and breakdown of cementation

Based on experimental observation, the softening behaviour for cemented clay occurs after the soil reaches the peak strength state ($\bar{\eta} = \mathrm{M}$ and $\Delta e \neq 0$). The crushing of soil-cementation structure also takes place during this stage. For simplicity, it is assumed that the crushing of soil-cementation structure commences after the peak state to reach the final critical state of deformation. During crushing, the effective stress state stays on the line defined by M but may travel along the line either upwards or downwards, depending on hardening or softening, respectively. Based on trial and error, the function for the crushing of soil-cementation structure is proposed,

$$dC = -2\left(\frac{C}{C_{in}}\right) \frac{\left|dp'_s\right|}{\sqrt{\left(\frac{q}{p'} - \mathrm{M}\right)}} \qquad \text{Eq. (6)}$$

where C_{in} is the value of the initial cementation strength.

SIMULATING THE BEHAVIOUR OF MA LAN LOESS

In this section, the Structured Cam Clay Model Extended for cementation effect is employed to simulate the behaviour of Ma Lan loess. The experimental data were reported by Li and Yao [8]. Value of model parameters identified for simulations are listed in Table 1.

Table 1 Values of model parameters of Malan loess

λ*	κ*	M*	e_{IC}*	ν*	*b*	*C*	ω	γ
0.122	0.03	0.98	1.403	**0.3**	1	30	**1**	**1**

Because limit data are available for the soil from this paper and previous publications, the authors are unable to determine the size of the initial yield surface $p'_{y,i}$. By trial and error, the an empirical equation is proposed to determine $p'_{y,i}$ based on the undrained peak shear strength q_{peak}.

$$p'_{y,i} = \frac{1.85 q_{peak}}{\mathrm{M}*} \qquad \text{Eq. (7)}$$

A comparison of the effective stress paths for Malan loess in undrained conventional triaxial tests between simulation and test results are shown in Figures 2 and 3. Six tests are simulated and compared with experimental observations. They are four shearing tests starting from isotropic stress states, and 2 tests from anisotropic stress states. The confining stresses vary from 200 kPa to 750 kPa. It can be seen that the general features of the effective stress paths of the loess are described well both qualitatively and quantitatively. The simulated deviatoric stress and strain relationship is shown in Figure 3, which is consistent qualitatively with experimental observation [2, 8]. It is seen that overall model simulations are in consistency reasonable well with experimental observation. From this study, the following points on modelling the stress and strain relationship of loess are observed.

(1) Unlike that of reconstituted soils, there are two additional factors contributing the softening for loess: (a) the crushing of soil structure, and (b) decementation. For the crushing of soil structure, stress paths keep the same stress ratio as M* and move downward along the critical state line. For decementation, cementation strength C reduces gradually to zero and the stress ratio also decreases. It is seen here that the softening on loess is largely influenced by decementation. (2) It may be concluded from the comparison that the basic features of the behaviour of loess can be captured by the Structured Cam Clay with cementation in particular, though more work is needed on aspects such as the determination of model parameters, the variation of cohesion with saturation and the removal of soil structure by loading. (3) It can also be seen from the behaviour of loess can be captured by conventional elastoplastic models in general, and the two key factors in such a model are the structure of the soil constituents and the suction force.

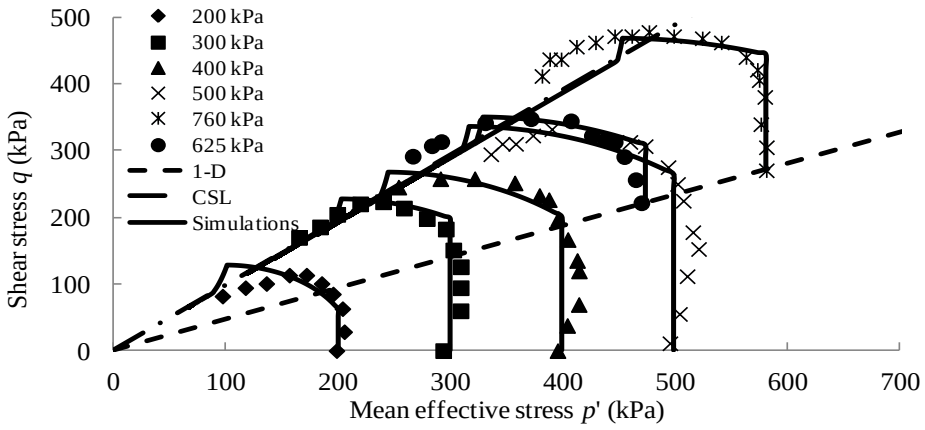

Fig 2. Effective stress paths for Malan loess measured and simulated

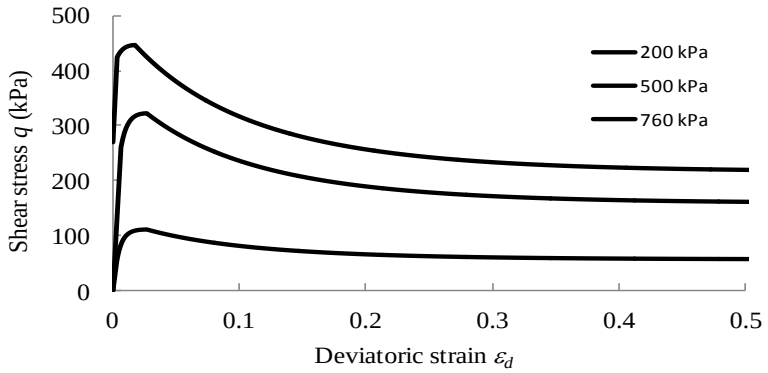

Fig 3. Deviatoric stress and strain relationship of Ma Lan loess simulated

CONCLUSION

Mechanical properties of loess are investigated and simulations of the stress and strain behaviour of the soil are made via the the thoretical framework of the Structured Cam Clay, and these simulations were compared with experimental observation. It is concluded that accurate prediction of the behaviour of loess is highly challenging because of complexity of the cementation amoung soil particles and collapsible nature of the structure with water as well as loading. It is seen that the Structured Cam Clay can provide approximate estimation of the behaviour of the loess. Therefore loess is a frictional material and its behaviour is dependent on the arrangement of and bonding amoung soil partices, essentially the same as other natural clays. To improve the accuracy of the simulation, further research within the Structured Cam Clay is needed in accurate representation of the development and removal of the cementation and structure of the soil with time, water and loading. An empirical equation for estimating the size of the initial structural yield surface is also suggested.

REFERENCES

[1] Chen C., Zhu Z., and Gao P, "Research on relationship between structure and deformation property of intact loess", *Rock and Soil Mechanics*, Vol. 27, No. 11, (2006),pp 1892-1896.

[2] Shao S., Luo A., Yu Q., and Zhou F., "Structural damage properties of Q_3 loess under triaxial loading and moistening", *Chinese Journal of Geotechnical Engineering*, Vol. 28, No. 12, (2006),pp.2078-2081.

[3] Leroueil S. and Hight D., "Compacted soils: from physics, to mechanics to hydraulic and mechanical behavior". *First Pan-American Conf. on Unsaturated Soils*, Cartagena de Indias, Colombia, (2013).

[4] Gens, A. and Nova, R., "Conceptual bases for constitutive model for bonded soil and weak rocks". *Geotechnical Engineering of Hard Soil-Soft Rocks*, Balkema, (1993).

[5] Taiebat M., Dafalias Y. F., Peek R., "A destructuration theory and its application to SANICLAY model", *Int. J. for Numerical and Analytical Methods in Geomechanics*. Vol. 34, No. 10, (2010),pp. 1009–1040.

[6] Horpibulsuk S., Liu M. D., Liyanapathirana S. and Suebsook J., "Behaviour of cemented clay simulated via the theoretical framework of the SCC model", *Computer and Geotechnique*, Vol. 37, No. 1, (2010),pp.1-9.

[7] Hu Z., Shen Z., and Xie D., "Deformation properties of structural loess", *Chinese Journal of Rock Mechanics and Engineering*, Vol. 23, No. 24, (2004),pp.4143-4145.

[8] Li J. and Yao Y., "Critical state model of Ko comsolidated structure loess", *J.Xi'an Univ. of Arch. & Tech.*(Natural Sience Edition), Vol. 42, No. 4, (2009),pp.533-537.

[9] Liu M. D. and Carter J. P., "Structured Cam Clay Model", *Canadian Geotechnical Journal.* Vol.39, No. 6, (2002),pp.1313-1332.

[10] Liu M. D. and Carter J. P., "The volumetric deformation of natural clays", *International Journal of Geomechanics*, ASCE, Vol. 3, No. 3/4, (2003),pp.236-252.

[11] Liu M. D. and Carter J. P. (2000), "Modelling the destructuring of soils during virgin compression", *Géotechnique*, Vol. 50(4), pp.479-483.